Universidad de Valladolid

ESCUELA DE INGENIERÍAS INDUSTRIALES

UNIVERSIDAD DE VALLADOLID

ESCUELA DE INGENIERIAS INDUSTRIALES

Máster en Ingeniería Industrial

ANALYSIS OF AN ARBITRARY SECONDARY CONCENTRATOR FOR THE SMALL PARTICLE HEAT EXCHANGE RECEIVER

Autor:

Alvarez De Soto, Jorge

María Teresa Parra Santos

San Diego State University

Valladolid, Septiembre 2016.

TFM REALIZADO EN PROGRAMA DE INTERCAMBIO

TÍTULO: Analysis of an arbitrary Secondary concentrator for the Small particle heat exchange Receiver

ALUMNO: JORGE ALVAREZ DE SOTO

FECHA: 29/08/2016

CENTRO: SDSU, solar Energy and Combustion Lab.

TUTOR: Dr. Fletcher J. Miller

Abstract

The design of a new method for the design of a new secondary concentrator for the Small Particle Heat Exchange Receiver using a Monte Carlo Ray Tracing method, based in Berchtold's thesis, is discussed in this thesis. The new method consists on generate the shape in SolidWorks, import it in ANSYS and use the nodes to generate the ray tracing in FORTRAN.

The main purpose of changing the secondary concentrator to a regular inlet shape is to increase the number of concentrator and in consequence the size of the heliostat field which improves the power generation efficiency and reduces the cost of electricity produced. The purpose of using a regular inlet is to close packed the concentrators in order not to have gaps between them.

FORTRAN is used to carry out the ray tracing for a concentrator with an arbitrary shape in order to choose the more efficient and lowest cost shape. FORTRAN is used in order to be compatible with MIRVAL, a FORTRAN code developed by Sandia National Laboratories that does the simulation of the heliostats and the receiver for a solar energy central receiver power plants. Due to the necessity of testing different shapes, SOLIDWORKS and ANSYS are used to generate the shape and import it into FORTRAN.

Matlab is used as a post processing of all the data generated by FORTRAN, in order to find the flux maps, and the power hitting the window.

Keywords

Concentrated Solar Power Plant, CSP, Secondary Concentrator, Terminal Concentrator, Monte Carlo Ray Tracing, Central Receiver System.

Acknowledgements

I wish to recognize in a special way my advisor, Professor Fletcher J. Miller, for his motivation, his support and guidance throughout the research process. It has been a privilege to work with such a curious man, his breadth of knowledge and perfectionism were a strong inspiration and encouragement for me.

Let me also acknowledge my Spanish advisor, Professor Teresa Parra, without whom it wouldn‘t have been possible to research for my Proyecto Fin de Carrera in the United States. I would also like to thank my colleagues of the Solar Energy and Combustion Lab for making my time in the lab enjoyable. I would like to particularly thank to Olivier Berchtold for his previous work on the CPC‘s modeling which was really helpful to fulfill this research.

Last but clearly not least, my family. I cannot thank enough my parents for their patience, encouragement and tremendous support during this year, especially my brothers that encourage me when nothing seemed to work out.

Table of Contents

Acronyms

CPC	Compound parabolic concentrator
CSP	Concentrated solar power
STE	Solar thermal electricity
PV	Photovoltaics
MCRT	Monte Carlo ray tracing
SPHER	Small Particle Heat Exchange Receiver
HTF	Heat transfer fluid
NV	Normal vector
PE	Primary energy
HEXHEX	Hexagonal inlet outlet
HEXBER	Berchtold shape with hexagonal inlet
BERS	Berchtold shape
WMO	World Meteorological Organization

Table of figures

1 Introduction.

The purpose of this chapter is to give the reader a basic overview about the objective of this thesis. It explains the importance of this research and the theoretical and computational method used during the thesis.

First, a brief introduction to solar energy is presented, and then we focus on Concentrated Solar Power (CSP).

1.1 Why renewable energy.

There is a pressing need to accelerate the development of advanced energy technologies in order to address the global challenges of clean energy, climate change and sustainable development.

The overall aim is to advance global development and uptake of key technologies to limit the global mean temperature increase to 2°C in the long term. The future accomplish of it will be directly related with the new efficient and renewable plants, since the annual greenhouse gas bulletin from the World Meteorological Organization, WMO, showed that in 2013 concentrations of CO_2 in the atmosphere were 142% of what they were before the Industrial Revolution. Existing conventional plants and those under construction may lock in greenhouse gases and especially in CO_2 emissions in order to accomplish the long term increased, as they will be operating for decades. [1]

Current emissions of major non-CO_2 greenhouse gases such as methane or nitrous oxide are significant for climate change in the next few decades or century, but these gases do not persist over time in the same way as carbon dioxide. [1]

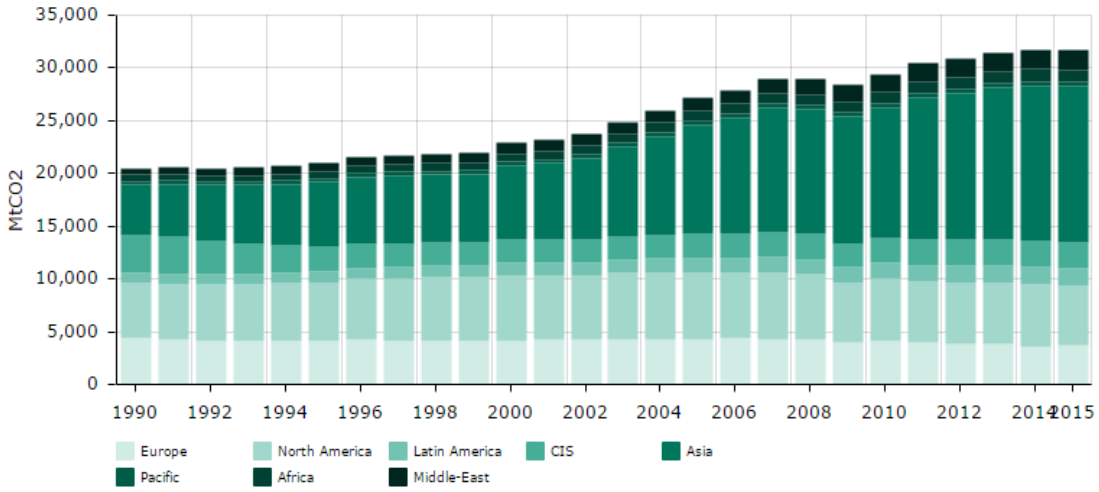

Figure 1-1 **CO_2** emissions worldwide [2]

As it is seen in the Figure 1-1 the CO_2 emissions have increased in the past 20 years, but thanks to the improvement in the renewable energies in the last years the average CO_2 emissions haven't increased as fast as in the previous years. [2]

A majority of the world's current electricity supply is generated from fossil fuels such as coal, oil and natural gas. These traditional energy sources face a number of challenges including rising prices, security concerns, and over dependence on imports from a limited number of countries, which have significant fossil fuel supplies, and growing environmental concerns over the climate change risks associated with power generation using fossil fuels. As a result of these and other challenges facing traditional energy sources, governments, businesses and consumers are increasingly supporting the development of alternative energy sources and new technologies for electricity generation. Renewable energy sources such as solar, biomass, geothermal, hydroelectric and wind power generation have emerged as potential alternatives which address some of these concerns. As opposed to fossil fuels, which draw on finite resources that may eventually become too expensive to retrieve, renewable energy sources are generally unlimited in availability. [3]

1.2 Climate change

The most critical factor about the increase in the CO_2 levels is the climate change, due to emissions from fossil fuel combustion, followed by aerosols and the CO_2 released by cement manufacture; the criticality of the increase in CO_2 versus others gases is its persistence over the time.

Climate change is a change in the statistical distribution of weather patterns when that change lasts for an extended period of time. Climate change may refer to a change in average weather conditions, or in the time variation of weather around longer-term average conditions. The evidence of it is clear. Our Earth is warming; average temperature has risen by 0.7°C over the past century and is projected to rise another 0.2 to 5°C over the next hundred years.

One of the most known effects of the climate changes is the warming process of the Earth which is commonly known as "greenhouse effect". This effect is related with the balance between the energy entering and leaving. If the energy is absorbed by the Earth, Earth warms, but if the energy is reflected back into space, the Earth doesn't warm, and if the absorbed energy is released back into space, Earth cools. [4]

In detail the effect depends in the sunlight that reaches Earth's surface, it can either be reflected back into space or absorbed by Earth. Once absorbed, the planet releases some of the energy back into the atmosphere as heat (also called infrared radiation). Greenhouse gases (GHGs) like water vapor (H_2O), carbon dioxide (CO_2), and methane (CH_4) absorb energy, slowing or preventing the loss of heat to space. In this way, GHGs act like a blanket, making Earth warmer than it would otherwise be.

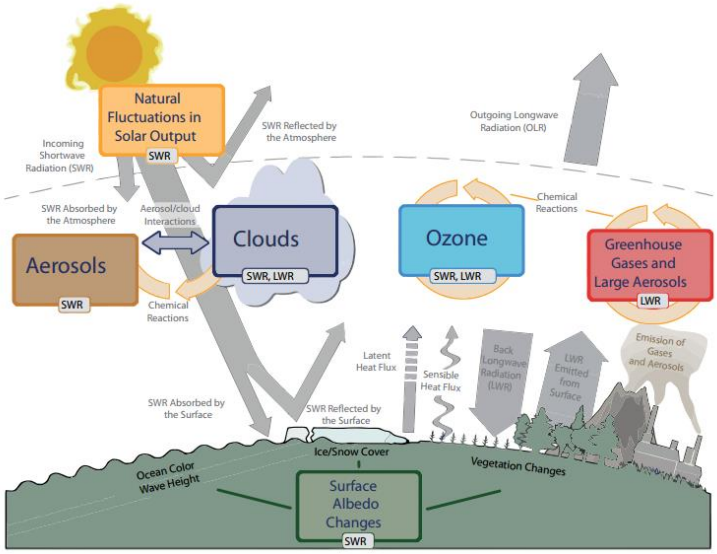

Figure 1-2 Explanation of the Greenhouse effect [5]

In order to minimize the greenhouse effect is mandatory to substitute the traditional ways to generate power which generated the greenhouse gases to a renewable energy like solar energy.

Emissions can be lower in two ways. Firstly, by lowering CO_2 emissions on the supply side, for example by switching electricity generation from fossil fuels to renewables, or deploying carbon capture and storage. Secondly, by lowering consumption emissions. [5] Since the second is related with the conscientiousness of the people is really hard to achieve without strong government mandates.

Generating electricity from renewable energy rather than fossil fuels offers not only power without emitting CO_2, but also significant public health benefits. The air and water pollution emitted by coal and natural gas plants is linked to breathing problems, neurological damage, heart attacks, and cancer. Replacing fossil fuels with renewable energy has been found to reduce premature mortality and lost workdays, and it reduces overall healthcare costs [6]

1.3 World Energy demand and Solar Energy

Trends in energy use are expected to increase all over the world as the population is growing together with its need for goods and comfort. [7]

A reliable forecast of energy resources, energy consumption and population in the future is a difficult task, due to the quantity of assumptions necessary to fulfill the trend.

Primary energy (PE) is an energy form found in nature that has not been subjected to any conversion or transformation process. It is energy contained in raw fuels, and other forms of energy received as input to a system. Primary energy can be non-renewable or renewable. [8]

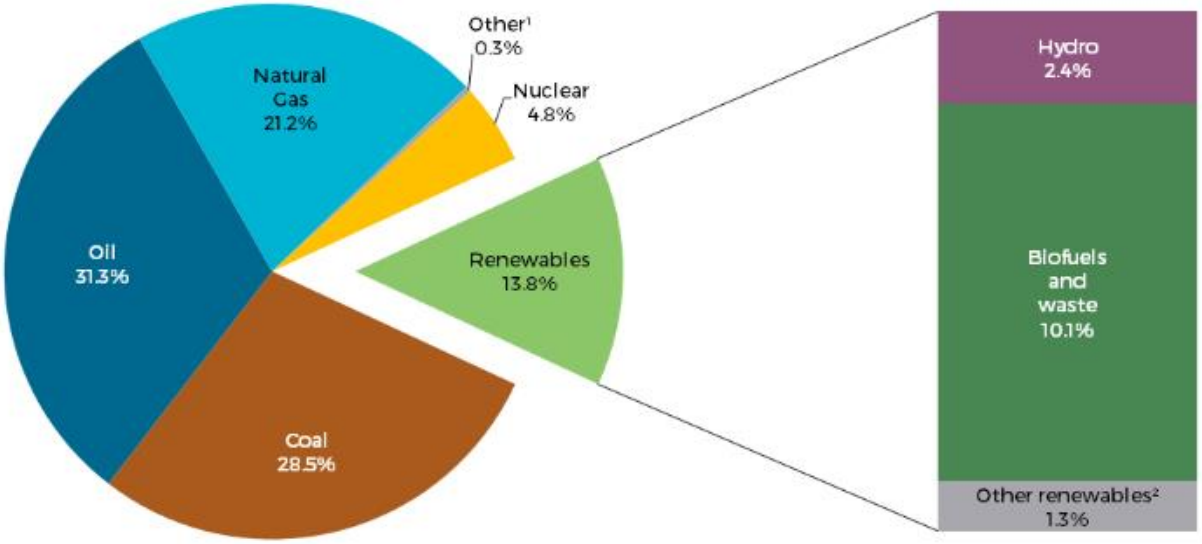

Figure 1-3 Fuel shares in world total primary energy supply in 2014 [5]

As can be seen in the Figure 1-3 the percent of renewables is really low, and in order to accomplish the CO_2 emissions is mandatory to develop the technology, as it appear in the Figure 1-4- the renewables are having an incredible growth .

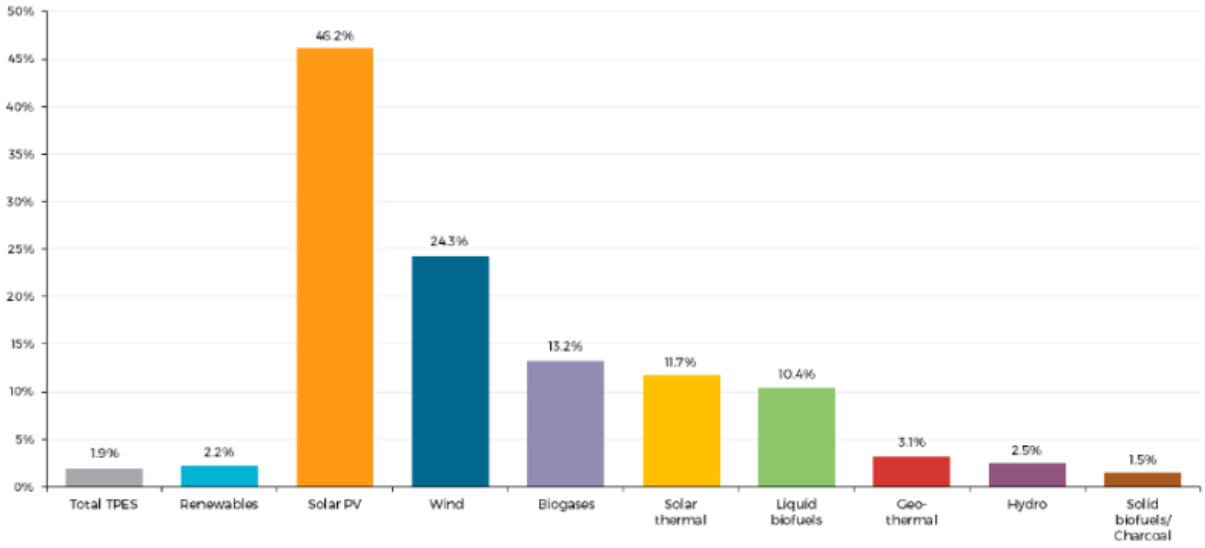

Figure 1-4-Annual growth rates of world renewables supply from 1990 to 2014 [5]

Since 1990, renewable energy has grown at an average annual rate of 2,2% . Although solar PV energy has grown especially, solar thermal has more benefits in order to accumulate the energy. The main reason of the growth of solar energy is that is the most abundant energy resource on earth, the terawatt hours reaching the surface of the planet every year are thousands of times bigger than the commercial primary energy consumed by humankind. [5]

1.4 Concentrated Solar power

The basic operation principle of a concentrated solar power (CSP) plant is to concentrate solar radiation into a receiver, specially designed for high absorption and to reduce heat loss. A fluid flowing through the receiver absorbs the heat, and high temperature–high pressure steam is generated to drive a turbine to produce electricity. It can be generated with traditional Rankine power cycles using steam turbines.

CSP plants use mirrors to concentrate the energy from the sun, on a receiver placed in the top of a tower, to drive traditional steam turbines or engines that create electricity. The thermal energy concentrated in a CSP plant can be stored and used to produce electricity when it is needed, day or night.

A heat-transfer fluid heated in the receiver is used to generate steam, which, in turn, is used in a conventional turbine generator to produce electricity. Some power towers use water/steam as the heat-transfer fluid. Other advanced designs are experimenting with molten nitrate salt because of its superior heat-transfer and energy-storage capabilities. The energy-storage capability, or thermal storage, allows the system to continue to dispatch electricity during cloudy weather or at night.

The CSP can be divided in four families, shown in the Figure 1-5.

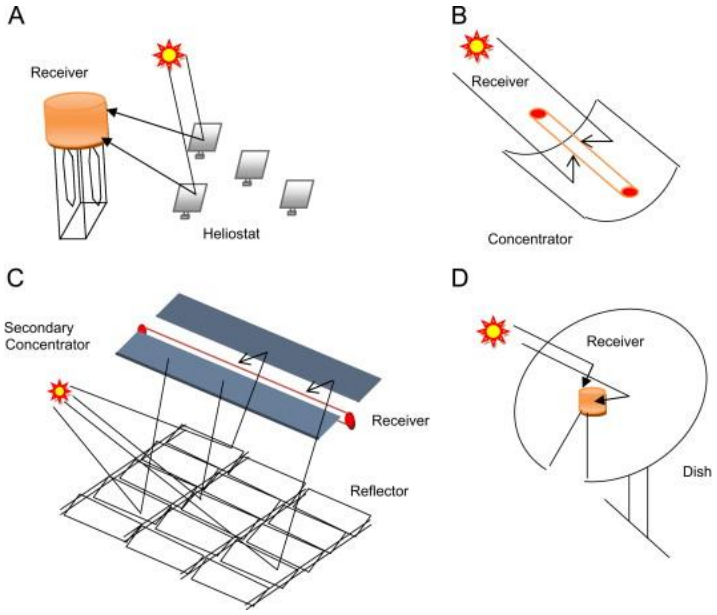

Figure 1-5 Basic concept of CSP families: (A) Central receiver, (B) parabolic trough, (C) linear Fresnel, (D) dish [9]

(A) Central receiver system, Power tower systems use a central receiver system, which allows for higher operating temperatures and thus greater efficiencies.

(B) Parabolic trough systems, use curved mirrors to focus the sun's energy onto a receiver tube that runs down the center of a trough.

(C) Compact Linear Fresnel Reflector, uses the principles of curved-mirror trough systems, but with long parallel rows of lower cost flat mirrors.

(D) Dish, mirrors are distributed over a parabolic dish surface to concentrate sunlight on a receiver fixed at the focal point.

In this thesis is studied the central receiver system, in which the receiver absorbs the sunlight from the heliostats and transfers the energy to a circulating fluid, the fluid is usually used to make steam for electricity generation, as can be seen in the.

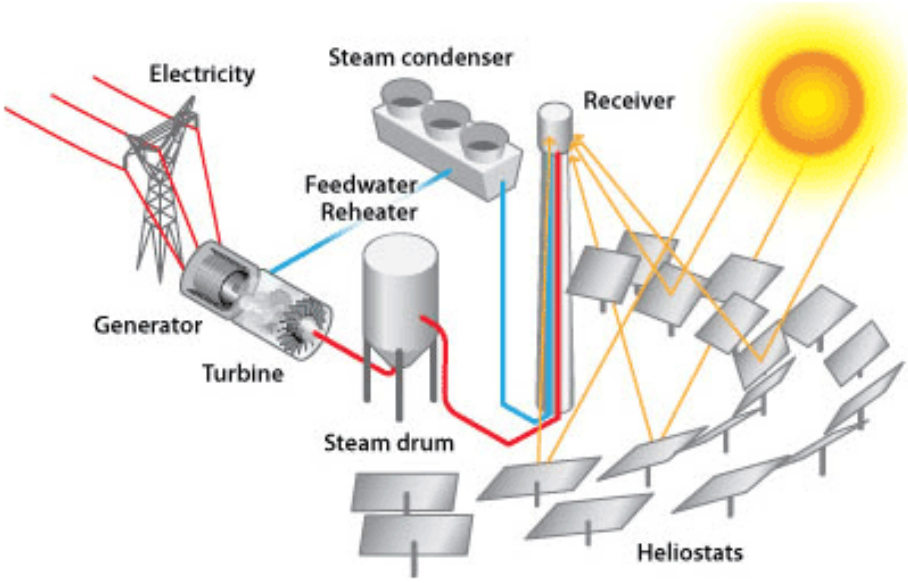

Figure 1-6 Scheme of a CSP plant [10]

The heliostat field is limited in the maximum achievable concentration ratio due to the incident angle spread from the sun, heliostat tracking and surface deviations and also minor effects like absorption of solar energy in the air.

1.4.1 Why Concentrated Solar Power instead of Photovoltaics

Generation of solar thermal electricity (STE) from concentrating solar power (CSP) plants has grown strongly worldwide, and it is predicted to grown even more in the next years.

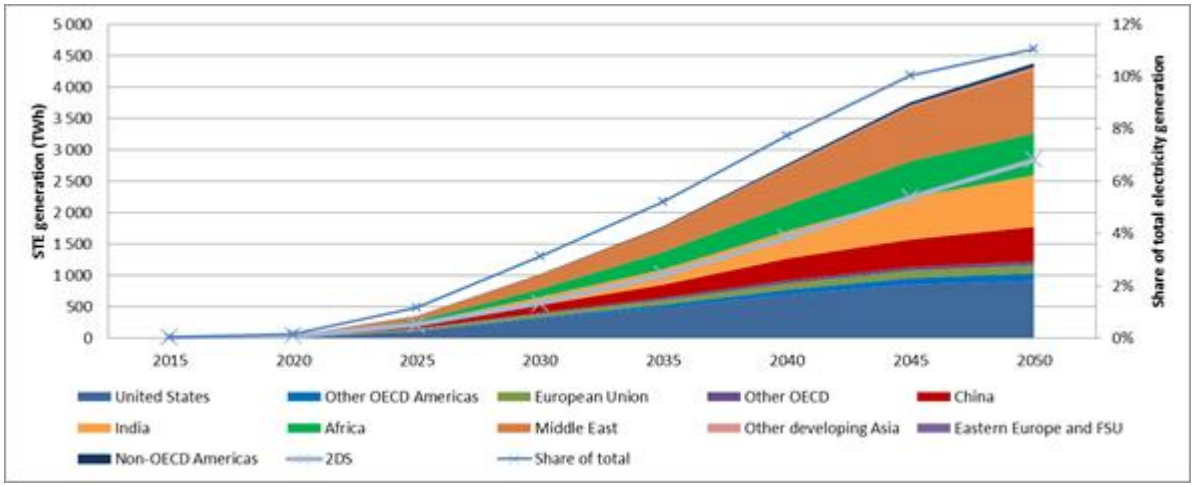

Figure 1-7 STE generation worldwide prediction [5]

One of the key benefits of choosing CSP over PV is that CSP plants can more easily provide ancillary services and provide dispatchable power on-demand using long-term storage. Combining these features in a hybrid power plant could make CSP competitive with PV in the future. [11] Current CSP plants are capable to store thermal energy for up to 16 hours, which means that their production profile can match the demand profile (just like a conventional power plant). PV is not dispatchable, as a feasible commercial energy storage system does not yet exist. Dispatchability will be increasingly important when and where renewable energies achieve high penetration rates, so two things can happen: CSP becomes a commercially viable solution before a commercial PV storage system is developed, carving its own market segment; or the PV industry quickly solves the storage issue and becomes the solar technology of choice. [12]

Other of the advantages of concentrating the sun's rays is that it allows higher working temperatures with good efficiency at collector level. This, in turn, allows better efficiency in converting heat into mechanical motion and, thus, electricity, as a consequence of the Carnot theorem.

STE from CSP plants is not broadly competitive today, but on-demand STE has higher value than PV electricity. Even in areas where afternoon peak time matches well with PV output, CSP plants offer a variety of ancillary services that are becoming increasingly valuable as shares of PV and wind (both variable renewables) increase in the electricity mix.

However the problem with CSP is the price of the generated electricity. In order to be competitive with all the others technologies the cost of the energy needs to be reduced by half.

Figure 1-8 Falling cost of concentrating solar power [13]

1.4.2 SPHER

The purpose of a SPHER is to heat a working gas in a solar receiver to a high temperature for powering a Brayton cycle gas turbine. The principal problem of most of the central receivers in the industry is that they use pipes to transfer the heat to the fluid, so the exterior surface of the pipes absorb the solar irradiation and transfer it to the heat transfer fluid(HTF) inside them. This way the pipes need to be heat up in order to exchange heat to the HTF, which provoke that the pipes are hotter than the HTF, which means higher thermal losses and limits the maximum achievable temperature due to materials limits. Moreover, the HTFs employed so far (oils, molten salts) degrade at temperatures over 800 K, which affect in the efficiency of the Rankine cycles.

Another challenge faced by current CSP plants is the large amount of cooling water required for Rankine cycle operation, which is a major concern, since the solar power plant are install in the regions which have more irradiation, which usually are dry regions, which are subjected to water shortages. This forced to use dry cooling methods, which increased the cost and decrease the efficiency of the system. [14]

The Small Particle Solar Receiver proposed by Hunt in 1979 is able to overcome the two previous limitations (provides higher outlet temperature and very significantly reduce the water requirements). This concept is based on employing a dispersion of carbon nanoparticles throughout a volume of gas to volumetrically absorb concentrated solar irradiation. [15]

It is essentially a large, pressurized vessel with a window (connected with the secondary concentrator, through which the concentrated solar irradiation enters) and an air-particle

mixture flowing inside, as schematically depicted in Figure 1-9. Since solar irradiation is absorbed volumetrically by the air-particle mixture, the walls are at lower temperature and do not limit the operating conditions anymore.

The purpose of the small particles is to absorb sunlight and exchange the heat to the gas functioning as a heat exchanger. Since the particles are so effective, and there are minimal losses through the walls the outlet temperature can excess of 1300 K.

The choice of the composition of the particles is determined by the desired operating temperature. Carbon nano-particles were chosen because they work as a selective absorber and the mixture of air and carbon can be treated as a single phase, and can be assume that the particles are at a local thermodynamic equilibrium with their surroundings.

The Small Particle Solar Receiver, in turn, would lead to more flexible operation, would exceedingly reduce the water requirements and would produce higher thermodynamic efficiency compared to lower temperature liquid cooled receivers.

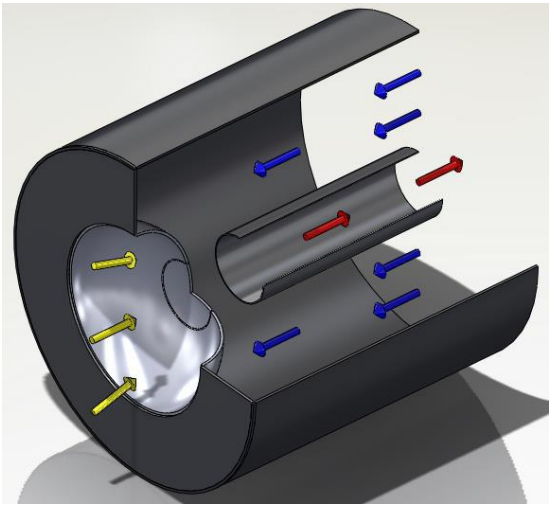

Figure 1-9 Schematic representation of the Small Particle Solar Receiver (yellow arrows: solar irradiation; blue arrows: air-particle mixture inlet; red arrows: air-particle mixture outlet).

The Small Particle Solar Receiver can also accommodate higher incident flux levels than any existing technology, which reduces the size of the solar receiver with the corresponding cost and thermal losses reduction.

1.4.3 Secondary concentrator

Pressurized volumetric receivers, Figure 1-10, have proven their feasibility and good performance, and their integration into gas turbine cycles has been demonstrated. But for that is mandatory to use a secondary concentrator, since the sunlight has to be concentrated into relatively small glass windows of the receiver. This also means that is not possible to position heliostats all around the tower, only those within the ellipse, resulting from the section boundary of the view cone with the ground plane, are usable. [16] [17]

The purpose of the secondary concentrators is to redirect solar beams reflected by the primary concentrators to the focal point or line. This component allow an increase in the concentrated solar flux density and hence lead to lower thermal radiation losses relative to the incident radiation. [18] Its purpose is to increase the maximum solar concentration ratio in the window, show in Figure 1-10. The concentrator sits on top of the receiver tower and increases the receiver area while concentrating the rays, as can be seen the concentrated radiation passes through a domed window, and is absorbed in an absorbed, where the heat is transferred to the fluid directly. [17]

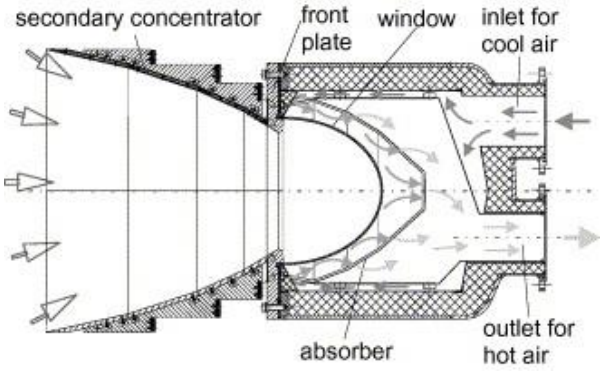

Figure 1-10 Secondary concentrator (Refos-concept).

As a general consideration, it should be noticed that in sunlight exploiting technologies, achieving the maximum efficiency is a key issue. When concentrating solar power (CSP) plants and solar furnace systems are considered, a relevant part of the efficiency of the overall system is due to the efficiency in light collection. Therefore, currently, there is a large interest in the development of techniques and methods to improve this facet.

Due to the fact that the receiver is generally angle insensitive and it is required to have a small entrance port to minimize radiation losses, a possible approach for the secondary mirror is to consider a secondary concentrator, usually a compound parabolic concentrator (CPC), as this geometry allows, at least in 2D, reaching the theoretical limit for sunlight concentration [6, 7]. In particular, CPCs can be very useful in large solar plants, where solar divergence prevents to obtain small focus areas, and, in high-temperature solar furnaces, where minimizing the entrance port dimensions is mandatory.

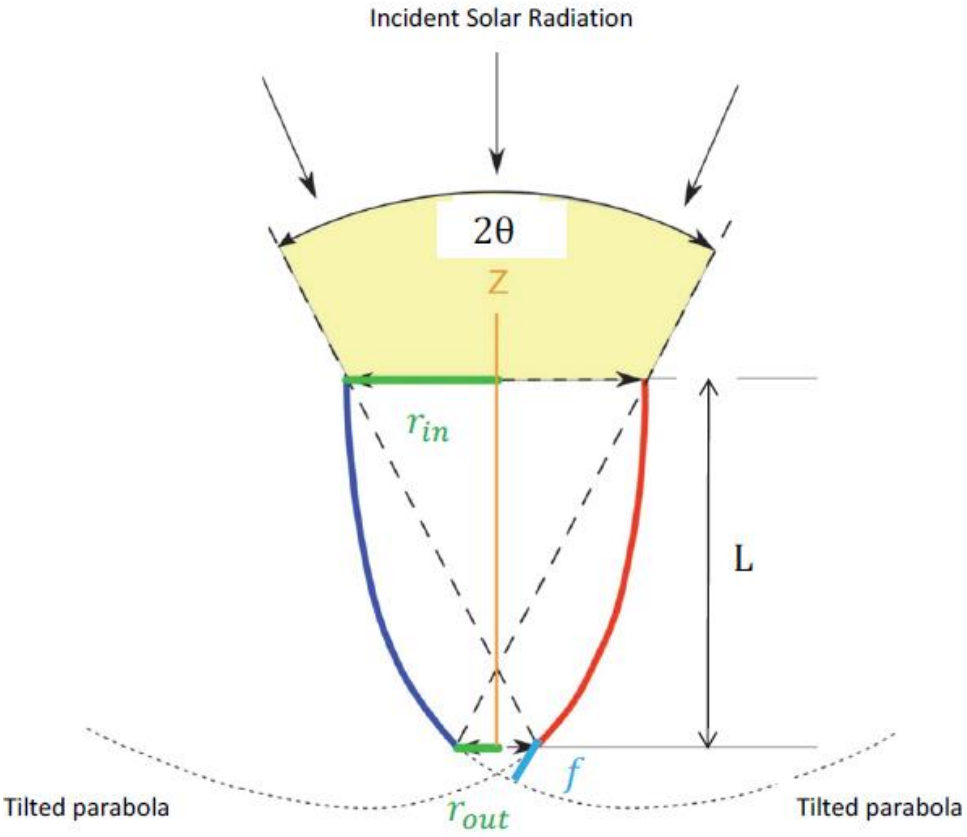

Figure 1-11 2D CPC (Berchtold modifications to Wikimedia commons) **[19]**

The CPC is the most efficient reflective geometry to collect light into the window in 2-D. [20] In 3 dimension the optimal solution is not evident. Previous researches made use of 3d CPCs [21], while another used polygons shapes for the secondary [22] , if we look at the astronomy studies for telescope, the concentrators are manufactured with a polygonal aperture and a circle outlet. [23] [24]

For this reason it is mandatory to test different shape in order to find the most efficient, and also taking into account the cost and that the shape allows to use more than one concentrator without losing any space between them(Figure 1-12).

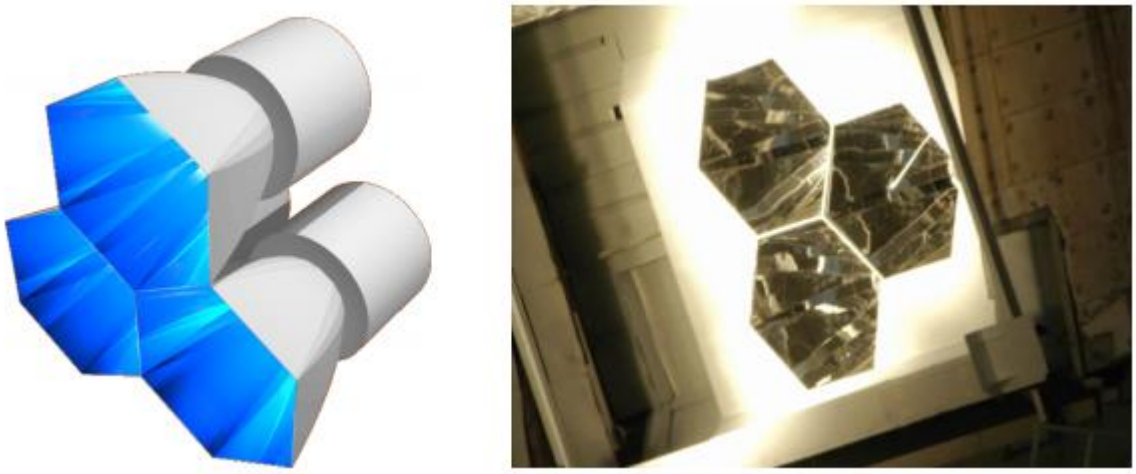

Figure 1-12 Multiple secondary concentrator SOLGATE solar receiver cluster [21]

1.5 Monte-Carlo Ray Tracing simulation (MCRT)

This thesis, as it modifies the secondary concentrator added in MIRVAL by Berchtold [19], uses a mathematical procedure called Monte Carlo Ray Tracing (MCRT). The MCRT is a numerical algorithm that works studying a large quantity of randomly generated numbers generated by a probabilistic model to find an approximate solution to a numerical problem that would be difficult to solve by other methods. In other words, the uncertain inputs in a model are represented by probability distributions.

With this the computer recalculates the model over and over again using different inputs, in order to simulate all possible outcomes. The results of the simulation is a distribution of possible outcomes, that is, the range of possible outcomes that could occur and the likelihood of any outcome occurring.

This is like running hundreds or thousands of "what-if" analyzes on your model, all in one go, but with the added advantage that the 'what-if' scenarios are generated with a frequency proportional to the probability we think they have of occurring.

In our case, the method is used to trace the rays from the sun to the heliostat field and then into the secondary concentrator. With this method is possible to determine qualitative and quantitative distribution of the rays' behavior, their direction and location of impact on the window, etc. [25]

1.6 MIRVAL

MIRVAL is a MCRT code developed by Sandia Laboratories in the 1970s with the purpose of detailed evaluation of fixed heliostat, field and receiver designs, and for computation of the solar thermal input to a receiver from a field of heliostats.[26]It is a FORTRAN code able to work with different receivers and types of heliostat for a solar energy central receiver power

plant, but it can be modify to evaluate any other receiver or heliostat, only changing a small number of subroutines. [26]

MIRVAL take into account the sun position, the non-uniform brightness of the sun's disc, the absorption of incoming rays in the atmosphere, the scattering of incoming rays by the atmosphere, the mirror-field and tower-receiver geometry, the reflectivity of mirror surface, the mirror guidance and imperfection in mirror guidance, the detailed mirror geometry including cant and figure of mirror facets, the small imperfections in mirror surface and the attenuation of reflected light in the atmosphere. The Combustion and Solar Energy Laboratory at SDSU modified the code in order to account spectral effects, and be able to run it with a secondary concentrator. [26] [19] [16]

MIRVAL is used as a base in this thesis to tracing the solar rays, it traces the rays to the point where they either get inside the receiver, following though the secondary and the window, or are lost to the environment.

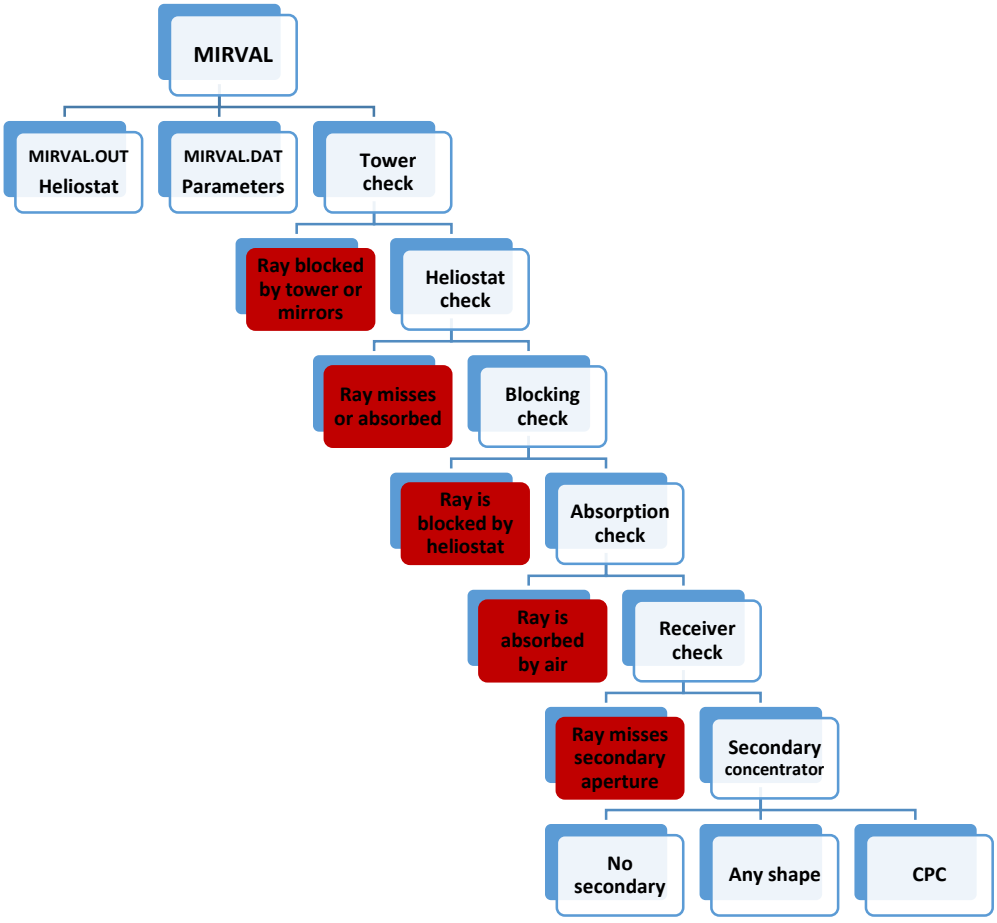

Figure 1-13 MIRVAL code scheme

1.7 Objective of this Proyecto fin de Carrera

The purpose of this research is to find a new shape for the secondary concentrator in order to be able to use multiple concentrators to increase the heliostat field and in consequence increase the efficiency and generate more power. The objective is to reduce the current limitation in the size of the heliostat field, which is related to the diameter and acceptance angle of the secondary concentrator, by modifying the shape of the secondary concentrator in order to allocate multiple concentrators at the top of the tower.

The current code works using the bisection method to calculate the intersection point using the equation of the shape, the limitations of it resides on the impossibility to test any other shape without finding the equation and in consequence modifying the code.

The main problem of trying to test any shape is the necessity to change the code to test a new shape and the difficulty to find an equation for all the shapes. To solve this a procedure is developed here that works with the nodes from ANSYS in order not to modify the code for any new simulation. This is an extremely powerful improvement, as it allows the analysis of any shape that can be drawn in SOLIDWORKS. The nodes from ANSYS are used to generate small planes with the purpose to find the intersection point in all of them but only in one of them the intersection is a point of the shape.

The remaining part of this thesis continues as follows. Chapter 2 simulation process, firstly is it explain the new inlet shape, the variables used by Berchtold, the new variables in order to run the code properly. Secondly it is explained how it was code the intersection and the reflection taking into account the imperfection, wavelength dependence. And thirdly the verification and the different test are presented.

2 Simulation

The ray tracing code presented in this thesis is based on Berthold's thesis, using the optimal parameters calculated by him [19]. These parameters include tilt angle, acceptance angle, and geometry of the secondary concentrator. As part of this research, a FORTRAN code was created in order to test different shapes for the secondary concentrator.

The main reason to continue using FORTRAN, is the purpose of implanting it in MIRVAL where the window code and receiver MCRT codes where implement, with the purpose of being able to make the test only running one program. Also due to its speed operating with matrices, which is a necessity in our case due to the quantity of planes, lines, and points used in the simulation, which are assigned as matrices.

And also because the purpose of the project is to implant it in MIRVAL, which was develop in FORTRAN.

2.1 Simulation design process

Multiple steps were used in this thesis in order to design the ray tracing simulation, with the objective to design a ray trace algorithm for any secondary concentrator.

The first step was to be able to modify the shape without having to modify the code all the time. For that the shape is generated in SOLIDWORKS, and then a mesh is generated in ANSYS and saved it in a .txt file with the name "shape.txt", and finally the mesh file is read in FORTRAN.

Figure 2-1 Scheme of how to generate the input file for FORTRAN

With FORTRAN the first part was to be able to read all the mesh information from the "shape.txt" file saved by ANSYS, and generate the plane with the nodes, secondly it was necessary to generate the intersection between all the planes and the ray and with that was developed the reflection subroutine which works with the intersection previously calculated.

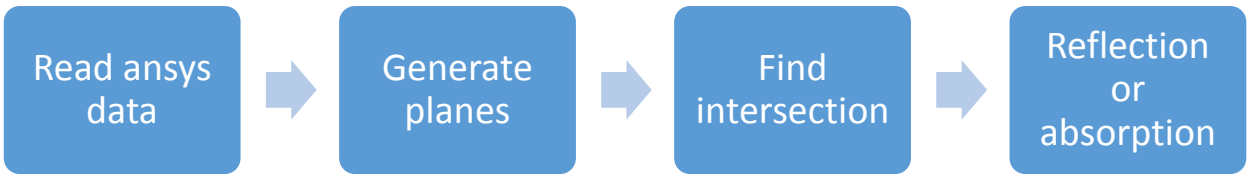

Figure 2-2 Scheme of the FORTRAN simulation design process

2.2 New inlet shape

As it was demonstrated by Eduardo Palomar, the heliostat field is limited by the CPC inlet, since the optical accuracy of the surface and other heliostat errors creates a deviation in the position and direction of the reflected rays, which becomes bigger in larger heliostat fields.

Due to the impossibility to modify the CPC dimensions since they are related with the window dimensions, the only way to increase the size of the field is to increase the number of windows and in consequence the number of secondary concentrator. With this purpose is mandatory to change the inlet, due to the impossibility to collocate more than one concentrator without losing some space between them. In order to avoid it, the entrance needs to be modified.

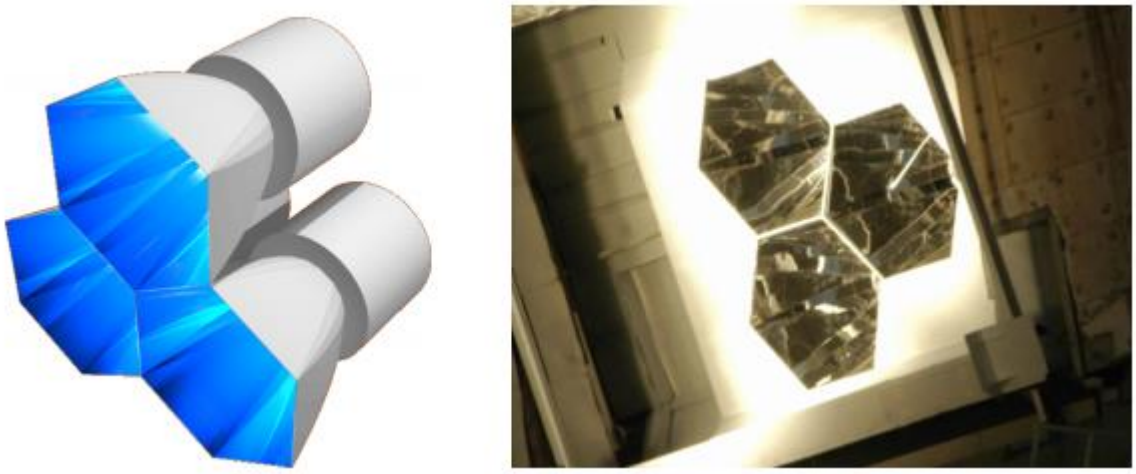

Figure 2-3 Multiple secondary concentrator SOLGATE solar receiver cluster [21]

The Figure 2-3 described the positions of the concentrators in order to increase the area of the heliostat field.

Another option not pursued in this thesis due to the difficulty of its manufacture, which will make it really expensive in compare with the other shapes would be CPC's pushed together as can be seen in the figure below.

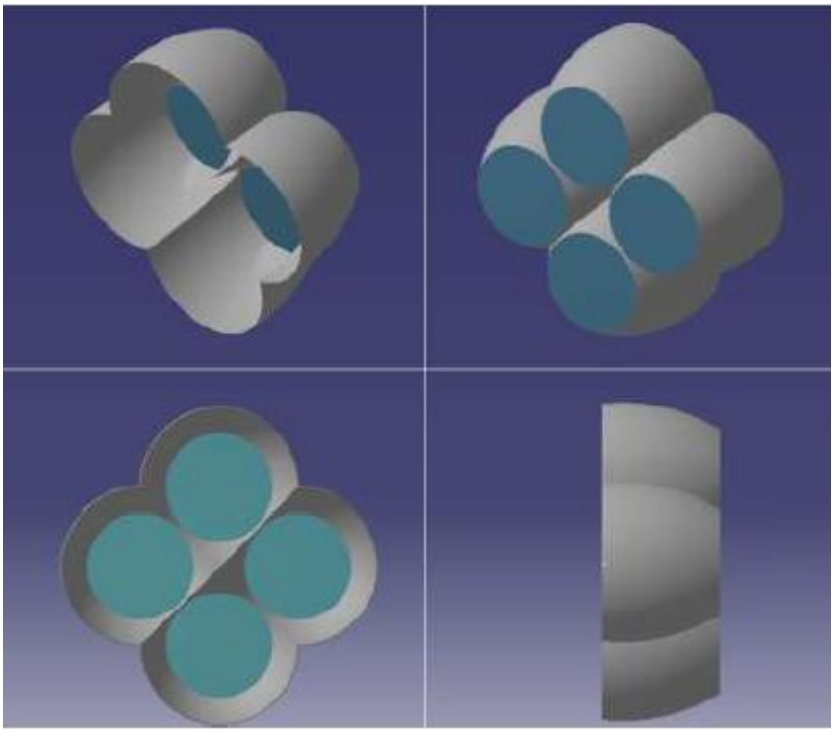

Figure 2-4 CPC's pushed together [16]

2.3 Simulation steps

First of all in order not to run MIRVAL during every of coding, we used an output file, *MIRVAL.FLX*, with more than 600.000 rays, generated with MIRVAL, which contains all the rays' coordinates, directions and secondary properties. These are used to calculate the intersection point of the rays with the planes from ANSYS.

As was said before the ability of being able to test any shape has a great inconvenience with the current code due to the different equations for any new shape and the necessity to change the code. Furthermore it may be impossible to find an equation for all the shapes. So it is mandatory to find a better way to generate the new shape.

To solve this inconvenient the shape is built in SOLIDWORKS, imported into ANSYS, meshed and then the resulting planes are used to calculate the intersection point in FORTRAN. This requires knowing SOLIDWORKS and ANSYS, and creating a file with the ANSYS nodes, but this problem is easier than modify the FORTRAN code for all the shapes.

The first step was to be able to import the ANSYS nodes in order to work with the new shape. The problem in that is the way ANSYS usually generates the nodes, since they are made without and order. Thus, it is easier to modify the ANSYS output in order to generate planes.

After that, the problem was to design the code to calculate the intersection with the planes generated by ANSYS, for this is mandatory to calculate the intersection with all the planes, and

check which intersection point is inside the plane, the intersection point has to be inside the three point that are generating the plane.

With the intersection point is possible to call the reflection subroutine, in order to trace the ray until it reaches the window, is absorbed, or is lost out the aperture.

After having the ray tracing for any shape, the next step was to modify the inlet and outlet to a regular shape in order to be able to install multiple concentrator in the same side of the tower, it was chosen a hexagon since it is the entrance which generate a honeycomb without the necessity of using different concentrator's shapes.

The code read the MIRVAL output file, imports the nodes information, makes the ray tracing for the real shape and at the end write out the information of the surviving rays, defined as rays that reached the window and a statistical output for the secondary concentrator.

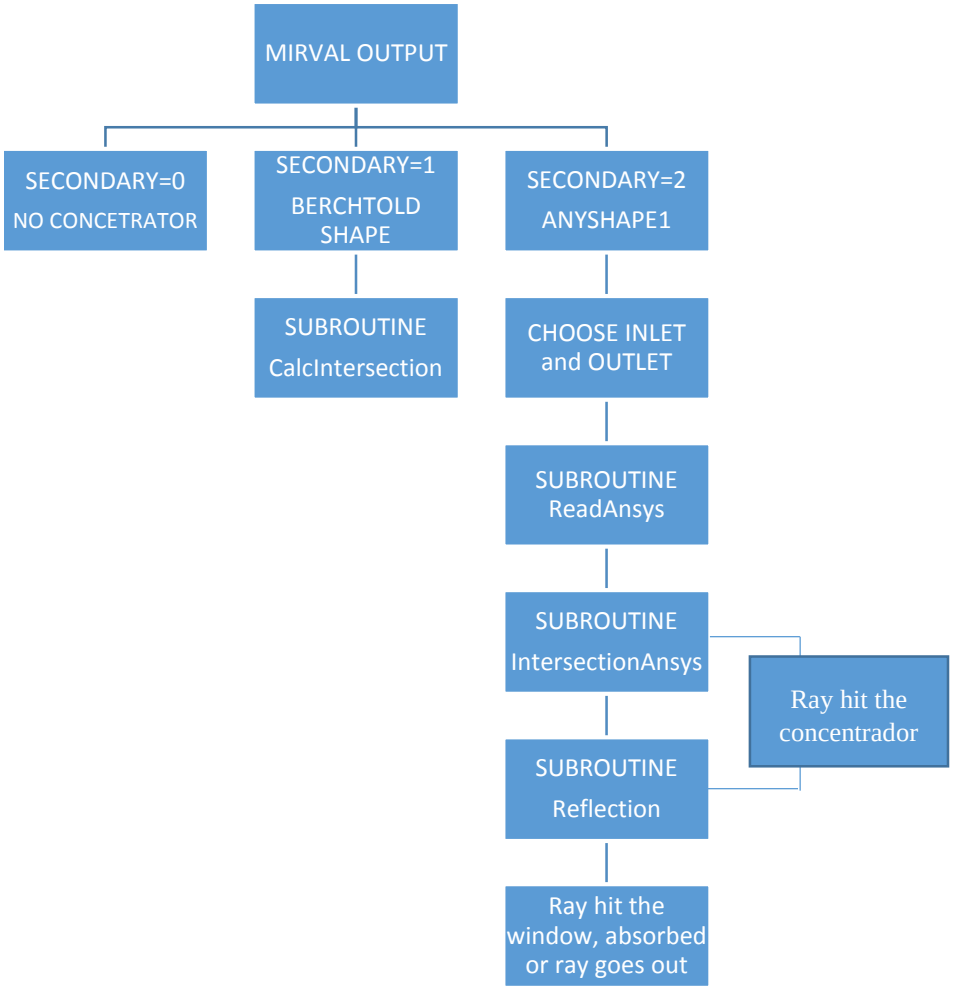

Figure 2-5 Simulation design flow chart

2.4 Berchtold's Variables

Before explaining the different secondary concentrator option and how to work with the new code, it is mandatory to understand Berchtold's variables in order to be able to work perfectly with the program.

Berchtold took into consideration the absorptivity of the concentrator, the slope and reflectance errors, considering them as an error in the direction after the reflection due to the impossibility to make a perfect shape, the spectral reflectance and the number of reflections. The relationship between variables and values can be seen in the following table.

	Value	**Explanation**
CPCUSEREFLCALC	0/1	Activate spectral reflectance.
CPCREFL	0.9629	CPC reflectivity.
CPCUSESLOPEERROR	0/1	Activates slope and reflectance errors.
CPCSLOPEERROR	0.003	Error in rad.
CPCRECLIM	10	Number maximum of reflections.

Table 2-1 Berchtold variables

The variable **CPCSLOPEERROR* is only use if **CPCUSESLOPEERROR* is equal to 1. The value of the **CPCREFL* is set to that value for the material's properties, but if **CPCUSEREFLCALC* is set to 1 the value of the reflectivity will change with the wavelength.

Also Berchtold calculated the optimal receiver tilt angle and in consequence the acceptance angle than need to be modified if the heliostat field is modified.

	Value	**Explanation**
CPCACCEPTANGLE	46	CPC acceptance angle
DELTAD	26	Receiver tilt angle

Table 2-2 Berchtold variables

This values where calculated by Berchtold, considering the heliostat field fixed for the National Solar Thermal Facility at Sandia Laboratories in New Mexico, which means that at the end for a new heliostat field will be necessary to calculate the optimal values.

2.5 New intersection method for different shapes

As it was explained in the simulation design process, the principal problem that appears in testing a combination of different shapes is the unknown equation of the new concentrator, which means it is mandatory to find another way to be able to calculate the intersection point of a ray and the concentrator.

Due to the required length of time to find an equation for the new possible concentrator and the necessity to change it for all the different possibilities, here we used the mesh nodes from ANSYS. The only problem about this is the necessary time to test all the planes for all the rays which will make the program slower from Berchtold's code.

A couple of new variable are used in order to be able to choose the subroutine that is going to be used, and the inlet and the outlet of the concentrator.

	Value	**Explanation**
Secondary	0	No secondary concentrator
Secondary	1	Berchtold's Code
Secondary	2	ANSYS' Code

Table 2-3 Secondary values to choose the different shapes

	Value	Explanation
cpchex	0	Circular inlet
cpchex	1	Hexagonal inlet

Table 2-4 Cpchex values to choose the different inlets

	Value	Explanation
outhex	0	Circular outlet
outhex	1	Hexagonal outlet

Table 2-5 Outhex values to choose the different inlets

In the Table 2-3 , it appears the explanation of the **Secondary* variable in order to choose the concentrator and the subroutine to use in the simulation, for the ANSYS's code is mandatory to save a .txt file with the ANSYS data.

In the Table 2-4 and Table 2-5 appears the meaning of the **cpchex* and **outhex* variables in order to modify the inlet or outlet of the concentrator.

So for a hexagonal inlet and hexagonal outlet is mandatory to set the variable **cpchex* and **outhex* to 1.

If any of the variables have a different value that is not show in the previous tables the code will stop and generate and error message.

2.6 Method of Solution

In order to run the program, it is mandatory to build the shape in SOLIDOWORKS, then import it in ANSYS, generate the mesh and copy all the nodes in a file, but first the *target system* need to be modify to *SLT*. If the target system is not modify the ANSYS will generate the nodes without generating the planes, which will make impossible for FORTRAN to work with the file.

This process seems to be unworthy to test a concentrator, for the quantity of time spend building the shape, but it is easier than modifying the code for any new concentrator.

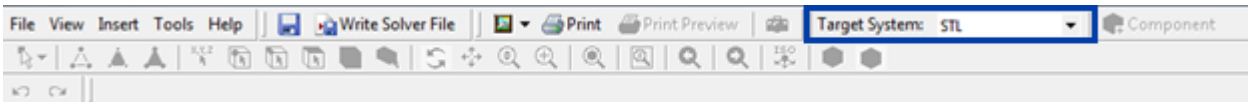

Figure 2-6 Target System: STL

The Figure 2-6 shows the modification, in a blue rectangle, to do in the mesh data in ANSYS, in the target system, in order that the file can work with the FORTRAN code.

Steps:

1. Build SOLIDWORKS shape.
2. Save in the format *.igs*.
3. Open Workbench ANSYS, file *final.wbpj*.
4. Import geometry, geometry, replace geometry, browse.
5. Thin/surface, select outer faces (value cero).
6. Mesh, refresh mesh, update refresh.
7. Change Target System to STL.
8. Open Model, write solver file.
9. Save it in .txt format with the name *shape.txt.*
10. Run FORTRAN.

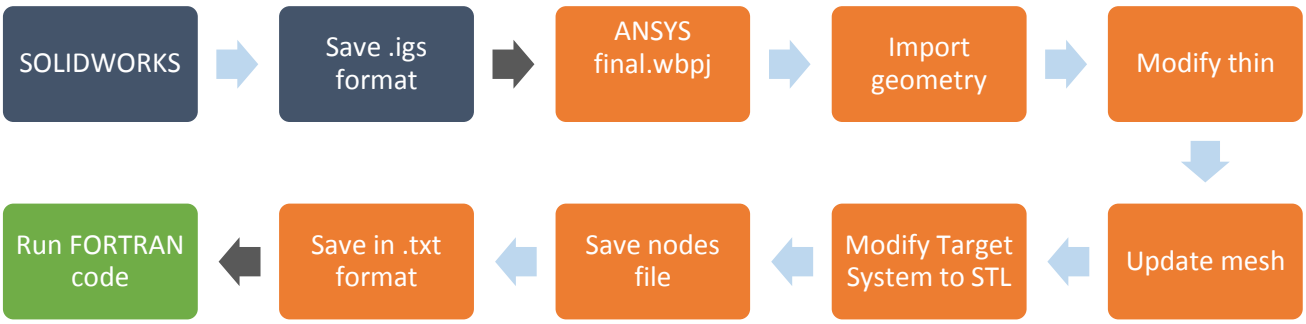

Figure 2-7 Testing process

The Figure 2-7 is a flow char of the process where the dark blue means that SOLIDWORKS is used, the orange are the steps in ANSYS and the green in FORTRAN.

2.7 Method of intersection

Berchtold made the code using the bisection method in order to find an approximation for the intersection point. This would be useful if we know the equation of the shapes. But, as it was said before, this is impossible for an arbitrary shape so a new intersection method need to be developed.

The method developed assumes that if we take really smalls planes the curvature of them will be insignificant. For that the nodes from ANSYS generate a plane, which is used to make the calculations, in order to test if they are (or which one is) hit by the ray. By increasing the number of nodes, we will find a point where the results do not change, and then we know we have sufficient points to approximate the curves surface as a many small planar elements.

Although ANSYS calculated the normal vector of the plane it was checked it and compare to see if it was faster to make the calculation of the plane or to work with the matrix imported from ANSYS. The main reason to check this is the slowness of FORTRAN working with the matrix compare with vectors.

The following equations explain how to create the plane with three points (point1, point2 and point3) which are the group of the closest three nodes that are used to generate a plane. Firstly two vectors are generate, which are used to generate the normal of the plane, since the cross product of two vectors will be orthogonal to both of these vectors, and then the equation of the plane is generated.

.

$$\begin{pmatrix} X1 \\ Y1 \\ Z1 \end{pmatrix} = \begin{pmatrix} Point1x \\ Point1y \\ Point1z \end{pmatrix} - \begin{pmatrix} Point2x \\ Point2y \\ Point2z \end{pmatrix}$$

Equation 2-1

$$\begin{pmatrix} X2 \\ Y2 \\ Z2 \end{pmatrix} = \begin{pmatrix} Point1x \\ Point1y \\ Point1z \end{pmatrix} - \begin{pmatrix} Point3x \\ Point3y \\ Point3z \end{pmatrix} \quad \text{Equation 2-2}$$

$$\begin{pmatrix} NormalvectorX \\ NormalvectorY \\ NormalvectorZ \end{pmatrix} = \begin{pmatrix} Y1 \cdot Z2 \\ Z1 \cdot X2 \\ X1 \cdot Y2 \end{pmatrix} - \begin{pmatrix} Z1 \cdot Y2 \\ X1 \cdot Z2 \\ Y1 \cdot X2 \end{pmatrix} \quad \text{Equation 2-3}$$

In the following figure appear the calculated normal and the ANSYS normal, as it is seen the difference is insignificant.

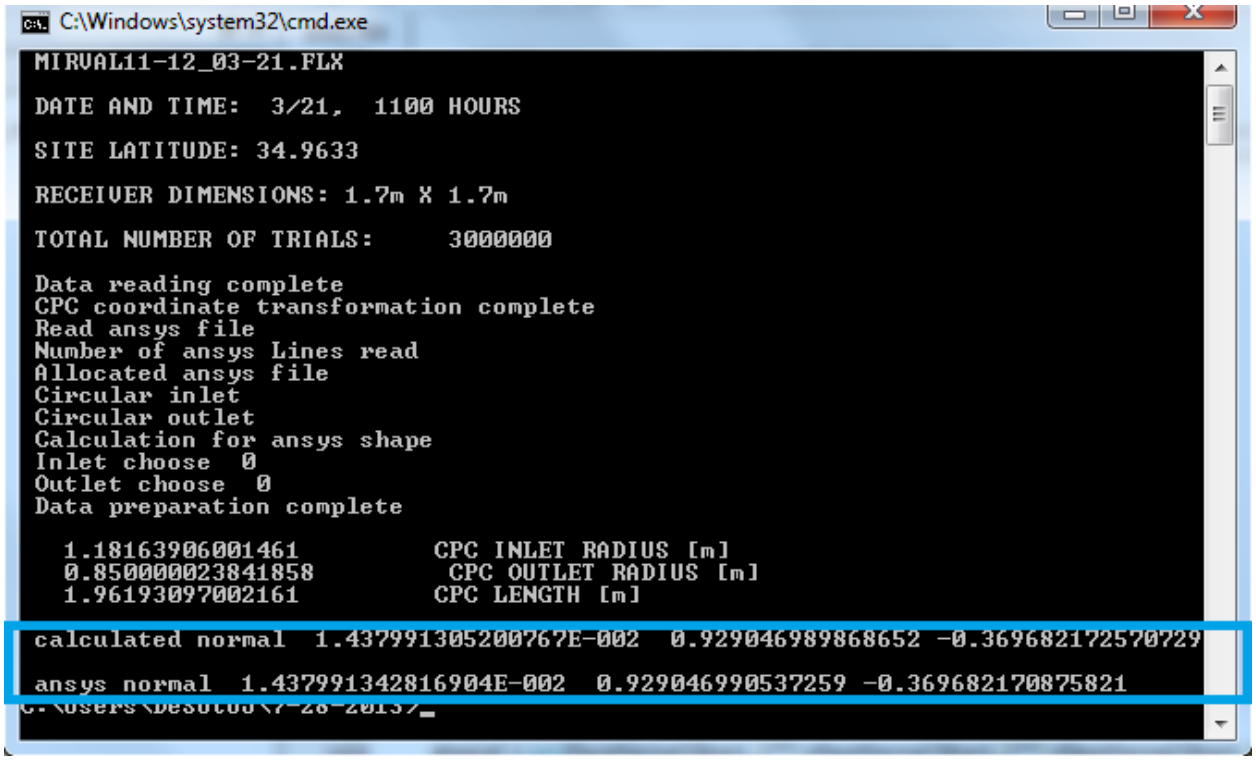

Figure 2-8 Normal plane calculated vs normal plane from ANSYS

Before using the normal vector (NV) is mandatory to normalize it, in order to be able to make the calculations. After normalizing the vector, to find the intersection point it is replace the values of the points for a line generated with the data from MIRVAL in the plane equation.

$$cte = NVx \cdot \big(XVAL(iRay) + t \cdot XCPC(iRay)\big) + NVy \cdot \big(YVAL(iRay) + t \cdot YCPC(iRay)\big) + NVz \cdot (ZVAL(iRay) + t \cdot ZCPC(iRay)) \quad \text{Equation 2-4}$$

Solving the Equation 2-4 the value of the variable t is found and with the following equation give us the intersection point.

$$\begin{pmatrix} IPx \\ IPy \\ IPz \end{pmatrix} = \begin{pmatrix} XVAL(iRay) + t \cdot XCPC(iRay) \\ YVAL(iRay) + t \cdot YCPC(iRay) \\ ZVAL(iRay) + t \cdot ZCPC(iRay) \end{pmatrix}$$ Equation 2-5

Now the last thing is to check if the intersection point is inside the three points, which will mean that the intersection point is in the shape, in consequence is the real intersection. This is done by comparing the intersection point with the nodes used to generate the plane; the condition is that the intersection point need to be bigger than the smallest of the three points but smaller than the bigger of them for the three exes, and also it is considered that the value of the z has to be the closest to the window, since it can happen that the intersection point is inside the plane but due to the curvature of the shape the real intersection is the next plane that is closer to the window.

Now that is possible to work with either of this intersection subroutines, a running time comparison is made in order to use the faster code.

	ANSYS planes	Calculated planes
Time (s)	589.824	697.917

Table 2-6 Time comparison using ANSYS planes and calculating the planes for the 03/21 between 11-12 for Berchtold's shape

Finally it was decided to use the ANSYS planes since is almost two minutes faster than calculating the planes, and as it can be seen in the Figure 2-8 the results are quite similar.

2.8 Method of reflection

The reflection is based on Berchtold's subroutine, taking into account that the intersection point has been previously calculated, the bisection method fulfilled by Berchtold is not used, is only needed to calculate the reflected ray direction.

The reflected ray direction is given by mirroring the incident ray on the surface. For that the normal face of the intersection plane is used. A simple way to determine the reflected ray's direction vector is subtracting twice the surface normal component of the incident ray direction vector from the incident direction vector:

$$\begin{pmatrix} v_{x,reflected} \\ v_{y,reflected} \\ v_{z,reflected} \end{pmatrix} = \begin{pmatrix} v_{x,incident} \\ v_{y,incident} \\ v_{z,incident} \end{pmatrix} - 2 \begin{pmatrix} n_x \\ n_y \\ n_z \end{pmatrix} \left(\begin{pmatrix} v_{x,incident} \\ v_{y,incident} \\ v_{z,incident} \end{pmatrix} * \begin{pmatrix} n_x \\ n_y \\ n_z \end{pmatrix} \right)$$ Equation 2-6 [19]

The reflected vector direction and the intersection point (new point of origin) are used to continue the tracing of the ray. The reflection subroutine was implemented in order to avoid the rays in which the Z component of the reflection is positive, which means that they will turn back and never hit the window, and also to avoid the rays which have a large number of reflections, which provoke the slowing down of the program.

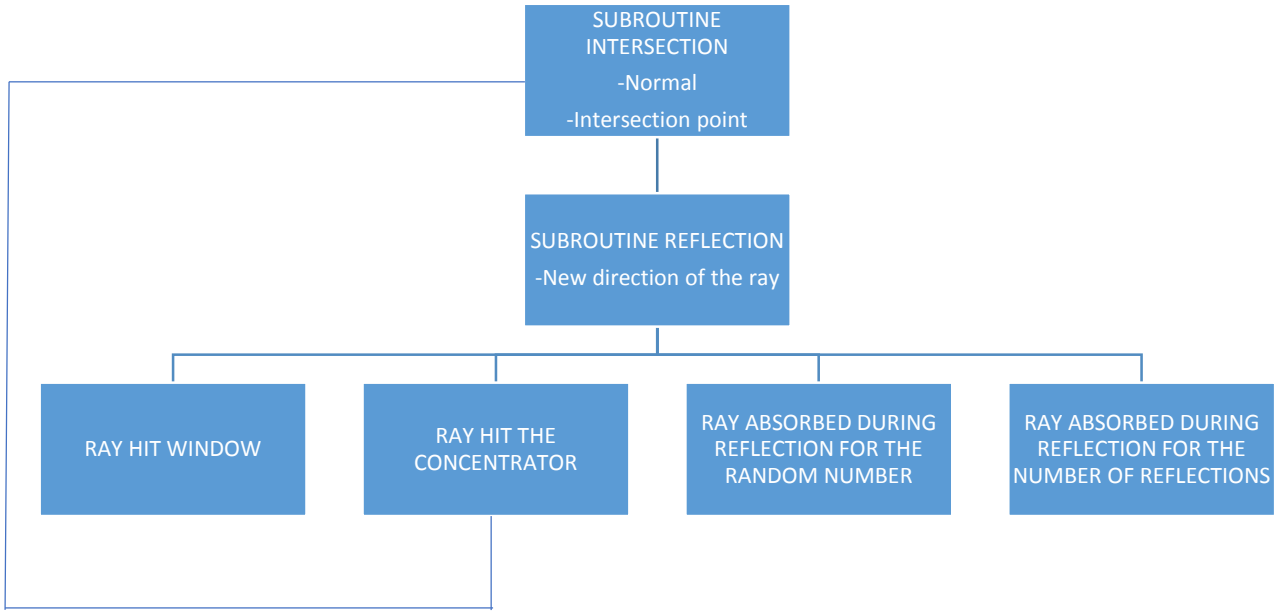

Figure 2-9 Reflection flow chart

As it is shown in the flow char above the possibilities after the reflection are:

- Hitting directly the window.
- Hitting again the secondary concentrator.
- Being absorbed during the reflection, a random number is generated for every intersection and if this number is bigger that the **CPCREFL*, the ray will be absorbed.
- Being absorbed during the reflection, due to the number of reflections.

2.9 3D Secondary concentrator with imperfection

In order to make a more realistic research of the concentrator, it is necessary to include certain deviation from the perfect implementation of the ideal concentrator. These deviations are caused by material limitations, environmental influences and mostly by manufacturing tolerances.

The principal problem of some of the new concentrators is the impossibility to manufacture a perfect shape since they will be a combination of different shapes. This leads to a deviation in reflected rays' directions.

For an ideal concentrator any ray that enters with an incident angle below the acceptance angle is accepted. But due to geometrically imperfections the rays at the very acceptance limit can end up being rejected, for that is taking into account the imperfections to try to simulate the imperfections and have a more realistic result.

2.10Wavelength dependence

In order to make the wavelength calculations to be more realistic, the reflectance data was split into 4 wavelength bands and approximated by polynomials. This allows the calculation of an exact value of reflectance for each wavelength and eliminates the need for a lookup table, thus making the execution of the code faster. [19]

2.11Verification

The necessity to verify the code is related to the assumption of no curvature in the generated planes and also due to the impossibility to make the calculations with all the decimals. Here we will compare Berchtold's code, which uses an equation and thus accounts for curvature, with the code developed here that approximates the same as many small flat surfaces.

Due to the impossibility to make these variables the same for the same ray, it is decided not to use them for the verification. Instead, we compare the results from Berchtold's code with the new code, without using absorption, random number and error in the shape.

For this as it was said before, is mandatory to turn the random subroutine off, in order to use the same random number for the same ray in both subroutines, and the reflection is considered to be 100%, in order not to have absorption, and is cancelled the errors in the shape, but not the error in the heliostat field, since it would be the same for both shapes.

The reason of making the random number constant is to avoid having different random numbers since some rays have different number of reflection which means they call the random number subroutine different times which supposed that the next ray will have a different random number, which makes it impossible to compare the two codes since the rejected rays are different.

There are some rays that have different number of reflections due to the difference in the intersection point and in the normal vector which makes a change in the number of reflections in same rays, due to the impossibility of using an exact number for all the calculations, which will supposed in calling the random subroutine a different numbers of times and in that case the absorbed rays will be different.

For the comparison it is mandatory to build the shape in SOLIDWORKS(Figure 2-10), with the equation used by Berchtold [19], presented below:

$$(r\cos(\theta_{max}) + z\sin(\theta_{max}))^2 + 2\,r_{out}((1+\sin(\theta_{max}))^2\,r - 2\,r_{out}\cos(\theta_{max})(2+\sin(\theta_{max}))\,z - r_{out}(1+\sin(\theta_{max}))\,(3+\sin(\theta_{max})) = 0 \quad \text{Equation 2-7}$$

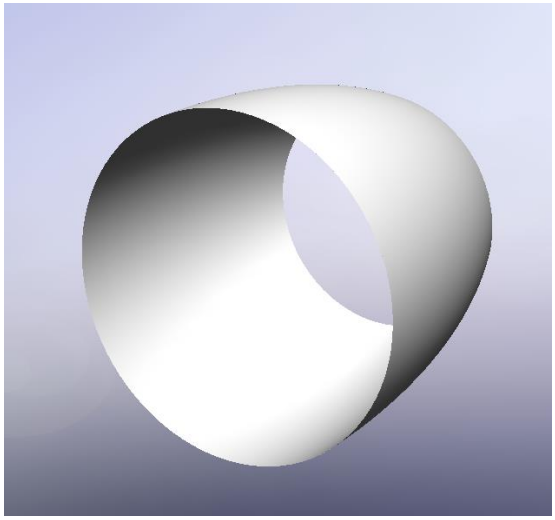

Figure 2-10 Berchtold's shape

The principal problem in ANSYS is to generate a fine mesh in order to minimize the error for the assumption of perfect planes. In the figure below the mesh used in the calculations is shown. It contains 13230 surface elements.

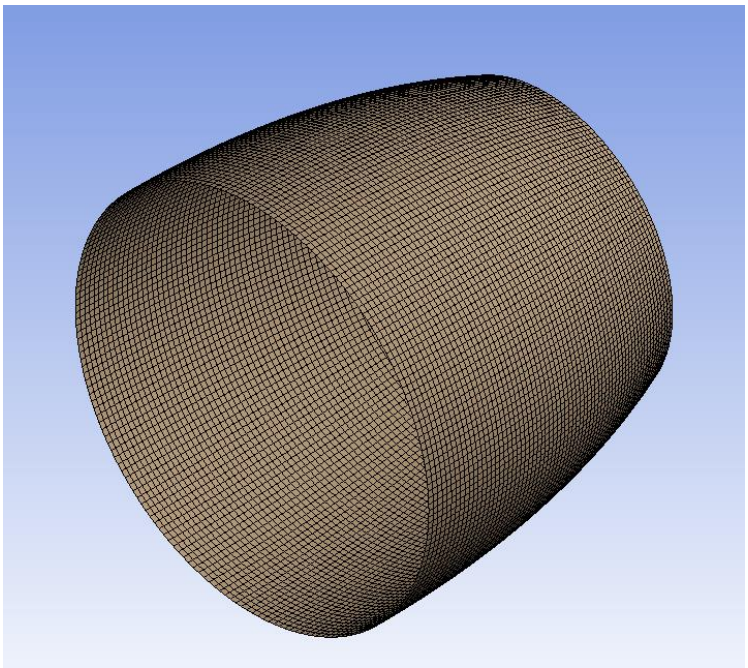

Figure 2-11 Berchtold's shape with mesh

The comparison between the incident power on the window for both code, Figure 2-12, shows that the power in the window is nearly the same, the difference is around 2kW (0.0003%) less with the new code. Secondly it shows that the distribution of the hitting rays is quite similar, so we can assume that the results from the new code are good enough to assume them as corrects.

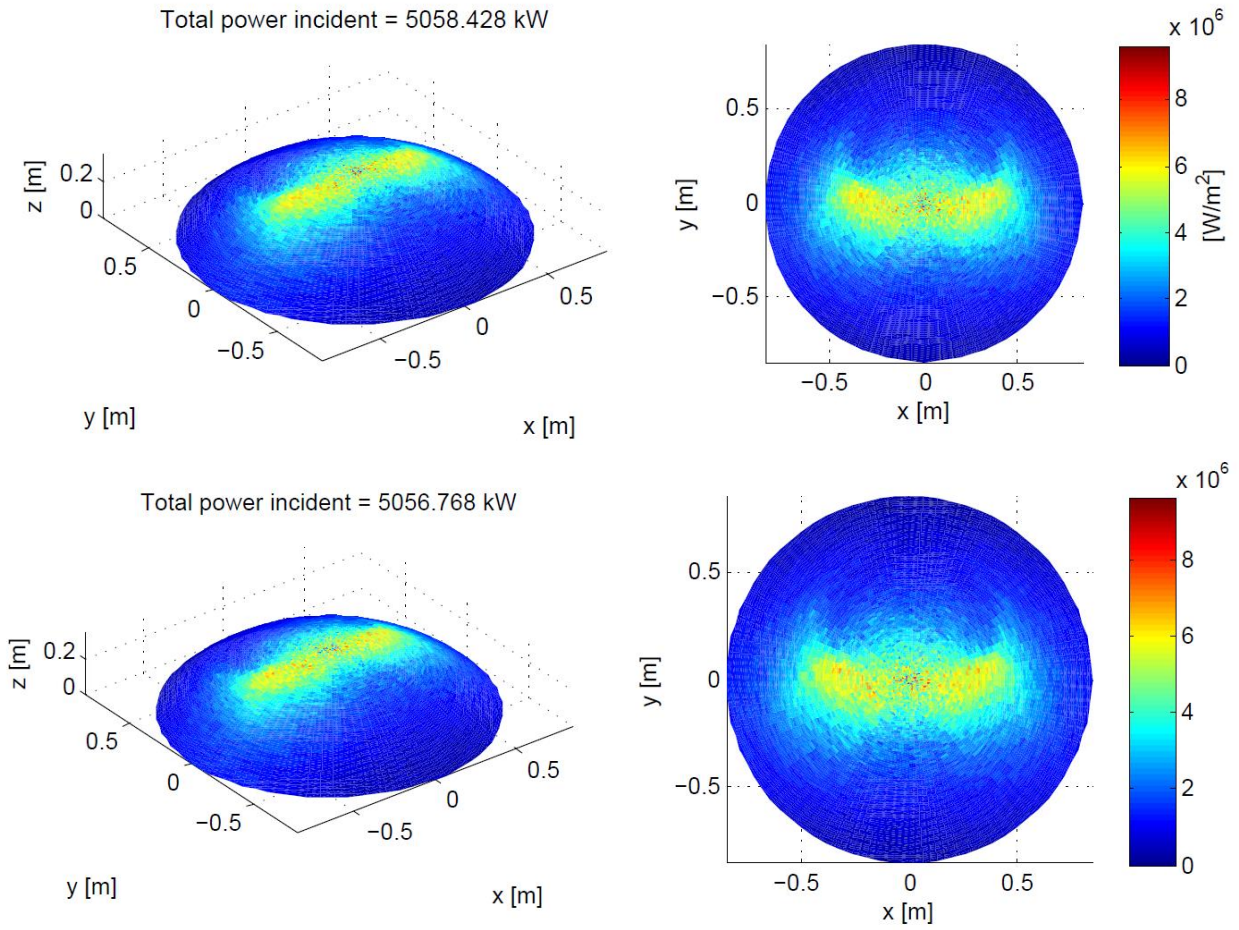

Figure 2-12 Berchtold's code vs New code for the 03-21 from 11-12

The principal problem of the new code is the running time since it is slower than the previous code, due to the necessity to test all the planes for all the rays.

	Berchtold's code	New code
Time (s)	11.8249	589.824

Table 2-7 Time comparison between Berchtold's code and the new Code for 3 million of trials.

As can be seen in the Table 2-7 the increase in the running time is around 58 times, but although the running time is quite big, it does not make an incredible change since it will be running less than 10 minutes.

Comparison of the different codes

	Berchtold's code	**New code**
PERCENTAGE OF ACCEPTED RAYS	96.36	96.33
POWER OF ACCEPTED RAYS	5058427.80 W	5056767.92 W
PERCENTAGE OF RAYS OUTSIDE ACCEPTANCE ANGLE	3.51	3.51
POWER OF RAYS OUTSIDE ACCEPTANCE ANGLE	184412.07 W	184412.073 W
PERCENTAGE OF RAYS MISSING CPC APERTURE	0	0
POWER OF RAYS MISSING CPC APERTURE	0	0
PERCENTAGE OF RAYS ACCEPTED WITHOUR REFLECTION	42.37	42.37
POWER OF RAYS ACCEPTED WITHOUR REFLECTION	2224338.77 W	2224338.77 W
PERCENTAGE OF RAYS ABSORBED IN REFLECTION	0	0
POWER OF RAYS ABSORBED IN REFLECTION	0	0
PERCENTAGE OF RAYS REJECTED AFTER REFLECTION	0.13	0.16
POWER OF RAYS REJECTED AFTER REFLECTION	6758.39 W	8418.27 W

Table 2-8 Comparison between the codes for all the possibilities for the rays

As it is seen the difference between the codes is related with the rays rejected after reflection, most probably due to the assumptions make with the planes, but this is insignificant due the different is less than a 0.05%.

3 Results

3.1 Influence of the different variables

The aim of this chapter is to understand the influence of the different variables in the window pattern. For that it is tested the shapes with different errors in the heliostat field and with different dimensions for the MIRVAL ray file.

The purpose is to find the accuracy for the different variable and the efficiency of the new shapes.

- Firstly Berchtold's shape is going to be tested to be compared with the new shapes.
- Secondly the hexagonal inlet-outlet is tested.
- Thirdly a mixed shape between this two is tested.

3.1.1 Berchtold shape

The difference between this test and the verification test is the absorptivity, random number and the error in the shape. The main reason of repeating this shape is to be able to compare it with the new shapes.

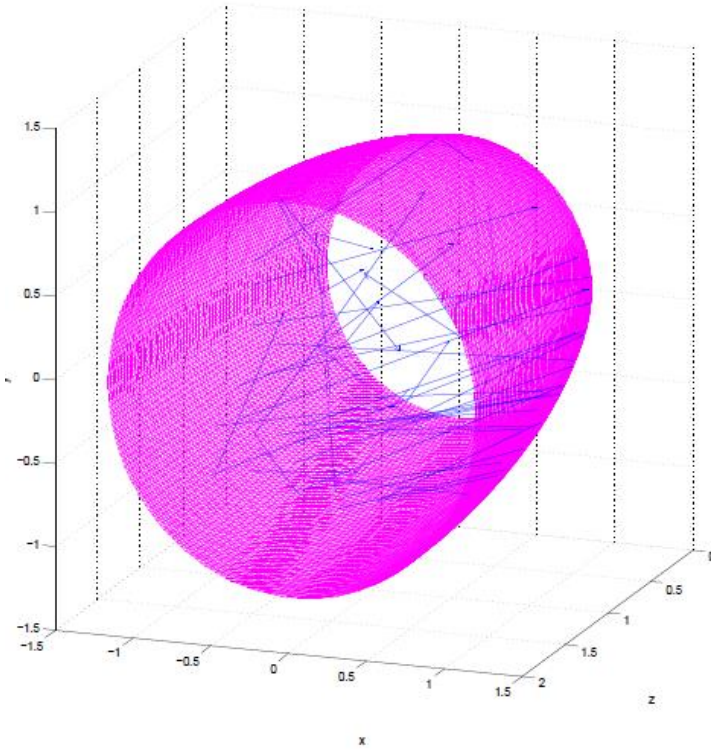

Figure 3-1 Ray tracing for Berchtold's shape, isometric view

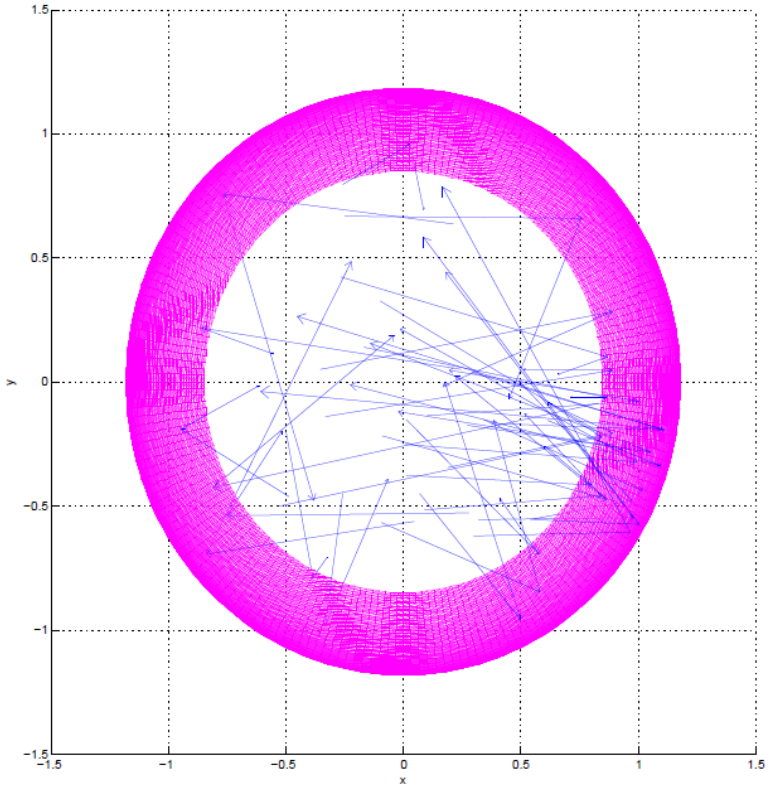

Figure 3-2 Ray tracing for Berchtold's shape, plane x-y

3.1.1.1 Test with error of 1.2mrad in the heliostat field and with 3.4 m of outlet file

Test for 3/21 at 07:00/08:00 hours:

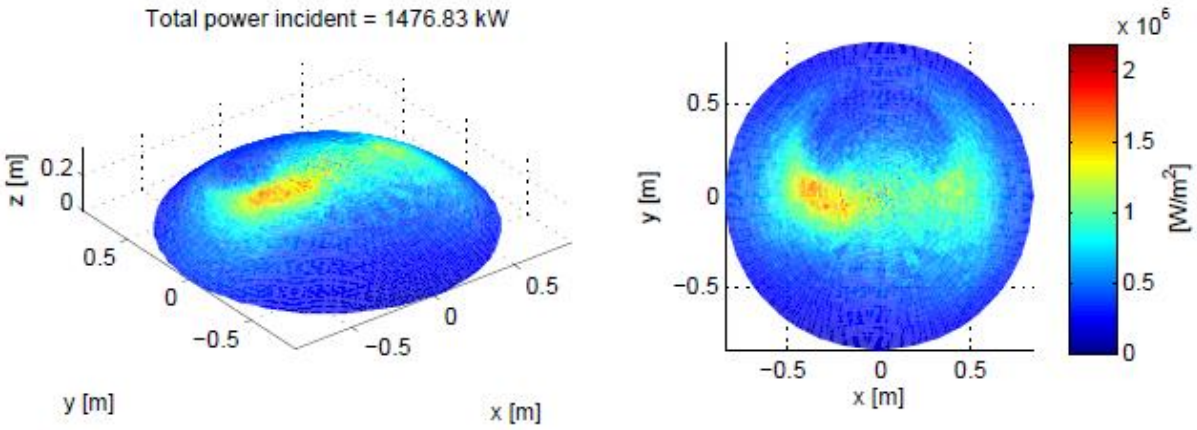

Figure 3-3 Test with error of 1.2mrad in the heliostat field and with 3.4 m of outlet file for 3/21 at 07:00/08:00 hours

Test for 3/21 at 11:00/12:00 hours:

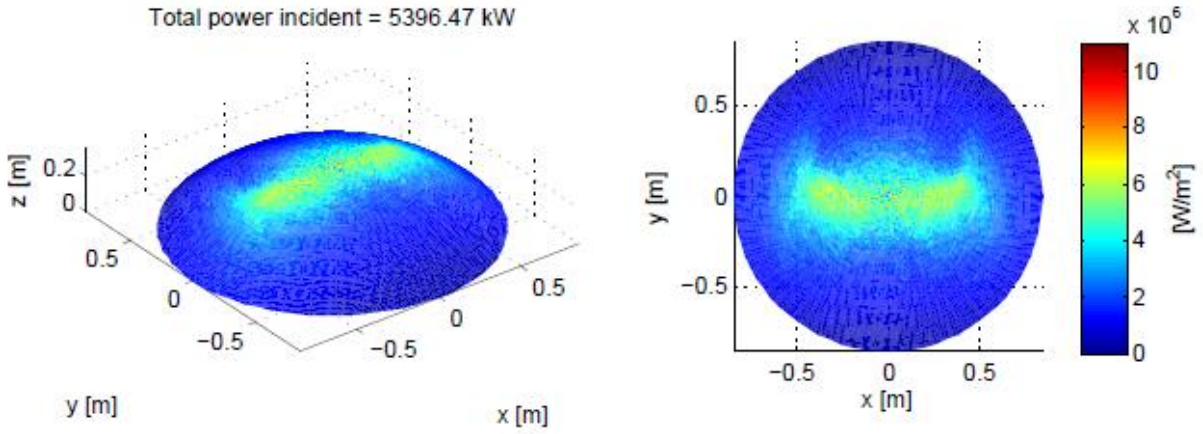

Figure 3-4 Test with error of 1.2mrad in the heliostat field and with 3.4 m of outlet file for 3/21 at 11:00/12:00 hours

Test for 3/21 at 15:00/16:00 hours:

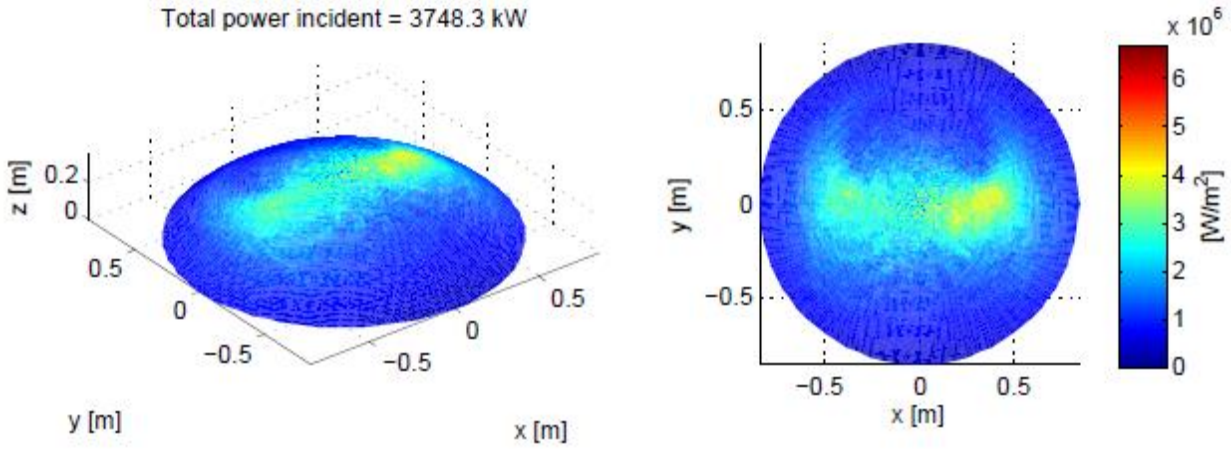

Figure 3-5 Test with error of 1.2mrad in the heliostat field and with 3.4 m of outlet file for 3/21 at 15:00/16:00 hours

3.1.1.2 Test without error in the heliostat field and with 3.4 m of outlet file

Test for 3/21 at 07:00/08:00 hours:

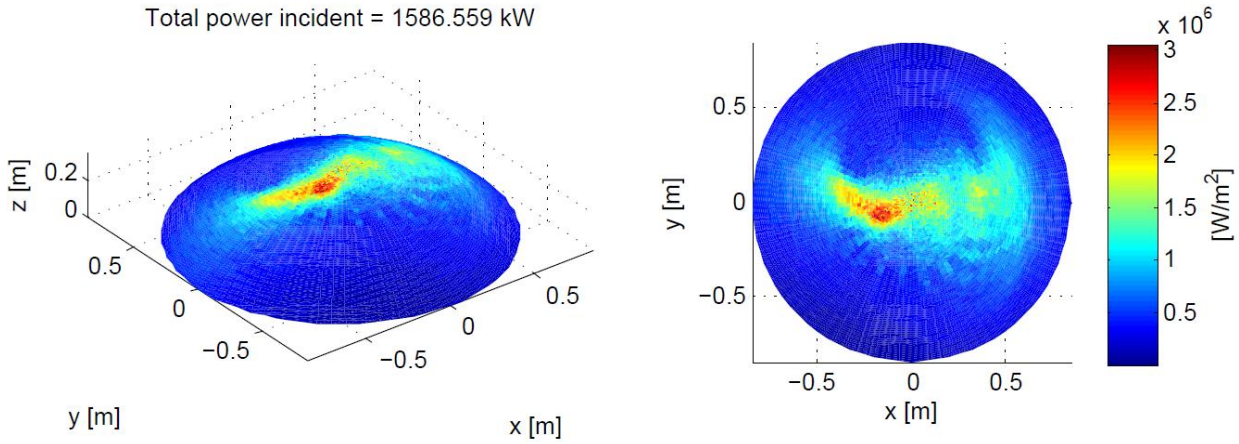

Figure 3-6 Test without error in the heliostat field and with 3.4 m of outlet file for 3/21 at 07:00/08:00 hours, different scale as the test with error of 1.2mrad in the heliostat field and with 3.4 m of outlet file for 3/21 at 07:00/08:00 hours

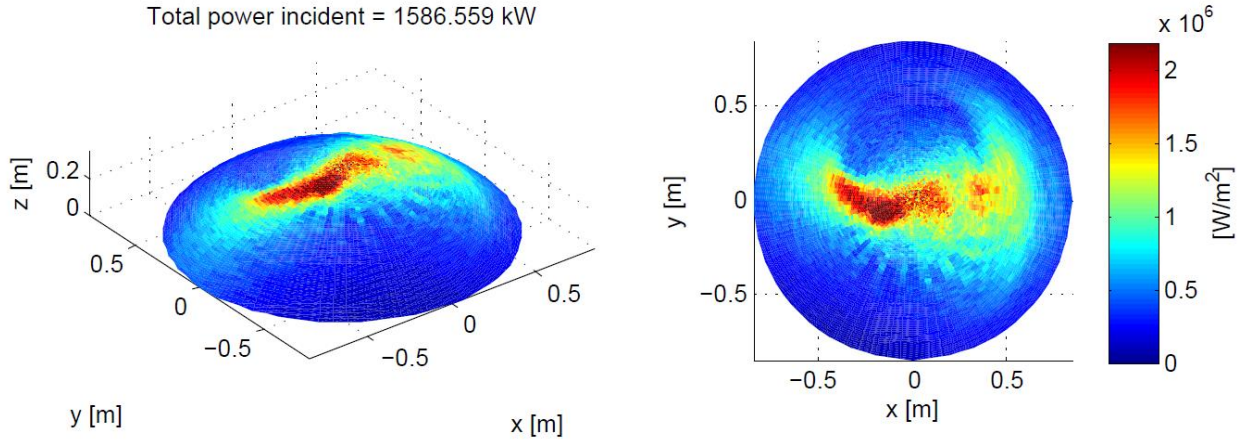

Figure 3-7 Test without error in the heliostat field and with 3.4 m of outlet file for 3/21 at 07:00/08:00 hours, same scale as the test with error of 1.2mrad in the heliostat field and with 3.4 m of outlet file for 3/21 at 07:00/08:00 hours

Test for 3/21 at 11:00/12:00 hours:

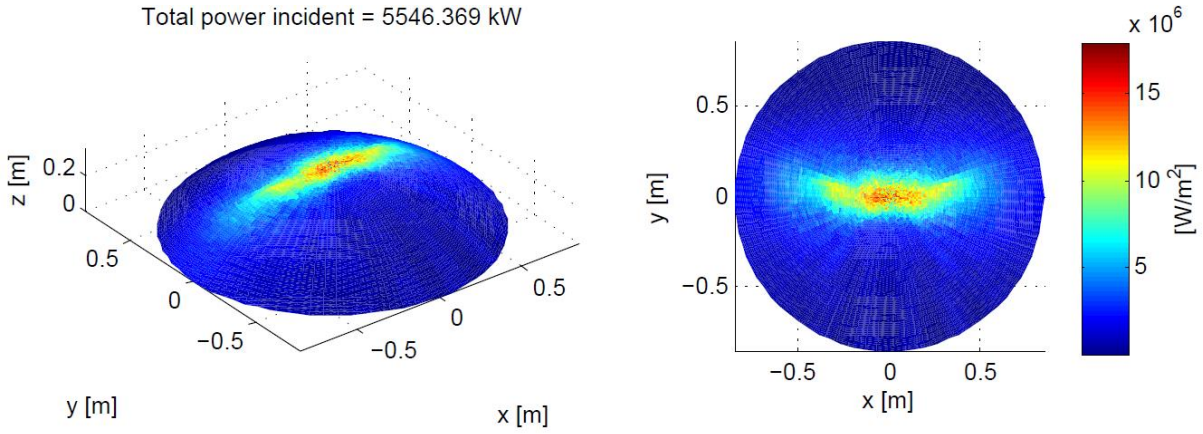

Figure 3-8 Test without error in the heliostat field and with 3.4 m of outlet file for 3/21 at 11:00/12:00 hours, different scale as the test with error of 1.2mrad in the heliostat field and with 3.4 m of outlet file for 3/21 at 11:00/12:00 hours

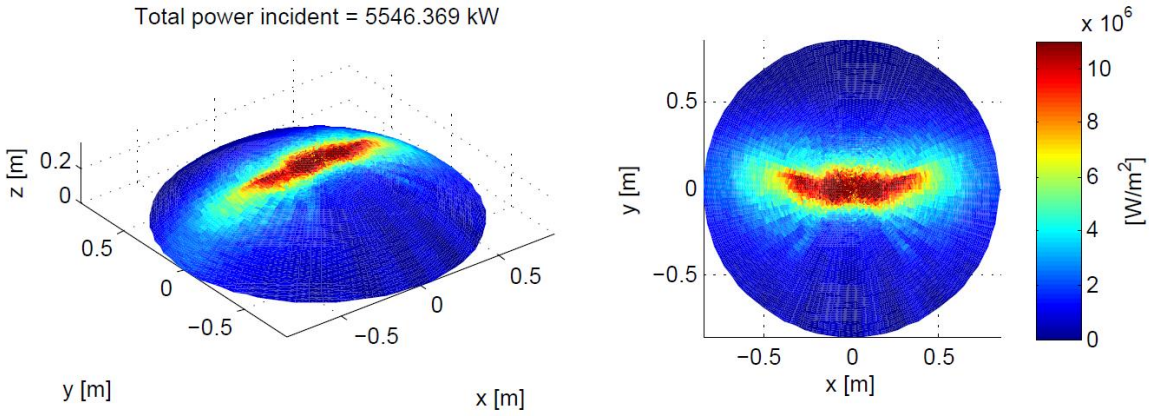

Figure 3-9 Test for 3/21 at 11:00/12:00 hours with same scale without error in the heliostat field and with 3.4 m of outlet file, same scale as the test with error of 1.2mrad in the heliostat field and with 3.4 m of outlet file for 3/21 at 11:00/12:00 hours

Test for 3/21 at 15:00/16:00 hours:

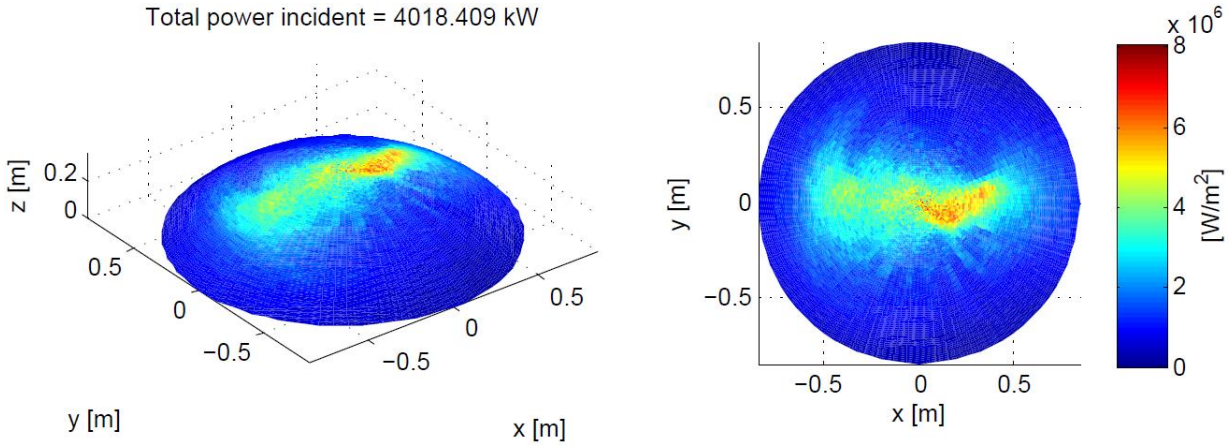

Figure 3-10 Test without error in the heliostat field and with 3.4 m of outlet file for 3/21 at 15:00/16:00 hours, different scale as the test with error of 1.2mrad in the heliostat field and with 3.4 m of outlet file for 3/21 at 15:00/16:00 hours

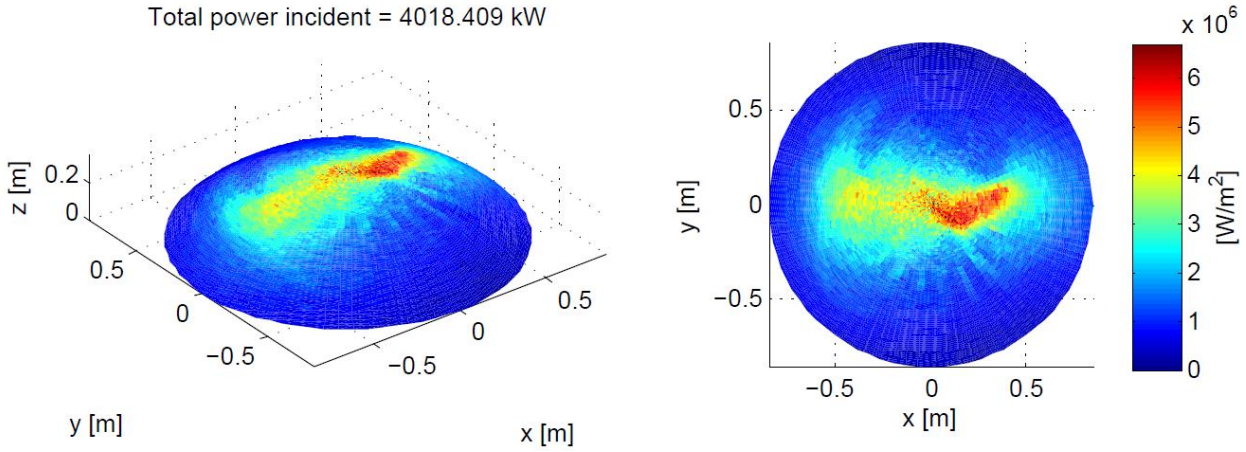

Figure 3-11 Test for 3/21 at 15:00/16:00 hours with same scale, without error in the heliostat field and with 3.4 m of outlet file , same scale as the test with error of 1.2mrad in the heliostat field and with 3.4 m of outlet file for 3/21 at 15:00/16:00 hours

The purpose of using the same scale is to demonstrate that the pattern is not modify for the error in the heliostat field, the difference is the power in the middle of the window that is increased without error.

3.1.1.3 Test without error in the heliostat field and with 1.7 m of outlet file

Test for 3/21 at 07:00/08:00 hours:

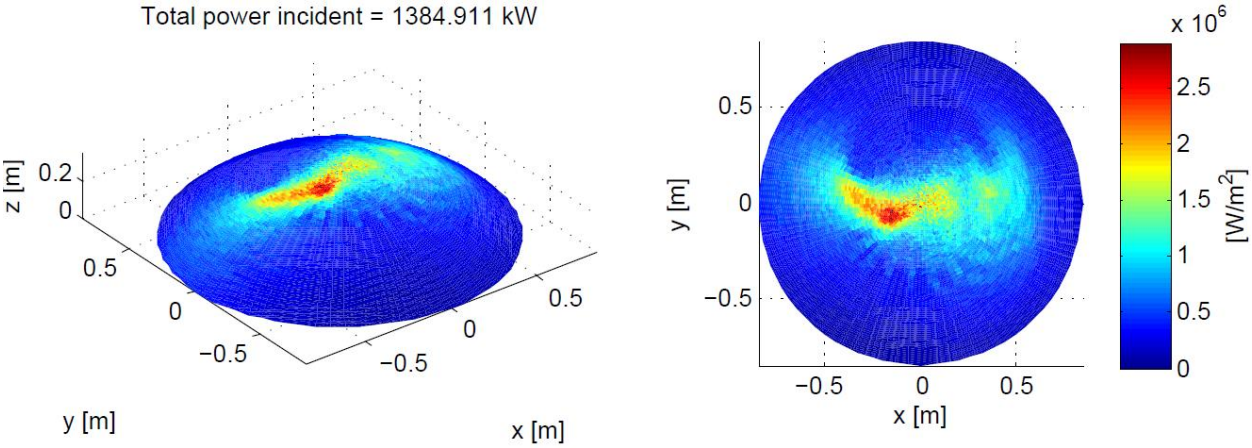

Figure 3-12 Test without error in the heliostat field and with 1.7 m of outlet file for 3/21 at 07:00/08:00 hours

Test for 3/21 at 11:00/12:00 hours:

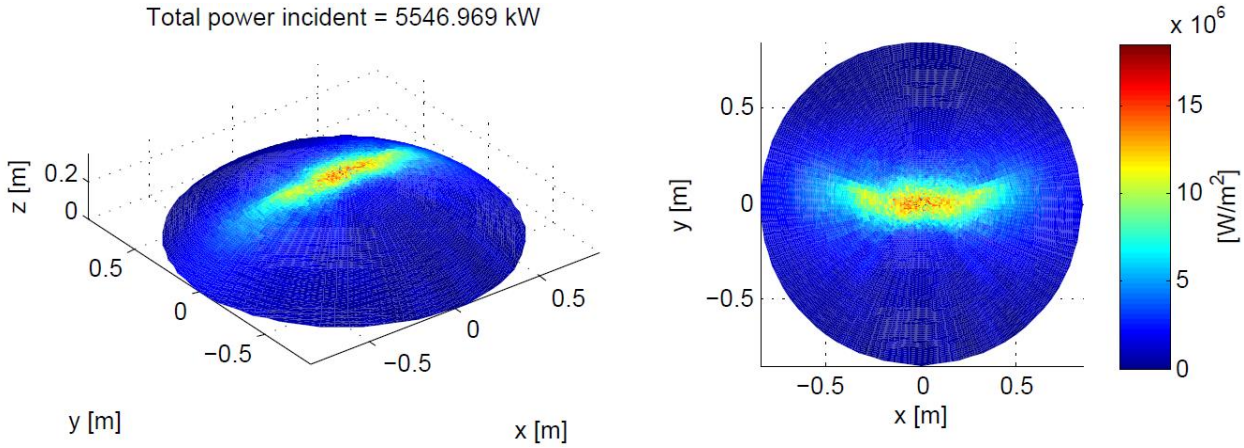

Figure 3-13 Test without error in the heliostat field and with 1.7 m of outlet file for 3/21 at 11:00/12:00 hours

Test for 3/21 at 15:00/16:00 hours:

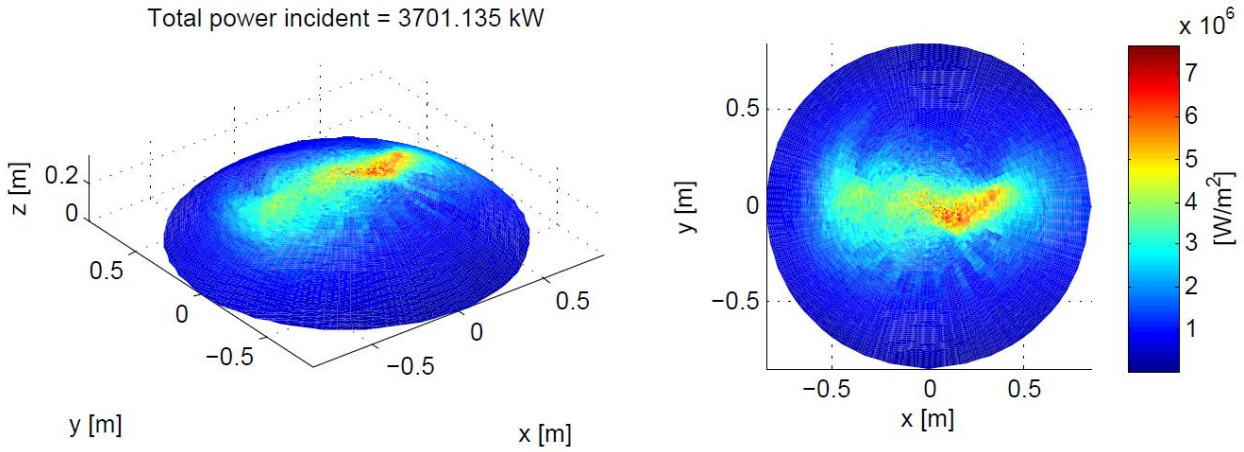

Figure 3-14 Test without error in the heliostat field and with 1.7 m of outlet file for 3/21 at 15:00/16:00 hours

3.1.1.4 Test with error of 1.2mrad in the heliostat field and with 1.7 m of outlet file

Test for 3/21 at 07:00/08:00 hours:

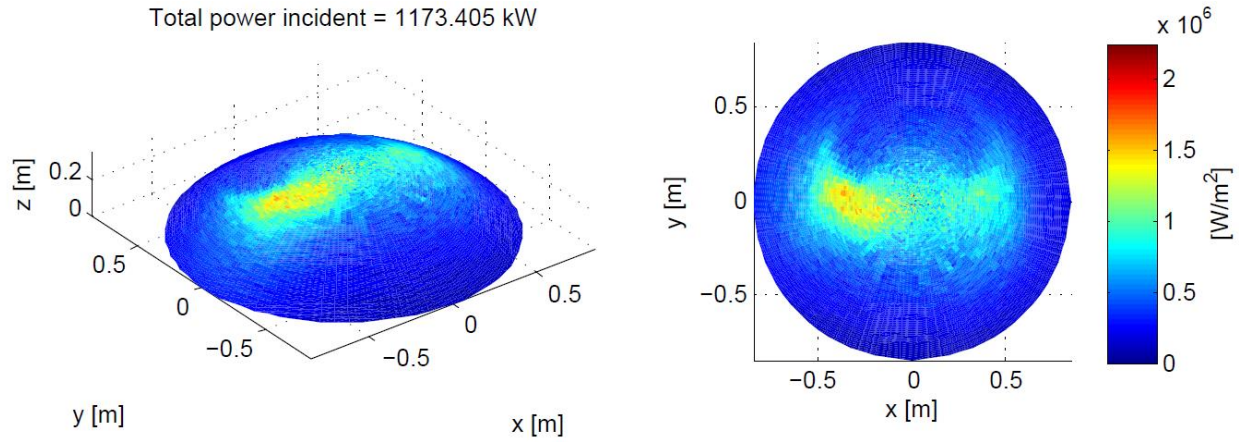

Figure 3-15 Test with error of 1.2mrad in the heliostat field and with 1.7 m of outlet file for 3/21 at 07:00/08:00 hours

Test for 3/21 at 11:00/12:00 hours:

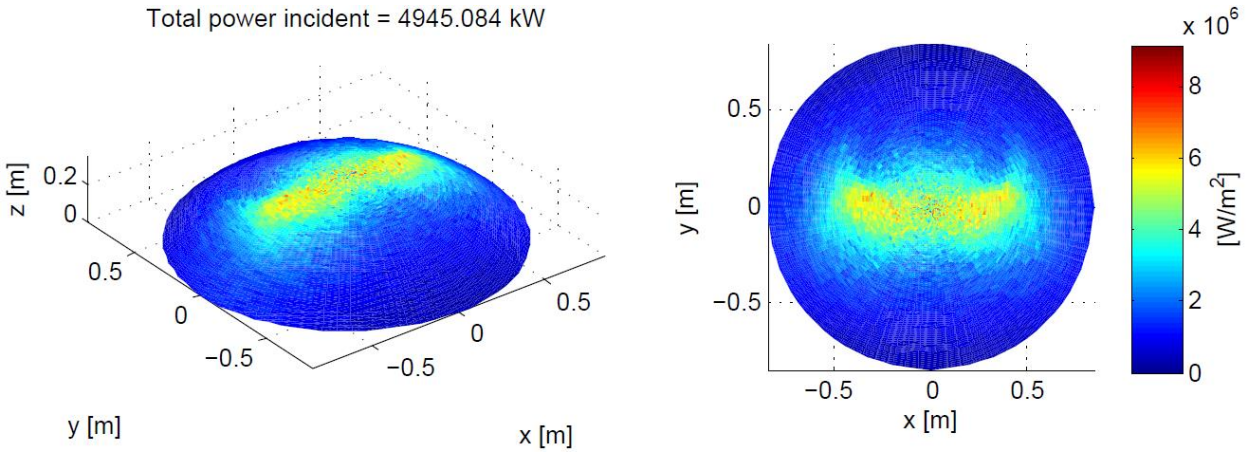

Figure 3-16 Test with error of 1.2mrad in the heliostat field and with 1.7 m of outlet file for 3/21 at 11:00/12:00 hours

Test for 3/21 at 15:00/16:00 hours:

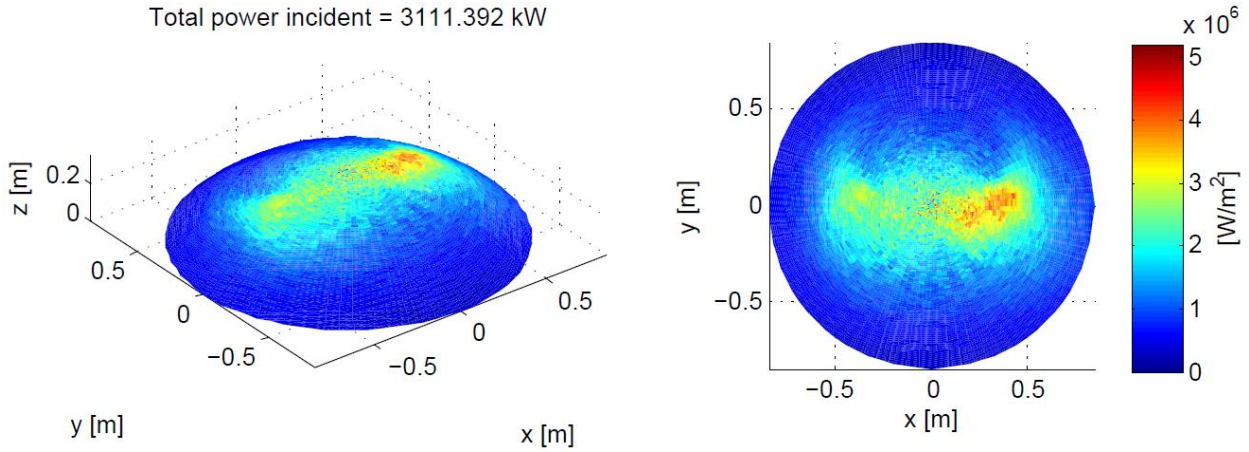

Figure 3-17 Test with error of 1.2mrad in the heliostat field and with 1.7 m of outlet file for 3/21 at 15:00/16:00 hours

3.1.1.5 Comparison

Variables	Day	Hour	Total Power Absorbed
Test with error of 1.2mrad in the heliostat field and with 3.4 m of outlet file	3-21	07:00/08:00	1476.83
	3-21	11:00/12:00	5396.47
	3-21	15:00/16:00	3748.3
Test without error in the heliostat field and with 3.4 m of outlet file	3-21	07:00/08:00	1586.56
	3-21	11:00/12:00	5546.37
	3-21	15:00/16:00	4018.41
Test without error in the heliostat field and with 1.7 m of outlet file	3-21	07:00/08:00	1384.91
	3-21	11:00/12:00	5546.97
	3-21	15:00/16:00	3701.14
Test with error of 1.2mrad in the heliostat field and with 1.7 m of outlet file	3-21	07:00/08:00	1173.40
	3-21	11:00/12:00	4945.08
	3-21	15:00/16:00	3111.39

Table 3-1 Comparison of the hitting power for different Mirval variables for Berchtold shape

3.1.2 Secondly the hexagonal inlet-outlet is tested

This shape is constructed generating inscribed hexagon in Berchtold´s shape. The main advantage of it is the facility of construction, since is made with planes, which leads to a really cheap concentrator. But the problem is that it does not use the entire window, since the exit is a hexagon too. For this shape is was used 10551 surface elements.

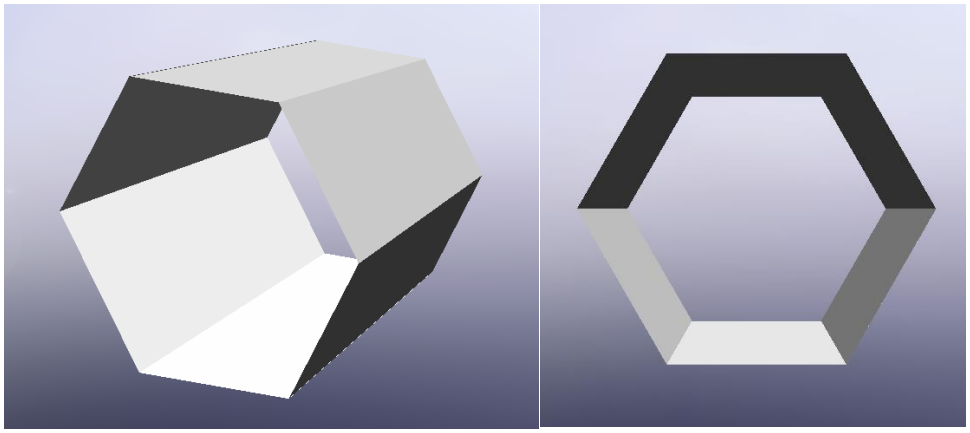

Figure 3-18 Hexagonal inlet with Berchtold's equation

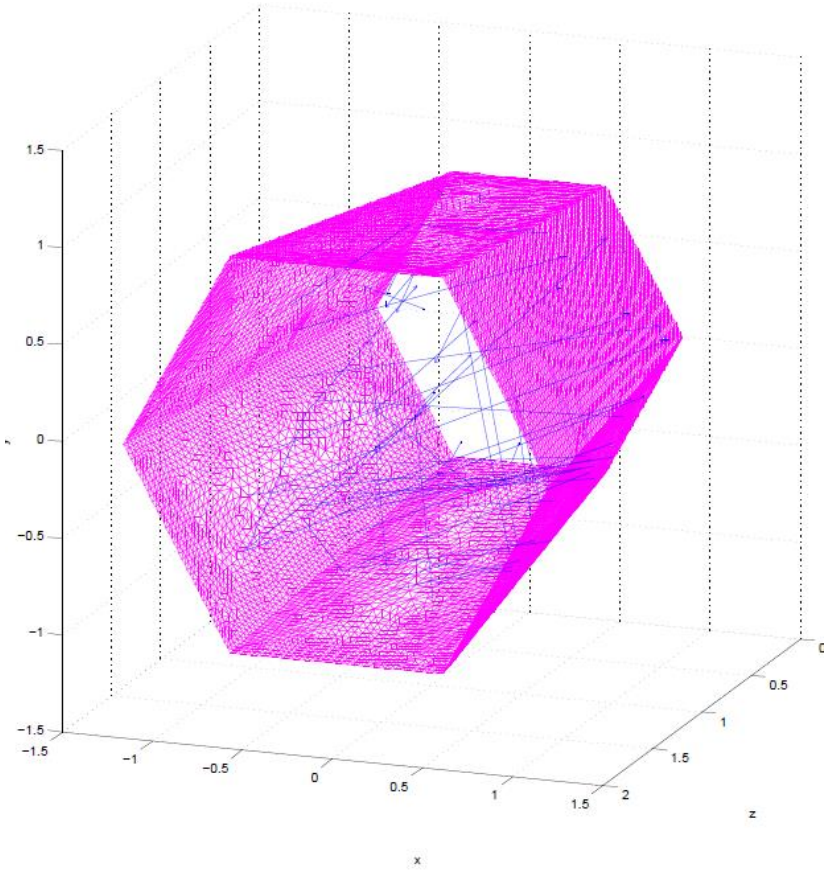

Figure 3-19 Ray tracing for hexagonal inlet and outlet, isometric view

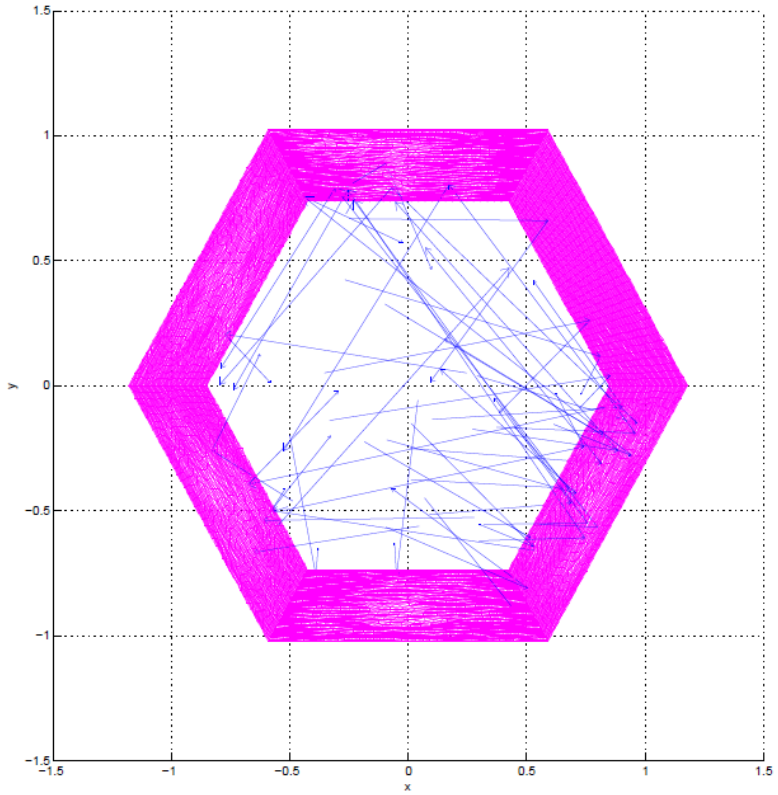

Figure 3-20 Ray tracing for hexagonal inlet and outlet, plane x-y

3.1.2.1 Test with error of 1.2mrad in the heliostat field and with 3.4 m of outlet file

Test for 3/21 at 07:00/08:00 hours:

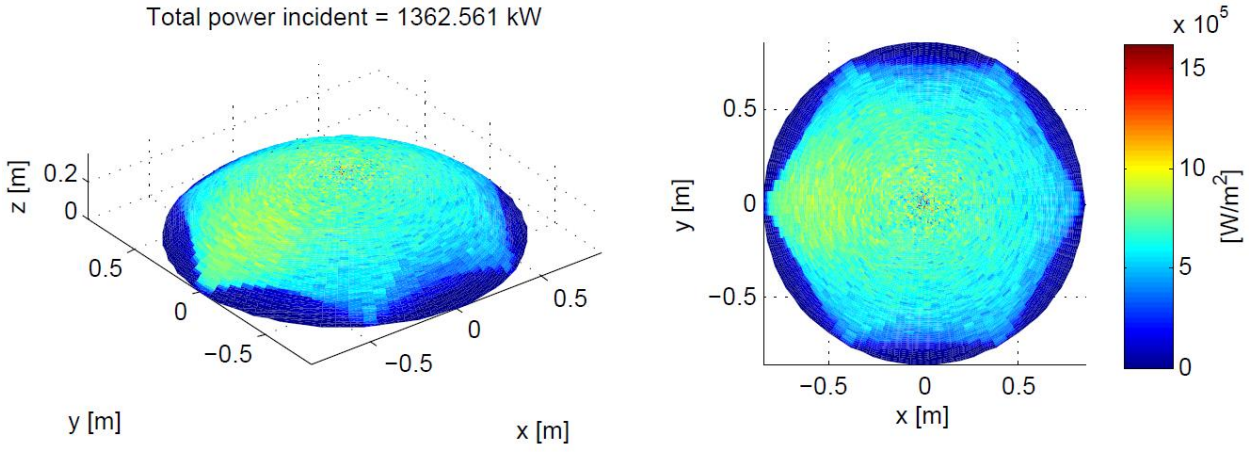

Figure 3-21 Test with error of 1.2mrad in the heliostat field and with 3.4 m of outlet file for 3/21 at 07:00/08:00 hours

Test for 3/21 at 11:00/12:00 hours:

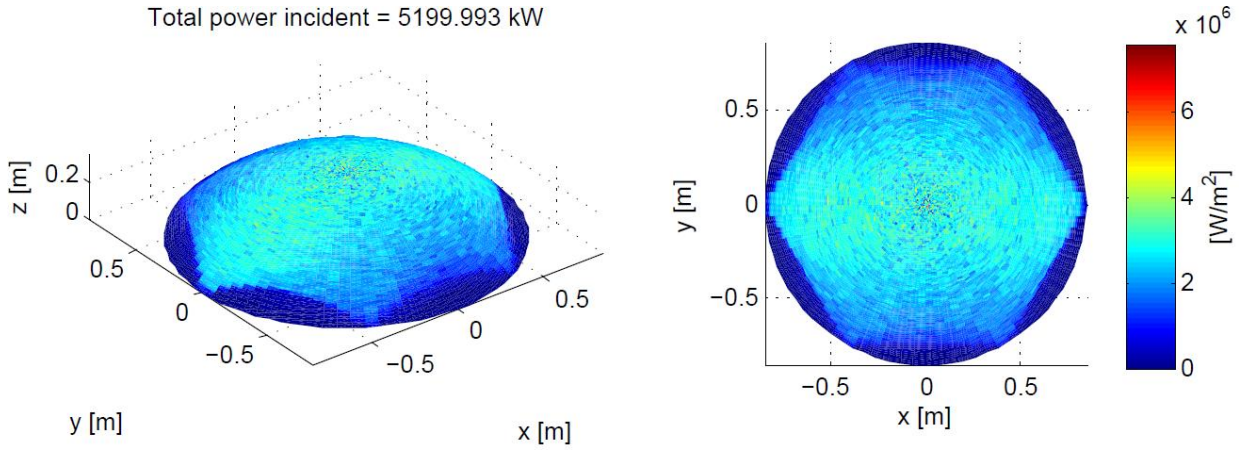

Figure 3-22 Test with error of 1.2mrad in the heliostat field and with 3.4 m of outlet file for 3/21 at 11:00/12:00 hours

Test for 3/21 at 15:00/16:00 hours:

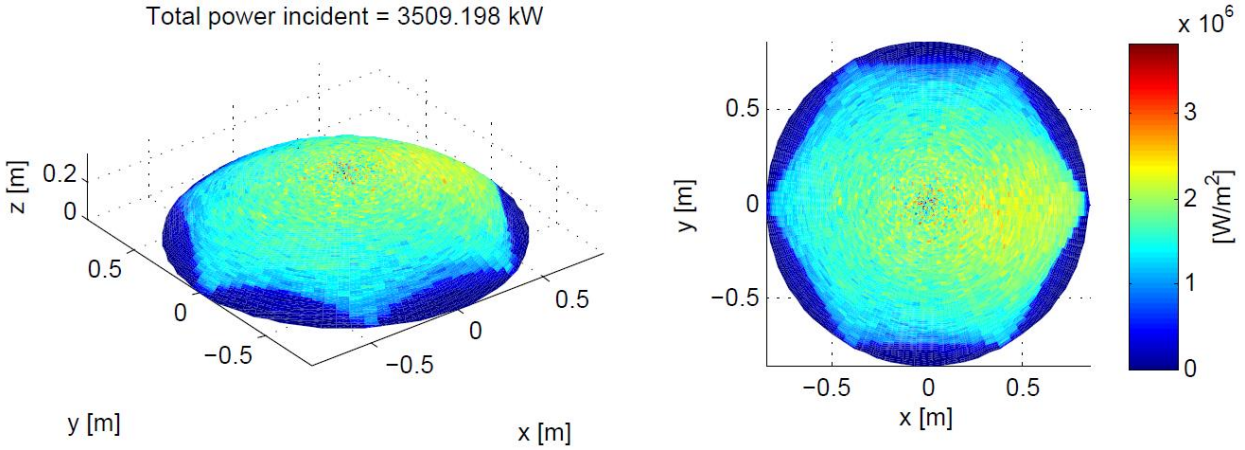

Figure 3-23 Test with error of 1.2mrad in the heliostat field and with 3.4 m of outlet file for 3/21 at 15:00/16:00 hours

3.1.2.2 Test without error in the heliostat field and with 3.4 m of outlet file

Test for 3/21 at 07:00/08:00 hours:

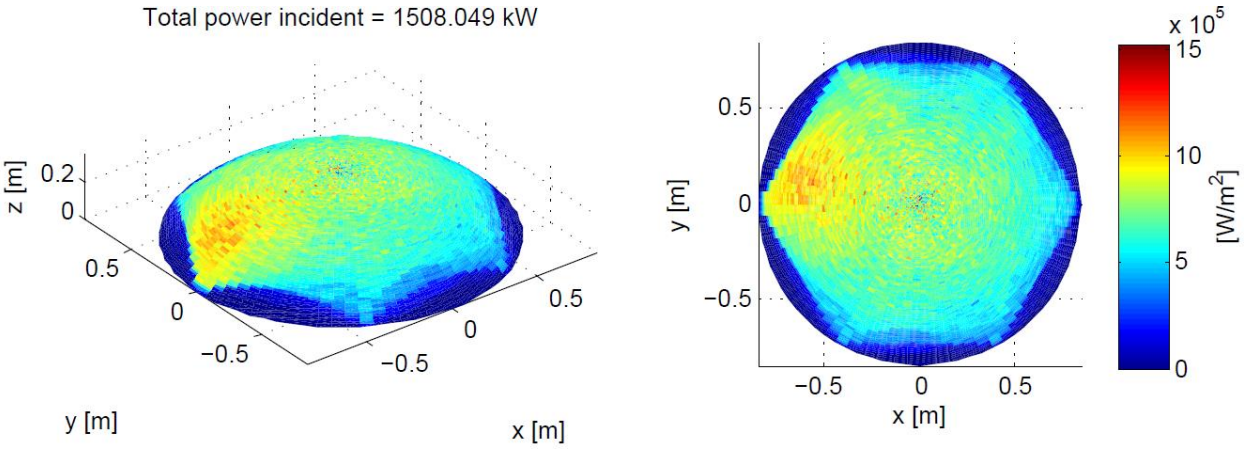

Figure 3-24 Test without error in the heliostat field and with 3.4 m of outlet file for 3/21 at 07:00/08:00 hours

Test for 3/21 at 11:00/12:00 hours:

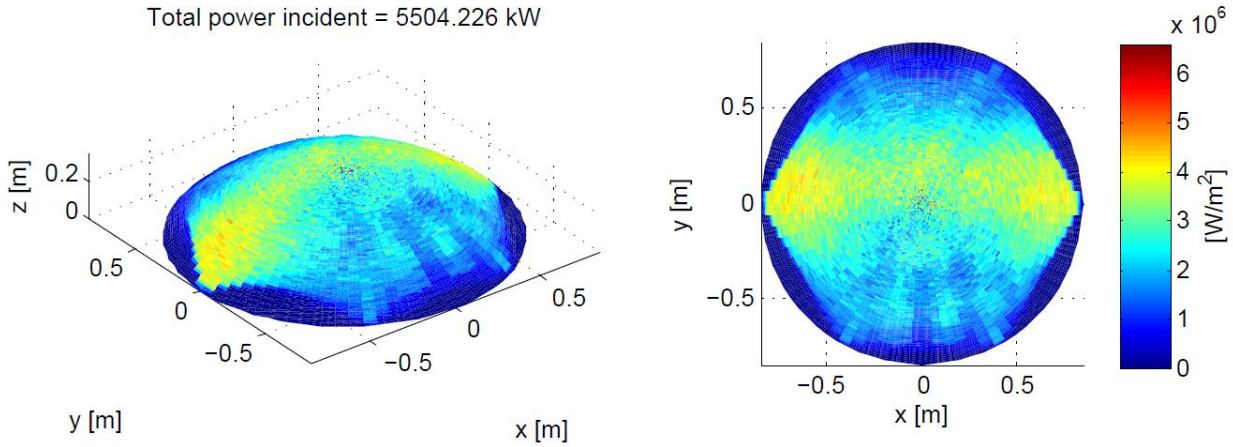

Figure 3-25 Test without error in the heliostat field and with 3.4 m of outlet file for 3/21 at 11:00/12:00 hours

Test for 3/21 at 15:00/16:00 hours:

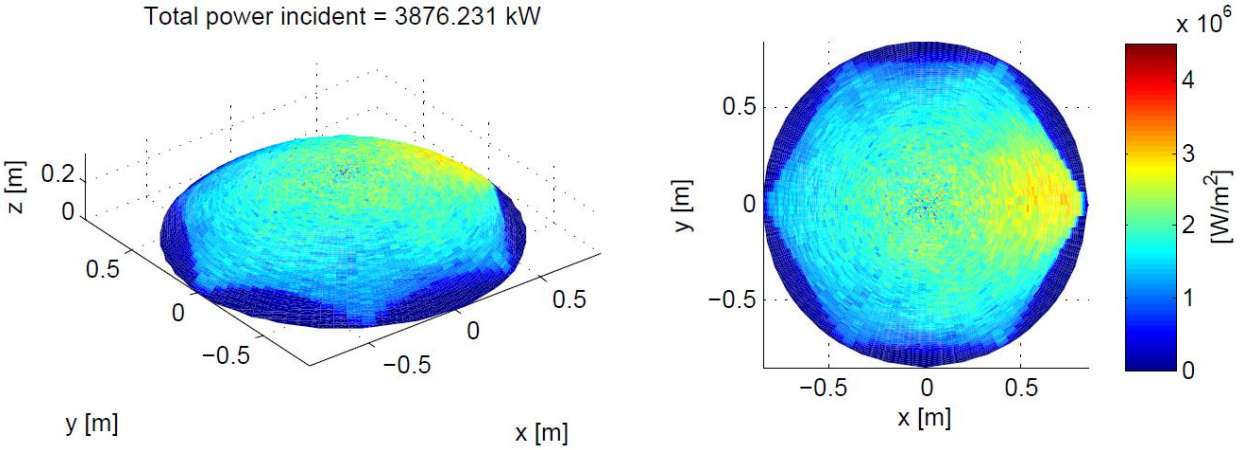

Figure 3-26 Test without error in the heliostat field and with 3.4 m of outlet file for 3/21 at 15:00/16:00 hours

3.1.2.3 Test without error in the heliostat field and with 1.7 m of outlet file

Test for 3/21 at 07:00/08:00 hours:

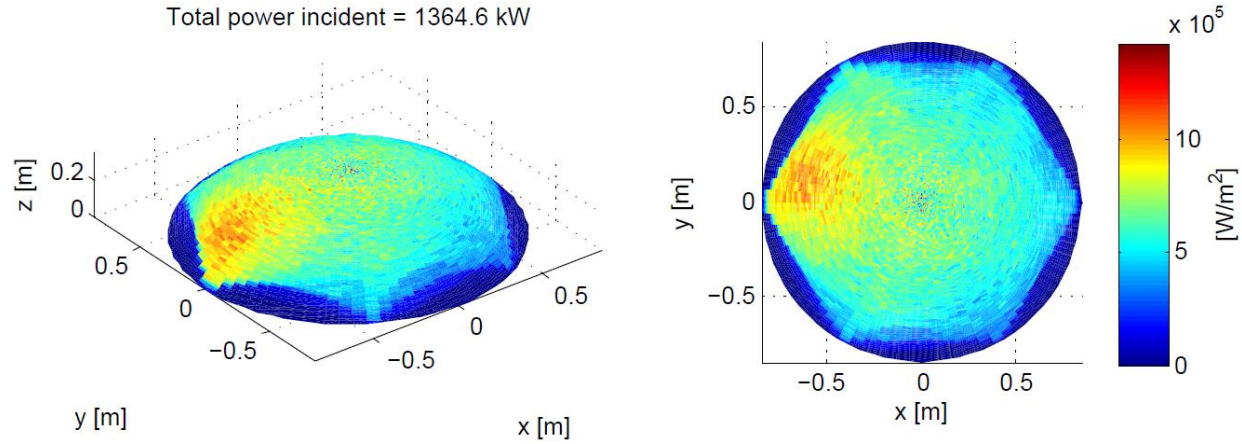

Figure 3-27 Test without error in the heliostat field and with 1.7 m of outlet file for 3/21 at 07:00/08:00 hours

Test for 3/21 at 11:00/12:00 hours:

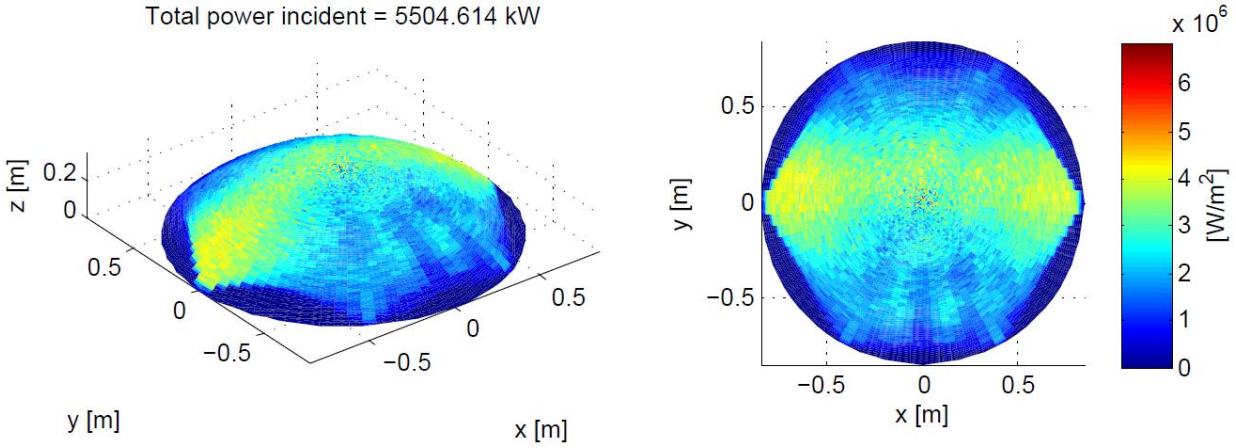

Figure 3-28 Test without error in the heliostat field and with 1.7 m of outlet for 3/21 at 11:00/12:00 hours

Test for 3/21 at 15:00/16:00 hours:

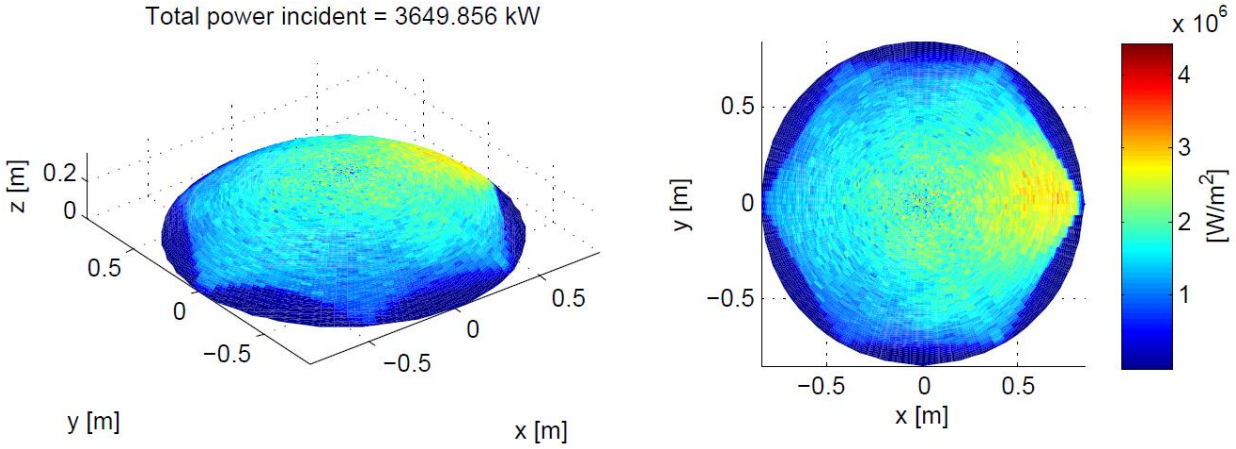

Figure 3-29 Test without error in the heliostat field and with 1.7 m of outlet for 3/21 at 15:00/16:00 hours

3.1.2.4 Test with error of 1.2mrad in the heliostat field and with 1.7 m of outlet file

Test for 3/21 at 07:00/08:00 hours:

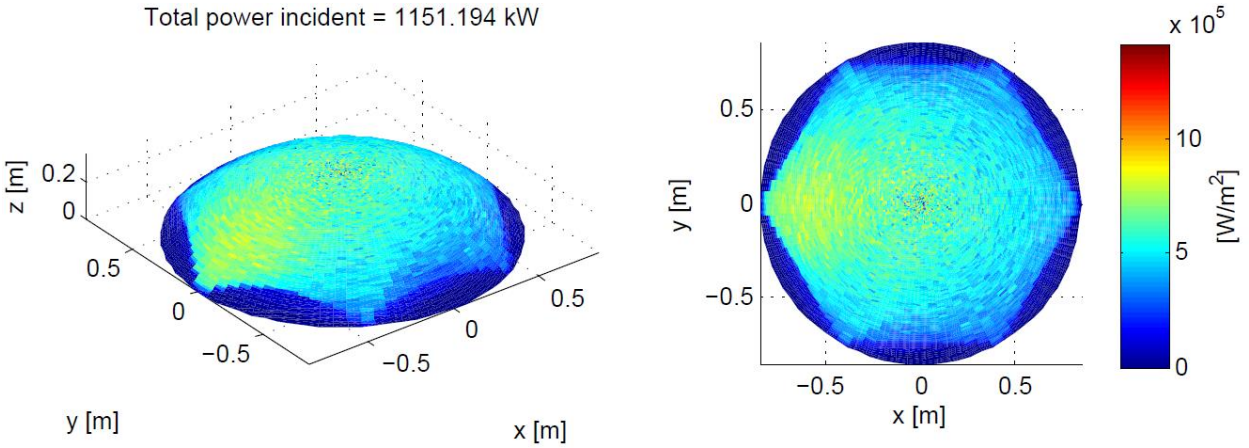

Figure 3-30 Test with error of 1.2mrad in the heliostat field and with 1.7 m of outlet for 3/21 at 07:00/08:00 hours

Test for 3/21 at 11:00/12:00 hours:

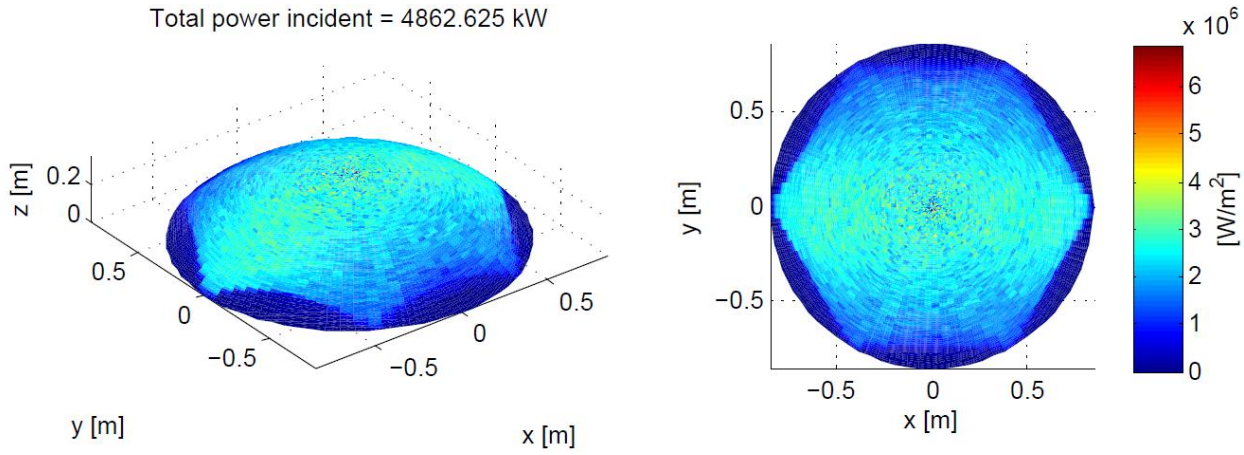

Figure 3-31 Test with error of 1.2mrad in the heliostat field and with 1.7 m of outlet for 3/21 at 11:00/12:00 hours

Test for 3/21 at 15:00/16:00 hours:

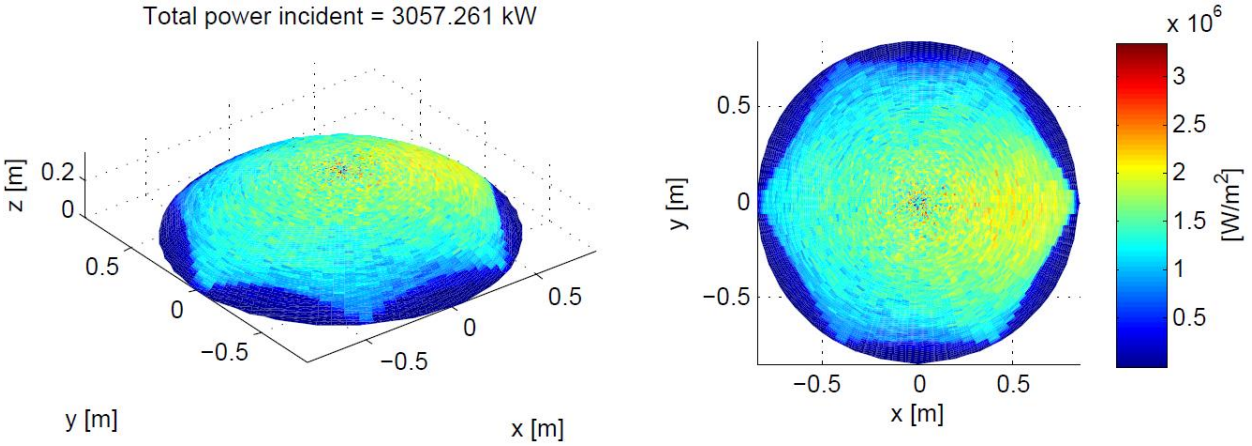

Figure 3-32 Test with error of 1.2mrad in the heliostat field and with 1.7 m of outlet for 3/21 at 15:00/16:00 hours

3.1.2.5 Comparison

Variables	**Day**	**Hour**	**Total Power Absorbed**
Test with error of 1.2mrad in the heliostat field and with 3.4 m of outlet file	3-21	07:00/08:00	1362.56
	3-21	11:00/12:00	5199.99
	3-21	15:00/16:00	3509.20
Test without error in the heliostat field and with 3.4 m of outlet file	3-21	07:00/08:00	1508.05
	3-21	11:00/12:00	5504.23
	3-21	15:00/16:00	3876.23
Test without error in the heliostat field and with 1.7 m of outlet file	3-21	07:00/08:00	1364.6
	3-21	11:00/12:00	5505.61
	3-21	15:00/16:00	3649.86
Test with error of 1.2mrad in the heliostat field and with 1.7 m of outlet file	3-21	07:00/08:00	1151.20
	3-21	11:00/12:00	4862.63
	3-21	15:00/16:00	3057.26

Table 3-2 MIRVAL variables

3.1.3 Berchtold shape with hexagonal entrance

This shape is based in Berchtold's shape with the particularity that the entrance is cut with an inscribed hexagon, as can be seen in the Figure 3-33, the purpose is to continue using the previous shape since it is the most efficiency shape and at the same time it is possible to allocate multiple concentrator. For this shape is was used 25372 surface elements.

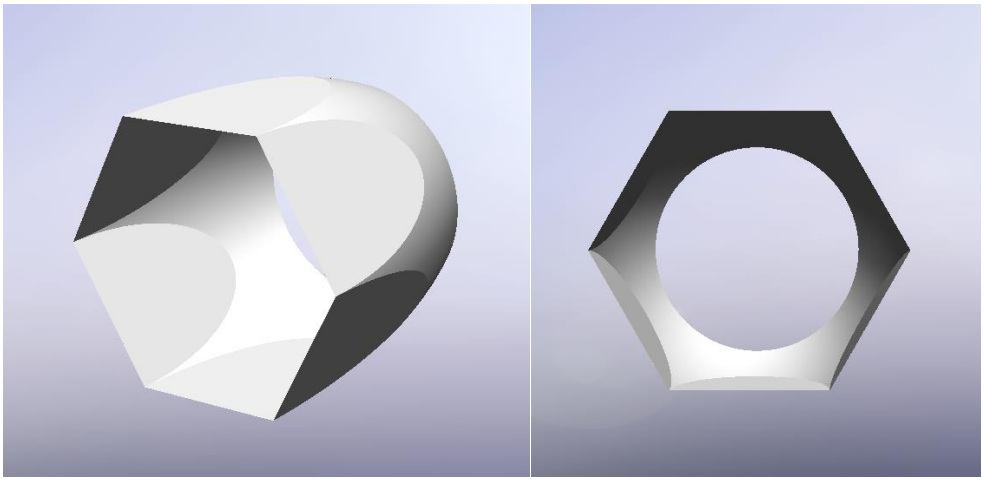

Figure 3-33 Hexagonal inlet with Berchtold's equation

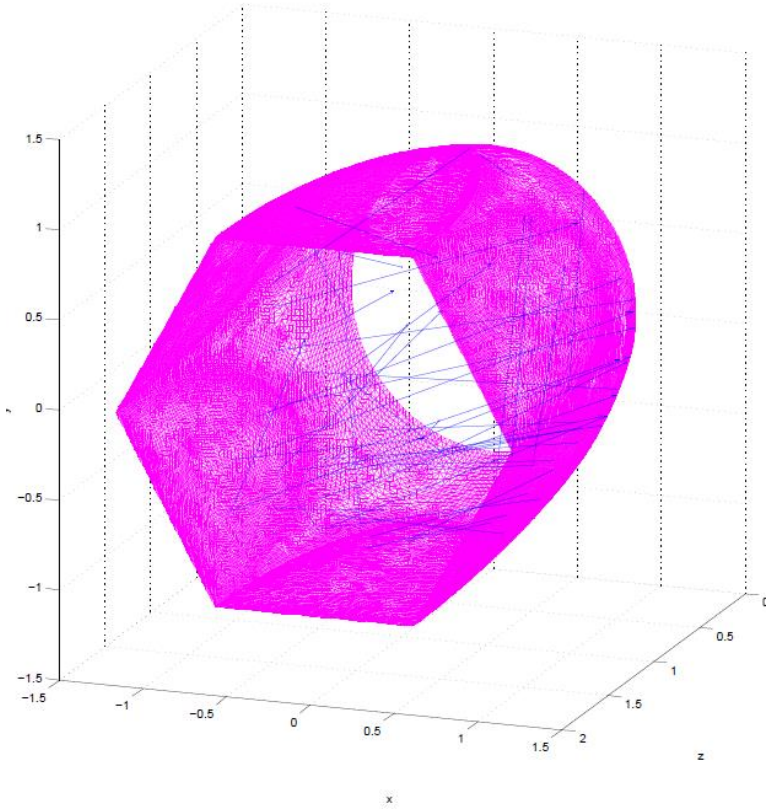

Figure 3-34 Ray tracing for hexagonal inlet with Berchtold's equation, isometric view

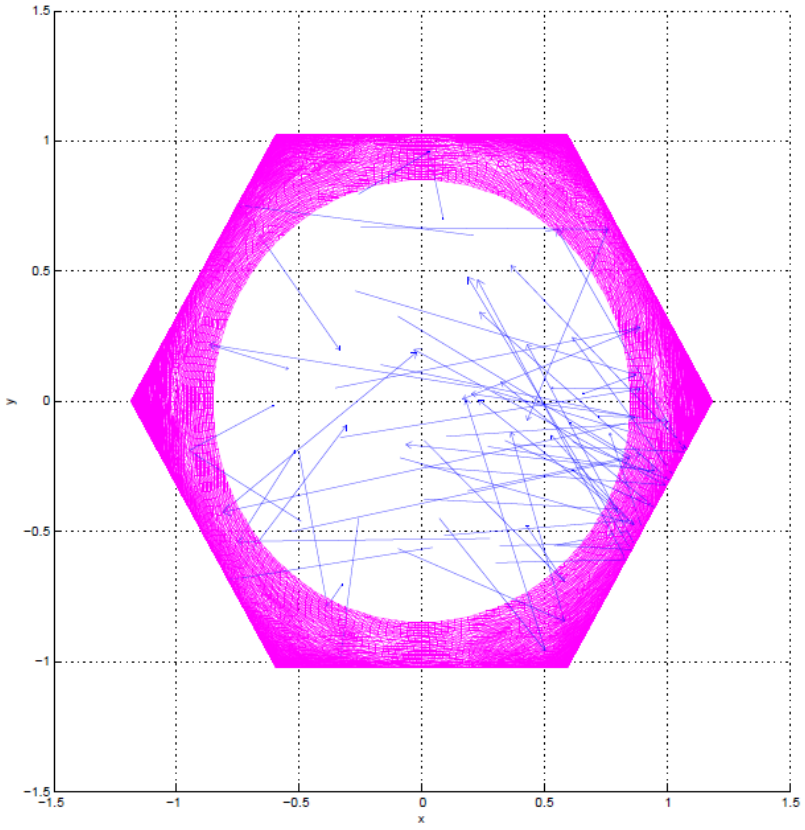

Figure 3-35 Ray tracing for hexagonal inlet with Berchtold's equation, plane x-y

3.1.3.1 Test with error of 1.2mrad in the heliostat field and with 3.4 m of outlet file

Test for 3/21 at 07:00/08:00 hours:

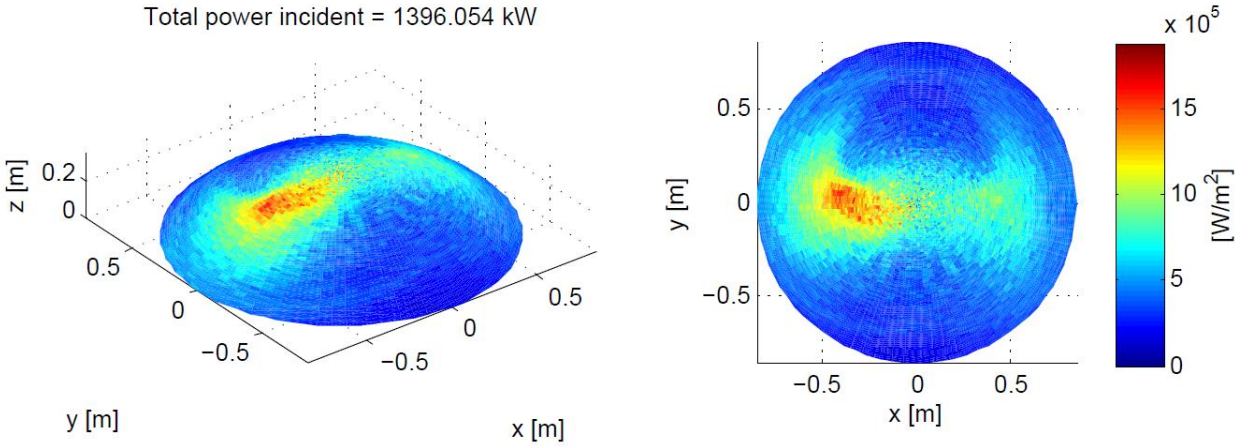

Figure 3-36 Test with error of 1.2mrad in the heliostat field and with 3.4 m of outlet for 3/21 at 07:00/08:00 hours

Test for 3/21 at 11:00/12:00 hours:

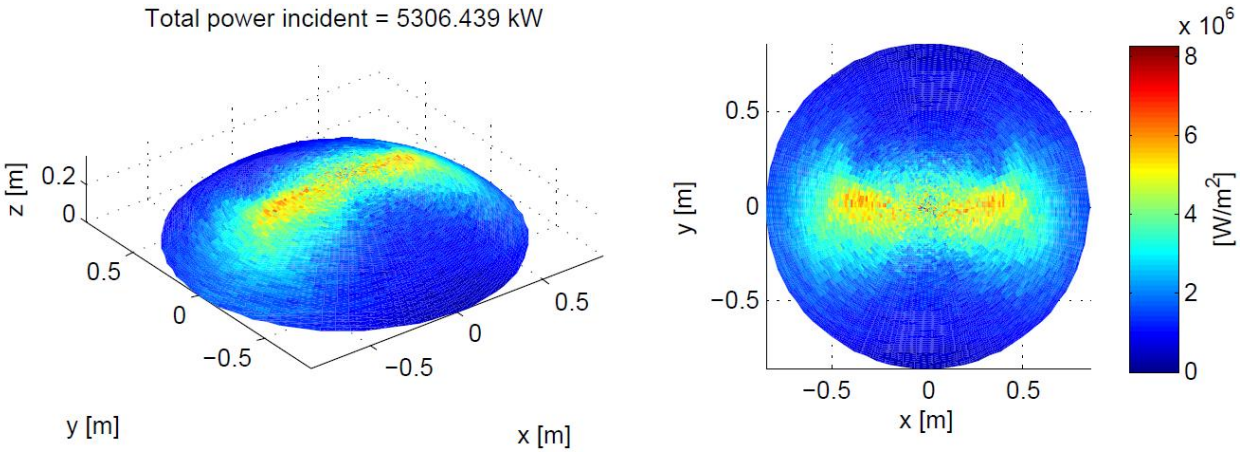

Figure 3-37 Test with error of 1.2mrad in the heliostat field and with 3.4 m of outlet for 3/21 at 11:00/12:00 hours

Test for 3/21 at 15:00/16:00 hours:

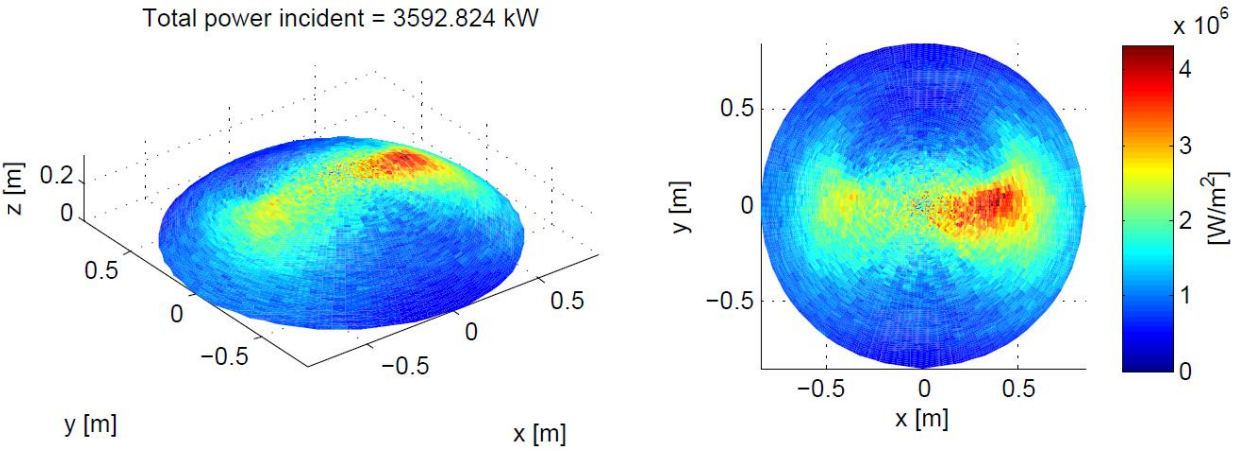

Figure 3-38 Test with error of 1.2mrad in the heliostat field and with 3.4 m of outlet for 3/21 at 15:00/16:00 hours

3.1.3.2 Test without error in the heliostat field and with 3.4 m of outlet file

Test for 3/21 at 07:00/08:00 hours:

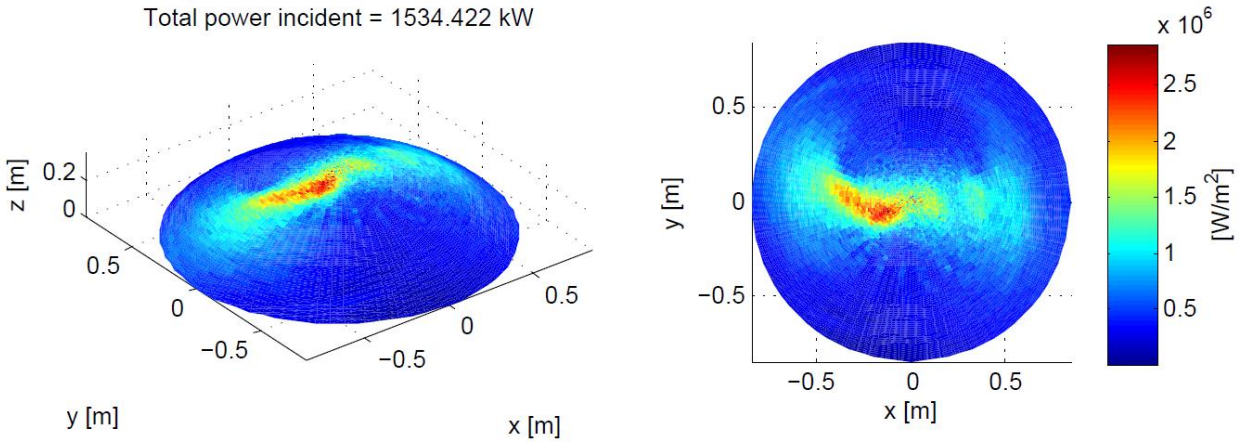

Figure 3-39 Test without error in the heliostat field and with 3.4 m of outlet for 3/21 at 07:00/08:00 hours

Test for 3/21 at 11:00/12:00 hours:

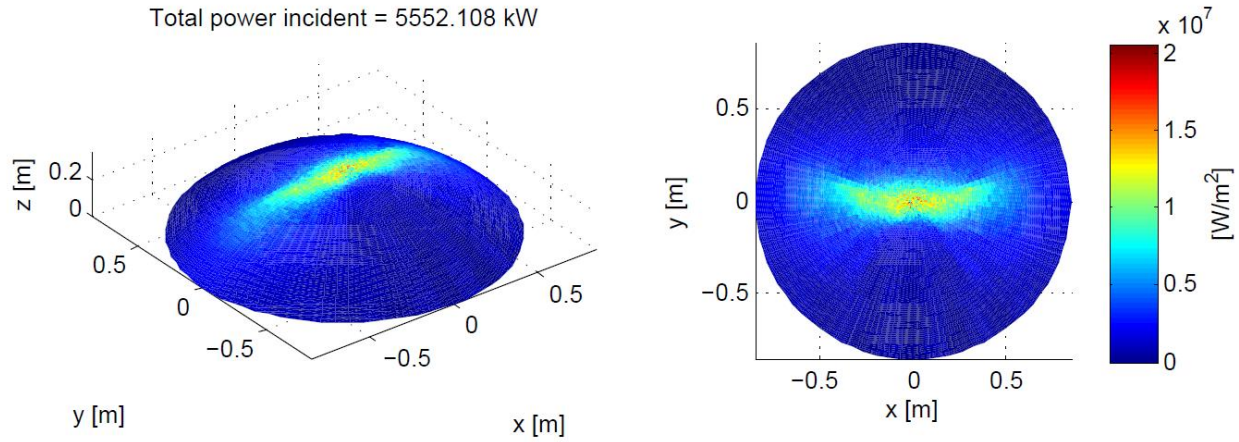

Figure 3-40 Test without error in the heliostat field and with 3.4 m of outlet for 3/21 at 11:00/12:00 hours

Test for 3/21 at 15:00/16:00 hours:

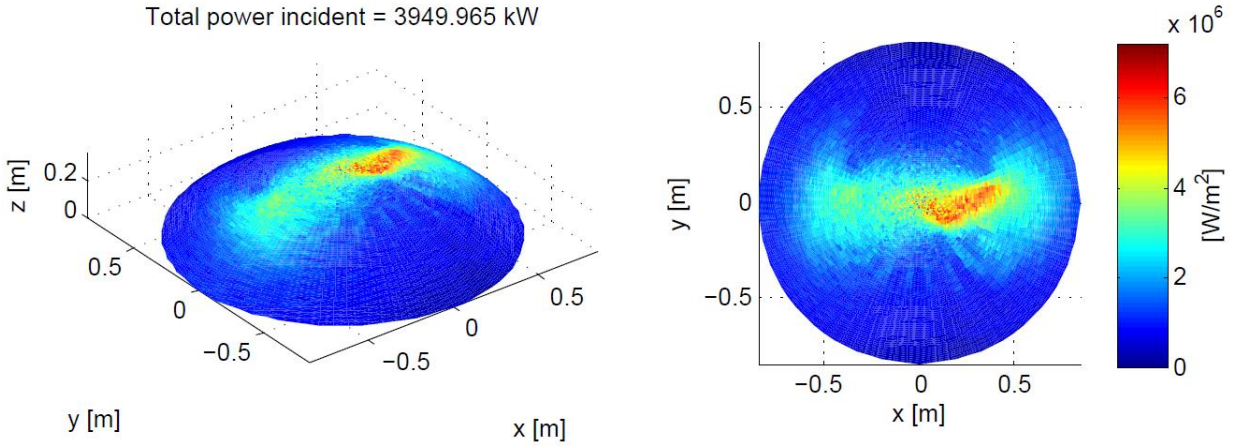

Figure 3-41 Test without error in the heliostat field and with 3.4 m of outlet for 3/21 at 15:00/16:00 hours

3.1.3.3 Test without error in the heliostat field and with 1.7 m of outlet file

Test for 3/21 at 07:00/08:00 hours:

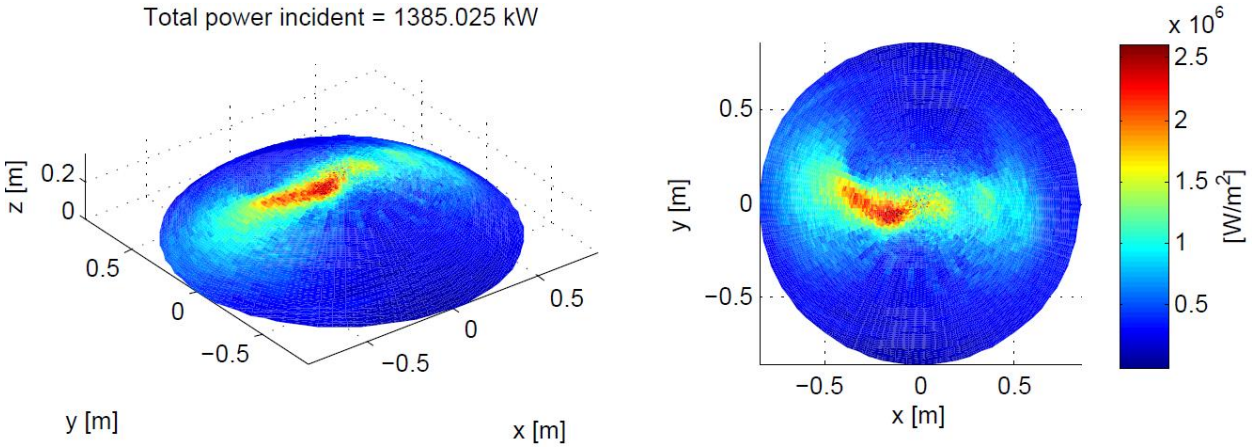

Figure 3-42 Test without error in the heliostat field and with 1.7m of outlet for 3/21 at 07:00/08:00 hours

Test for 3/21 at 11:00/12:00 hours:

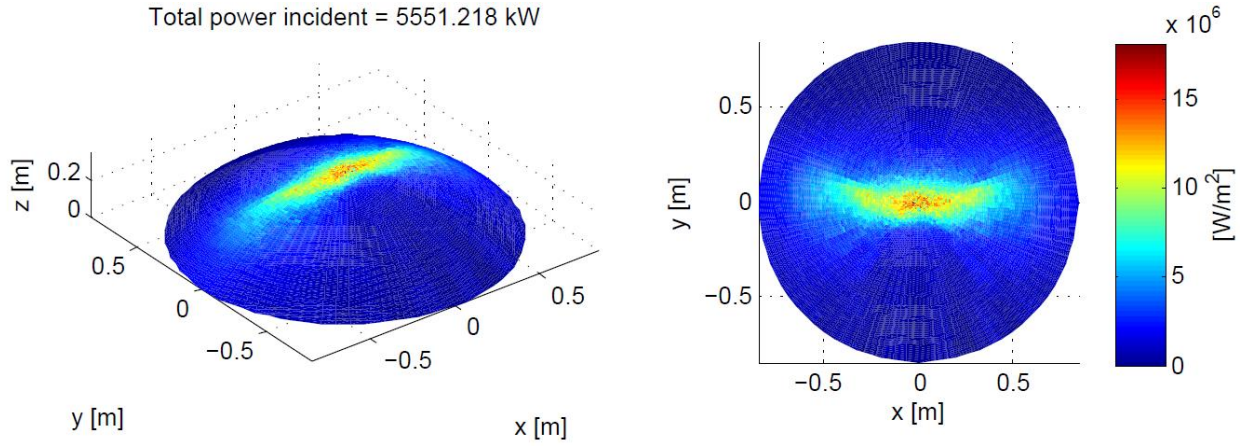

Figure 3-43 Test without error in the heliostat field and with 1.7 m of outlet for 3/21 at 11:00/12:00 hours

Test for 3/21 at 15:00/16:00 hours:

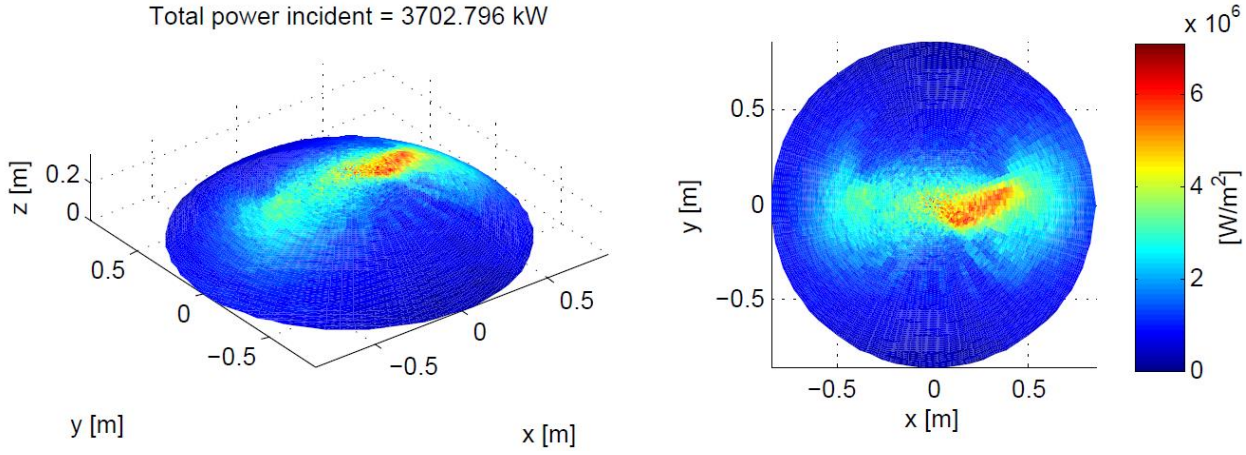

Figure 3-44 Test without error in the heliostat field and with 1.7 m of outlet for 3/21 at 15:00/16:00 hours

3.1.3.4 Test with error of 1.2mrad in the heliostat field and with 1.7 m of outlet file

Test for 3/21 at 07:00/08:00 hours:

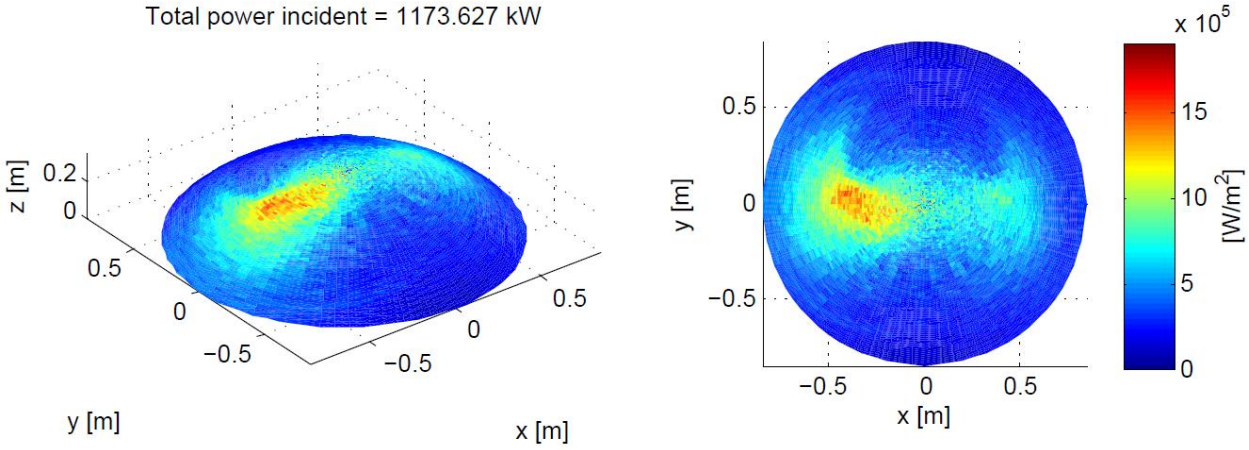

Figure 3-45 Test with error of 1.2mrad in the heliostat field and with 1.7 m of outlet for 3/21 at 07:00/08:00 hours

Test for 3/21 at 11:00/12:00 hours:

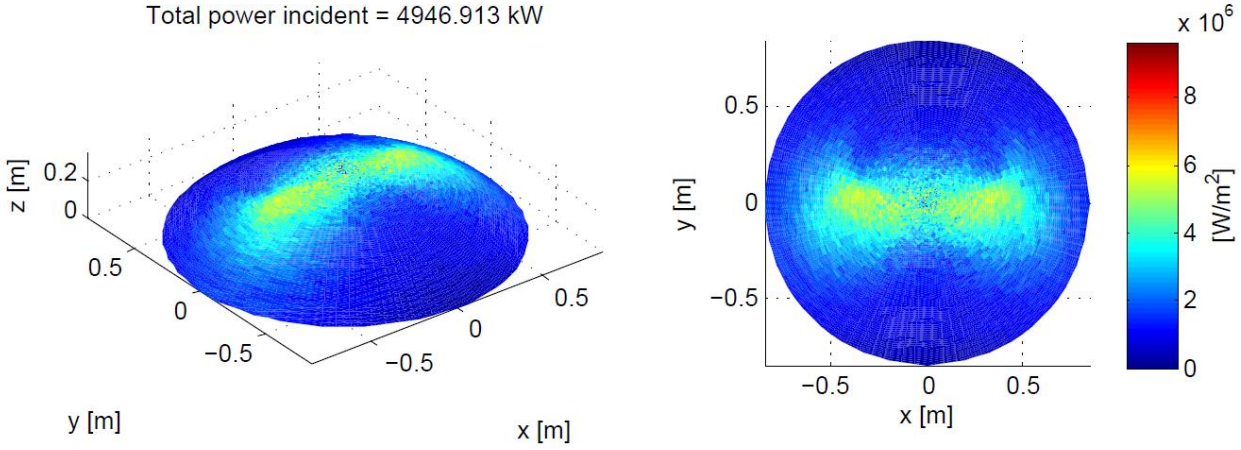

Figure 3-46 Test with error of 1.2mrad in the heliostat field and with 1.7 m of outlet for 3/21 at 11:00/12:00 hours

Test for 3/21 at 15:00/16:00 hours:

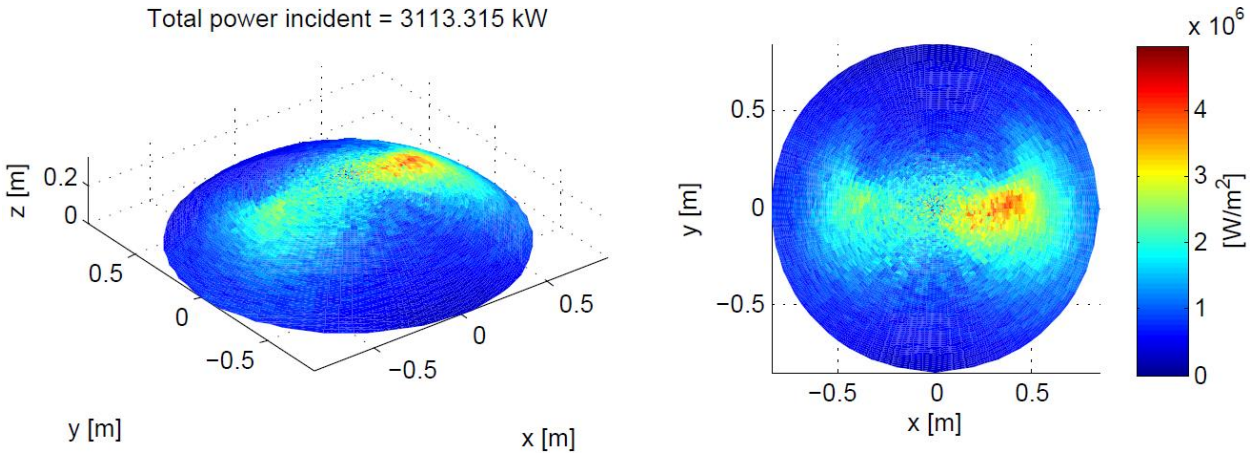

Figure 3-47 Test with error of 1.2mrad in the heliostat field and with 1.7 m of outlet for 3/21 at 15:00/16:00 hours

3.1.3.5 Comparison

Variables	**Day**	**Hour**	**Total Power Absorbed**
Test with error of 1.2mrad in the heliostat field and with 3.4 m of outlet file	3-21	07:00/08:00	1396.05
	3-21	11:00/12:00	5306.44
	3-21	15:00/16:00	3592.82
Test without error in the heliostat field and with 3.4 m of outlet file	3-21	07:00/08:00	1534.42
	3-21	11:00/12:00	5552.11
	3-21	15:00/16:00	3949.97
Test without error in the heliostat field and with 1.7 m of outlet file	3-21	07:00/08:00	1385.03
	3-21	11:00/12:00	5551.22
	3-21	15:00/16:00	3702.80
Test with error of 1.2mrad in the heliostat field and with 1.7 m of outlet file	3-21	07:00/08:00	1173.63
	3-21	11:00/12:00	4946.92
	3-21	15:00/16:00	3113.32

Table 3-3 Power comparison HEXBER

3.1.4 Ray comparison 03-21 from 11-12

The purpose is to understand why the difference in the power is not so important although the inlet was modify, which means that the percentage of rays missing CPC aperture will increase.

The Berchtold hexagonal shape is worse than Berchtold shape but is able to increase the amount of power thanks to the percentage of rays rejected after reflection; this may be related to the planes.

The main problem of the hexagon inlet-outlet shape is the percentage of rays rejected after reflection which increase due to the absence of curvature in the shape which will make more rays to go back, and also the percentage of rays absorbed in reflection, this has to be also related with the absence of curvature in the shape which does not focus all the rays in the window, and the number of reflections increase.

Comparison of the rays 03-21 from 11-12 with error and 3.4m outlet file

	BERCHTOLD	HEXHEX	HEXBER
PERCENTAGE OF ACCEPTED RAYS	94.18	92.31	94.20
POWER OF ACCEPTED RAYS	5396470.10W	5199992.83W	5306439.26W
PERCENTAGE OF RAYS OUTSIDE ACCEPTANCE ANGLE	3.49	3.55	3.55
POWER OF RAYS OUTSIDE ACCEPTANCE ANGLE	199938.33W	199938.33W	199938.33W
PERCENTAGE OF RAYS MISSING CPC APERTURE	2.23	3.95	3.95
POWER OF RAYS MISSING CPC APERTURE	127710.95W	222133.03W	222133.03W
PERCENTAGE OF RAYS ACCEPTED WITHOUT REFLECTION	41.15	36.13	41.41
POWER OF RAYS ACCEPTED WITHOUT REFLECTION	2358147.92W	2035589.76W	2332769.49W
PERCENTAGE OF RAYS ABSORBED IN REFLECTION	2.20	3.09	2.29
POWER OF RAYS ABSORBED IN REFLECTION	125896.72W	174224.87W	128879.08W
PERCENTAGE OF RAYS REJECTED AFTER REFLECTION	0.17	1.13	4.59-002
POWER OF RAYS REJECTED AFTER REFLECTION	9957.27W	63684.32W	2583.67W

Table 3-4 Comparison of the different percentage of the rays

3.1.5 Comparison

Variables	Day	Hour	Total Power Absorbed BERCHTOLD	Total Power Absorbed HEXHEX	Total Power Absorbed HEXBER
Error of 1.2mrad 3.4m of outlet file	3-21	07:00/08:00	1476.83	1362.56	1396.05
	3-21	11:00/12:00	5396.47	5199.99	5306.44
	3-21	15:00/16:00	3748.3	3509.20	3592.82
3.4 m of outlet file	3-21	07:00/08:00	1586.56	1508.05	1534.42
	3-21	11:00/12:00	5546.37	5504.23	5552.11
	3-21	15:00/16:00	4018.41	3876.23	3949.97
1.7 m of outlet file	3-21	07:00/08:00	1384.91	1364.6	1385.03
	3-21	11:00/12:00	5546.97	5505.61	5551.22
	3-21	15:00/16:00	3701.14	3649.86	3702.80
Error of 1.2mrad 1.7m of outlet file	3-21	07:00/08:00	1173.40	1151.20	1173.63
	3-21	11:00/12:00	4945.08	4862.63	4946.92
	3-21	15:00/16:00	3111.39	3057.26	3113.32

Table 3-5 Power comparison between the shapes

As can be seen the difference in the power is almost the same between the shapes, and also the window pattern is almost constant.

So it is assumed that the comparison can be done for any MIRVAL file, it is going to be used the error in the heliostat field in order to have a more realistic pattern, since it does not increase the running time of the simulation and a 1.7m of outlet file since the run time is lower.

3.2 Test for different days and hours a year

The aim of this chapter is to compare different days for the concentrator with the purpose of finding the more efficient, the cheapest and easiest to build and with an inlet that do not waste space between concentrators.

For this has been tested the previous shapes:

- Firstly Berchtold's shape is going to be tested to be compared with any new shape.
- Secondly the hexagonal inlet-outlet is tested, taking into account that not all the window is been used.
- Thirdly a mixed shape between this two is tested.

3.2.1 Berchtold shape

3.2.1.1 Test for 3/21 at 07:00/08:00 hours

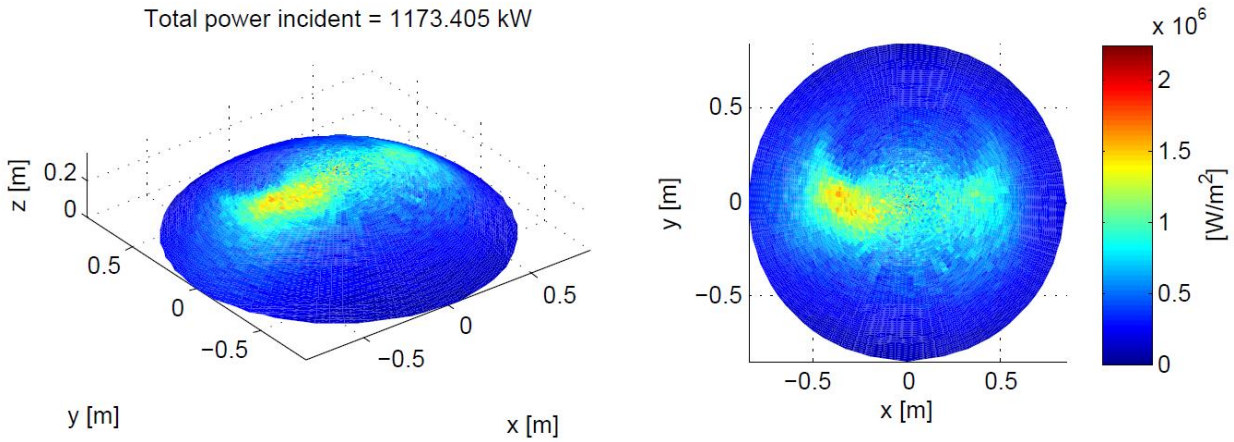

Figure 3-48 Test for Berchtold shape for 3/21 at 07:00/08:00 hours

3.2.1.2 Test for 3/21 at 11:00/12:00 hours

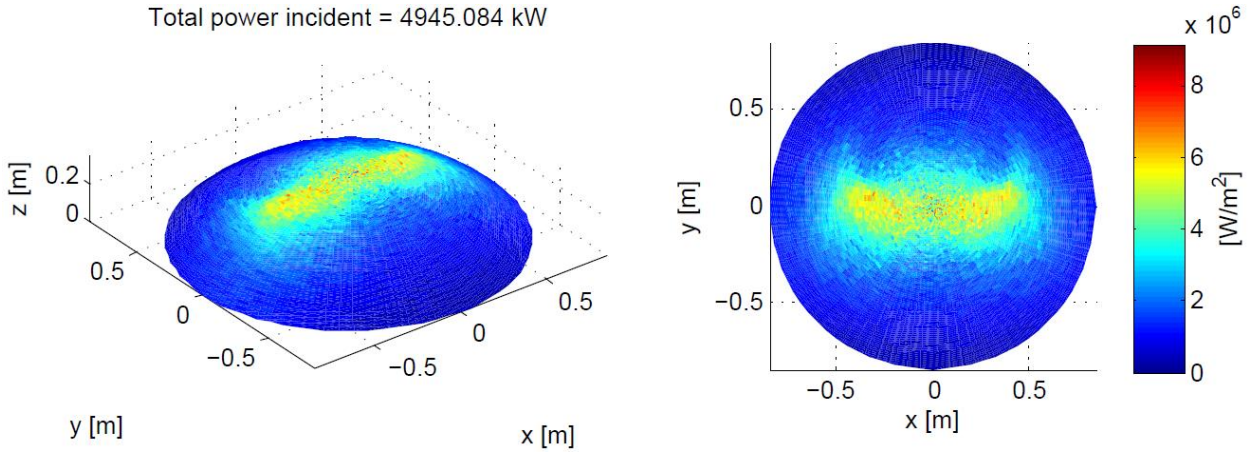

Figure 3-49 Test for Berchtold shape for 3/21 at 11:00/12:00 hours

3.2.1.3 Test for 3/21 at 15:00/16:00 hours

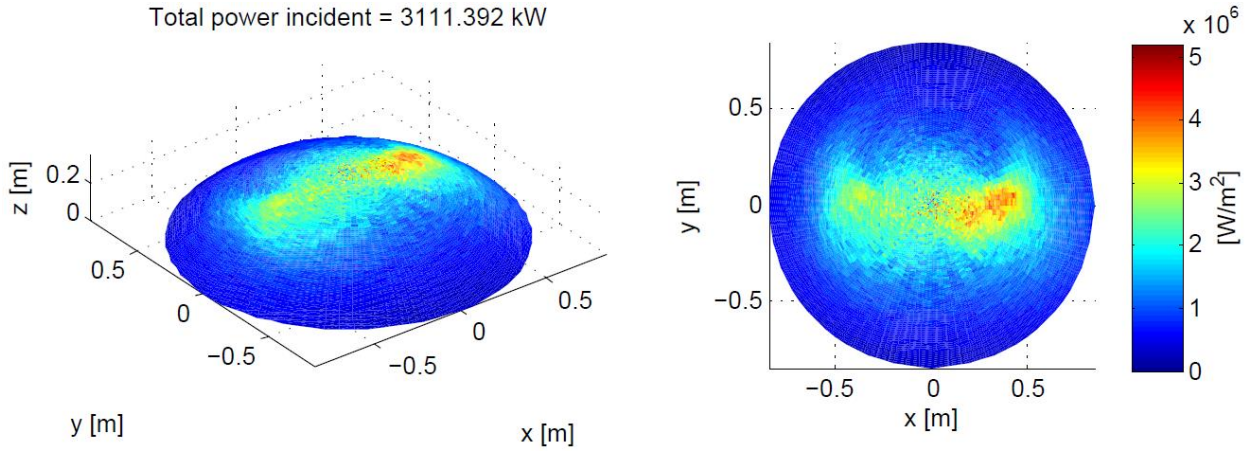

Figure 3-50 Test for Berchtold shape for 3/21 at 15:00/16:00 hours

3.2.1.4 Test for 6/21 at 07:00/08:00 hours

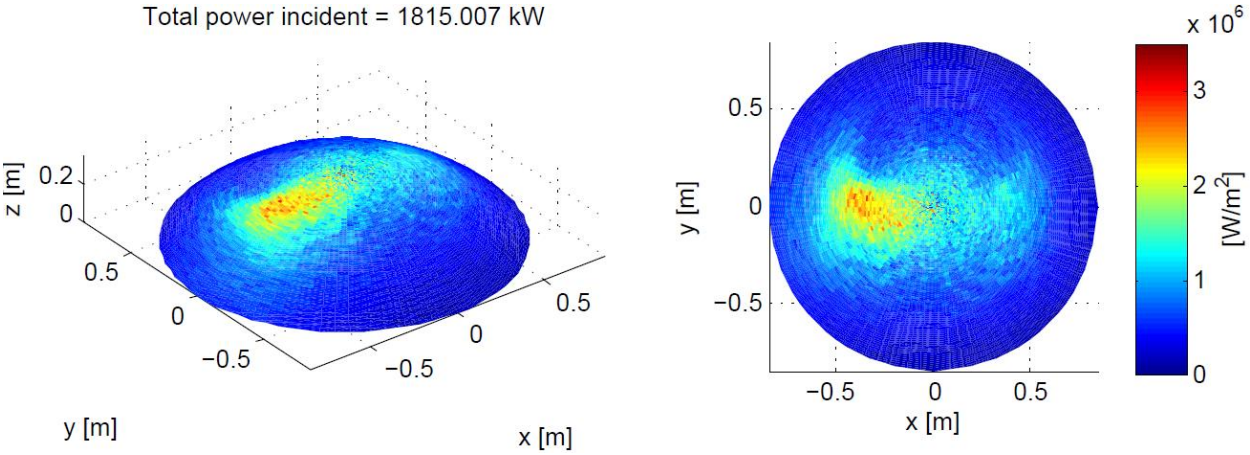

Figure 3-51 Test for Berchtold shape for 6/21 at 07:00/08:00 hours

3.2.1.5 Test for 6/21 at 11:00/12:00 hours

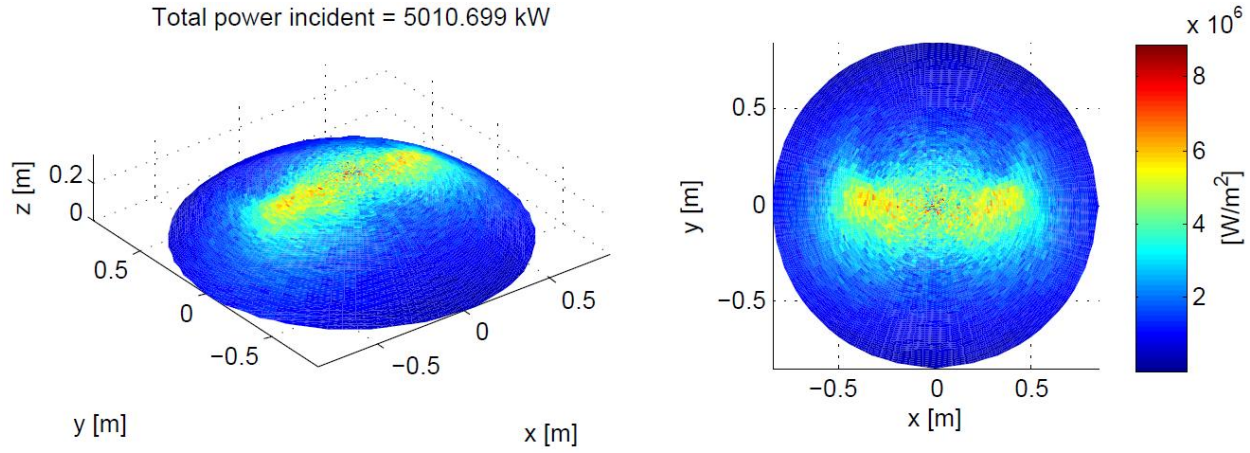

Figure 3-52 Test for Berchtold shape for 6/21 at 11:00/12:00 hours

3.2.1.6 Test for 6/21 at 15:00/16:00 hours

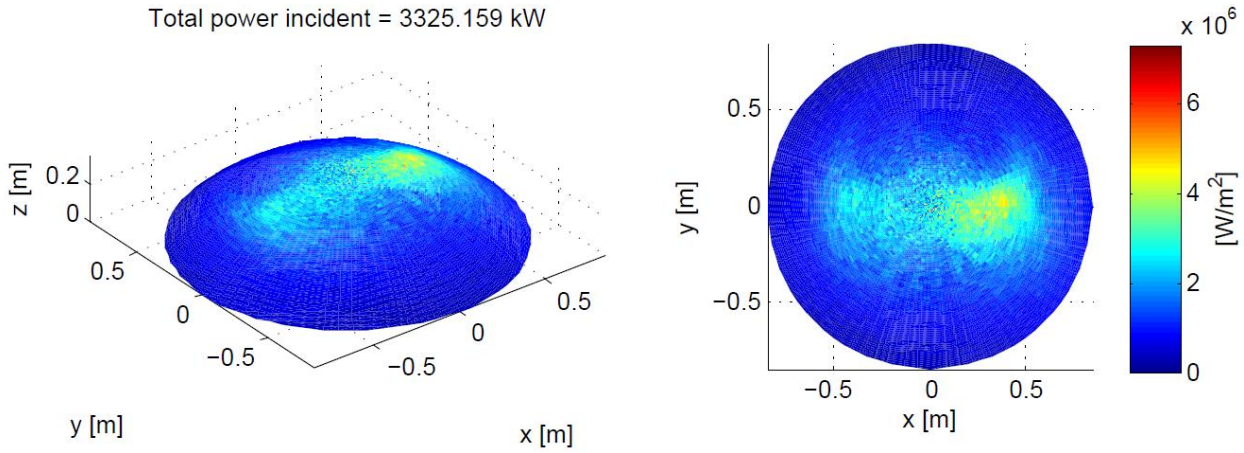

Figure 3-53 Test for Berchtold shape for 6/21 at 15:00/16:00 hours

3.2.1.7 Test for 9/21 at 07:00/08:00 hours

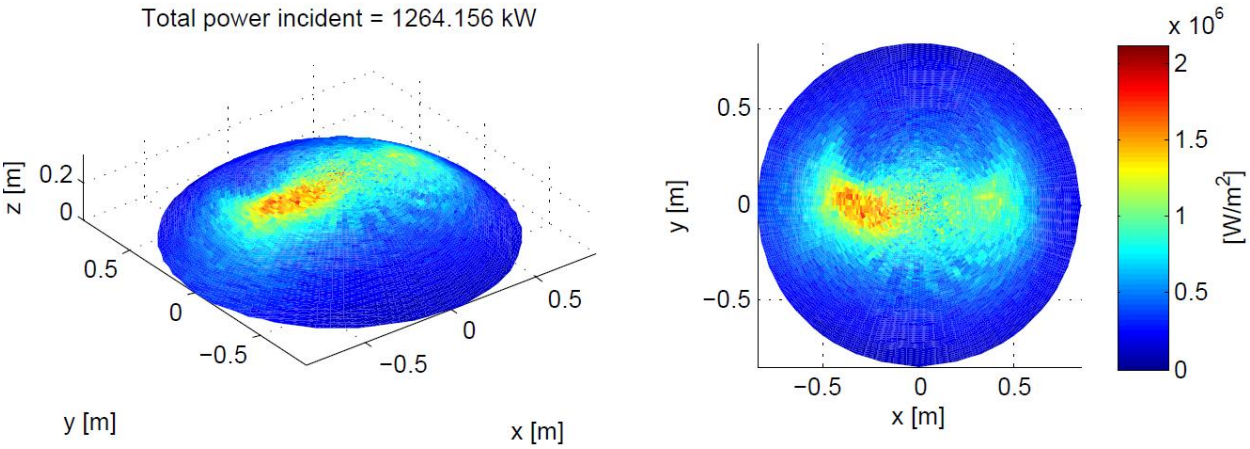

Figure 3-54 Test for Berchtold shape for 9/21 at 07:00/08:00 hours

3.2.1.8 Test for 9/21 at 11:00/12:00 hours

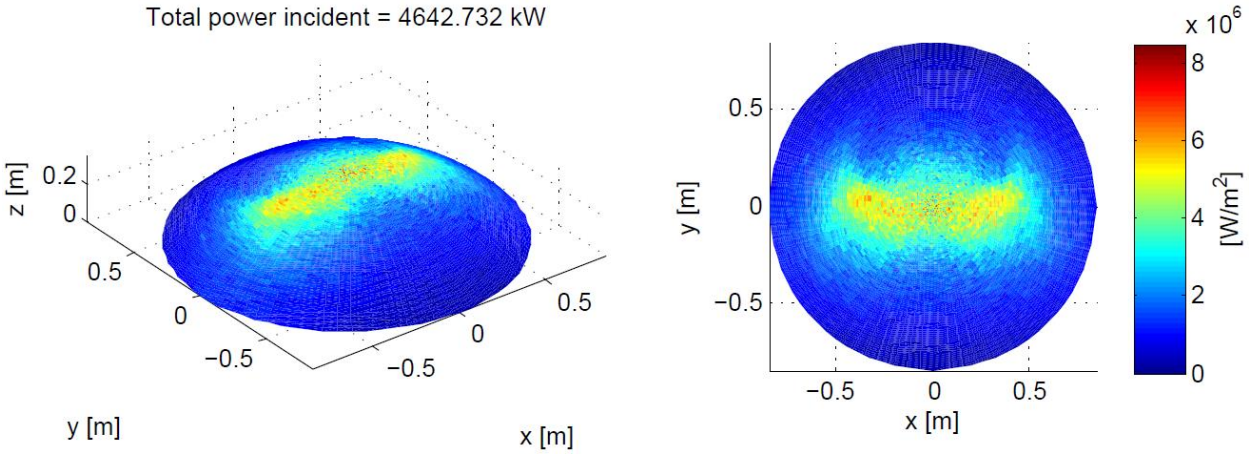

Figure 3-55 Test for Berchtold shape for 9/21 at 11:00/12:00 hours

3.2.1.9 Test for 9/21 at 15:00/16:00 hours

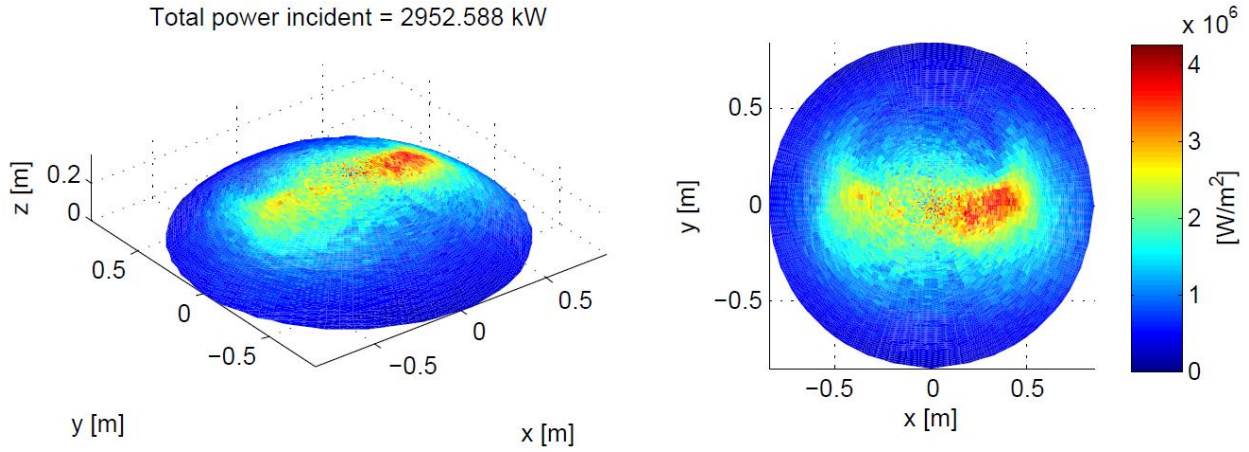

Figure 3-56 Test for Berchtold shape for 9/21 at 15:00/16:00 hours

3.2.1.10 Test for 12/21 at 11:00/12:00 hours

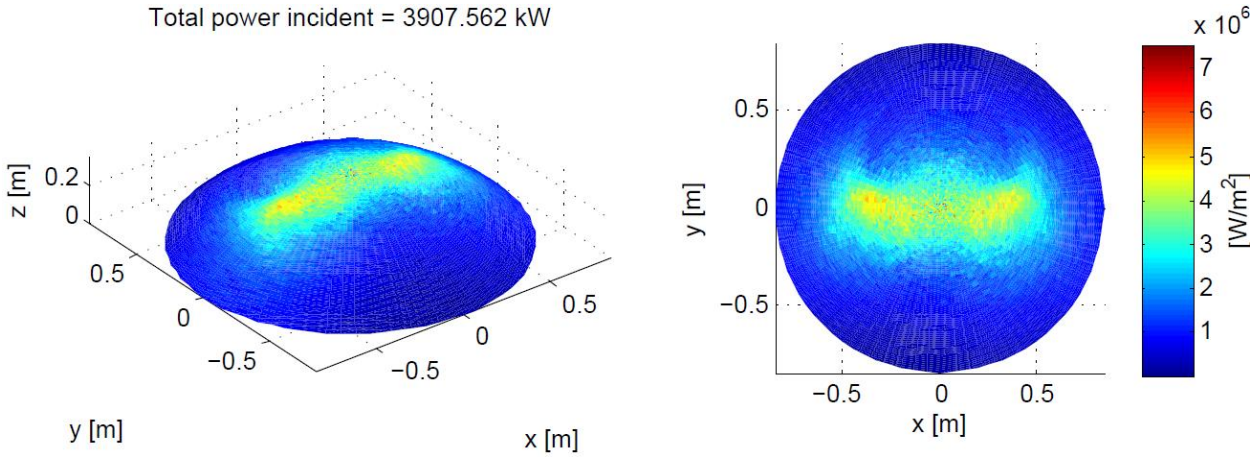

Figure 3-57 Test for Berchtold shape for 12/21 at 11:00/12:00 hours

3.2.1.11 Test for 12/21 at 15:00/16:00 hours

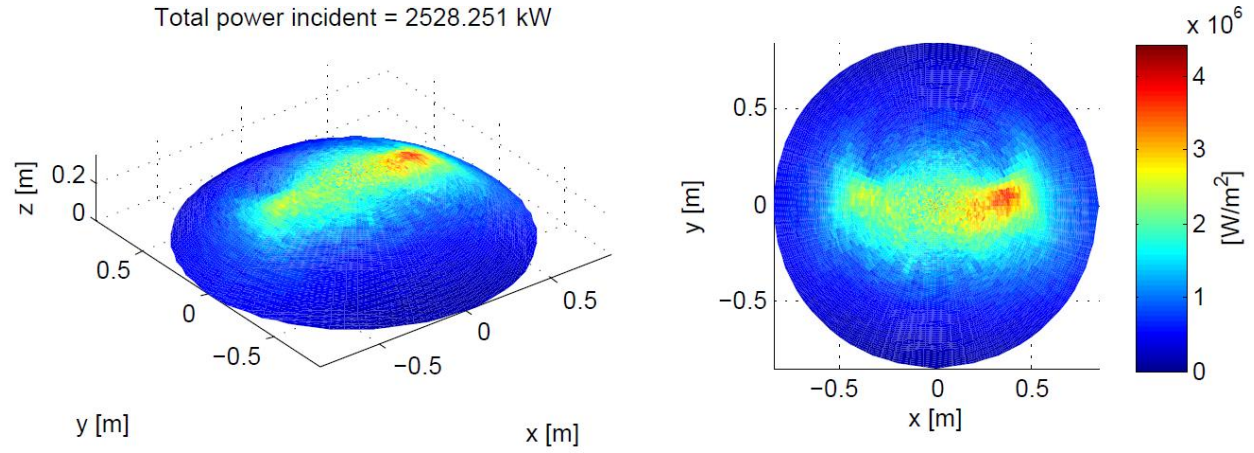

Figure 3-58 Test for Berchtold shape for 12/21 at 15:00/16:00 hours

3.2.1.12 Comparison of the hitting power

Day	Hour	Total Power Absorbed
3-21	07:00/08:00	1173.40
	11:00/12:00	4945.08
	15:00/16:00	3111.39
6-21	07:00/08:00	1815.00
	11:00/12:00	5010.70
	15:00/16:00	3325.16
9-21	07:00/08:00	1264.16
	11:00/12:00	4642.73
	15:00/16:00	2952.59
12-21	07:00/08:00	-----
	11:00/12:00	3907.56
	15:00/16:00	2528.25

Table 3-6 Comparison of the hitting power

3.2.2 The hexagonal inlet-outlet is tested

The main advantages of this shape is the facility of construction, since is made with planes, which leads to a really cheap concentrator. But the problem is that it does not use all the window, since the exit is a hexagon too.

3.2.2.1 Test for 3/21 at 07:00/08:00 hours

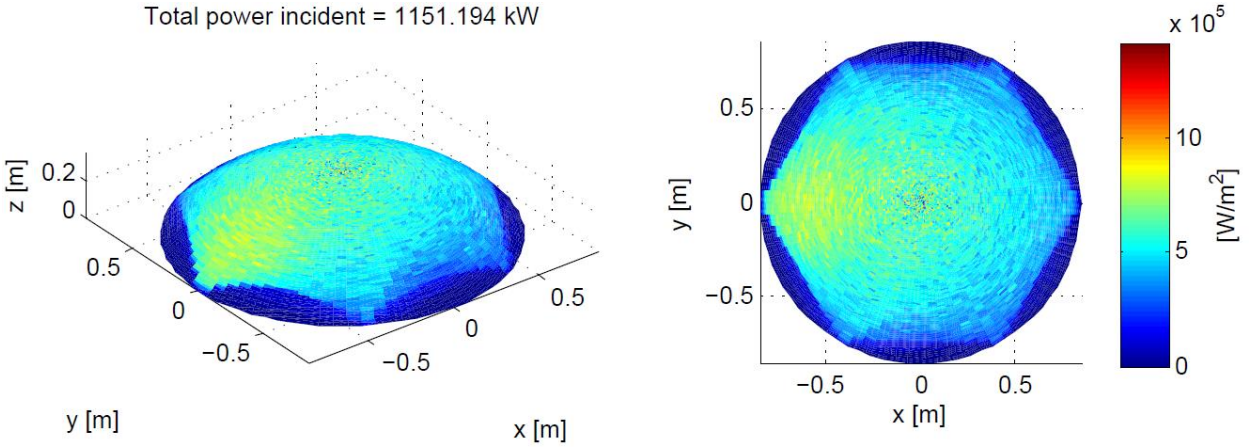

Figure 3-59 Test for hexagonal inlet-outlet for 03/21 at 07:00/08:00 hours

3.2.2.2 Test for 3/21 at 11:00/12:00 hours

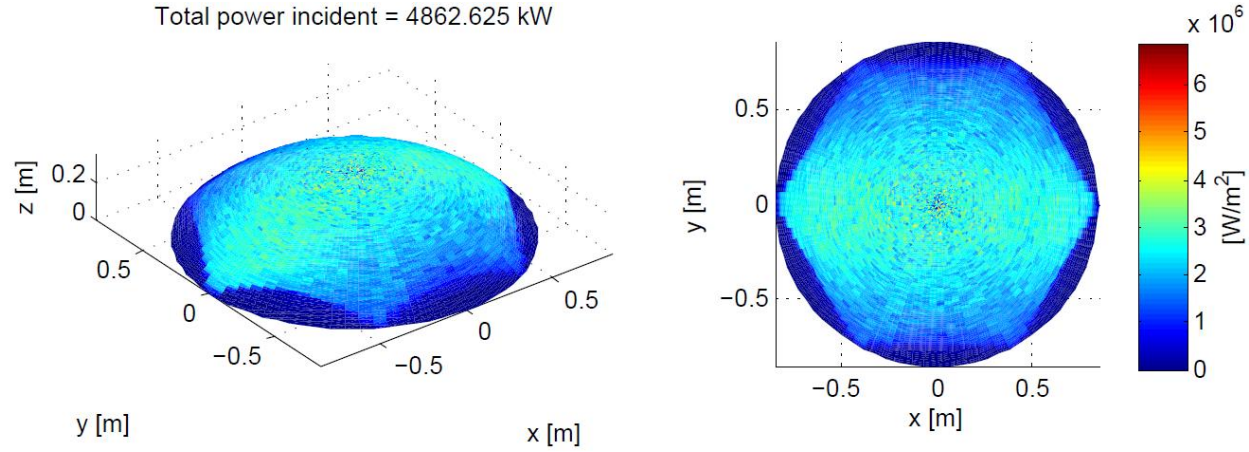

Figure 3-60 Test for hexagonal inlet-outlet for 03/21 at 11:00/12:00 hours

3.2.2.3 Test for 3/21 at 15:00/16:00 hours

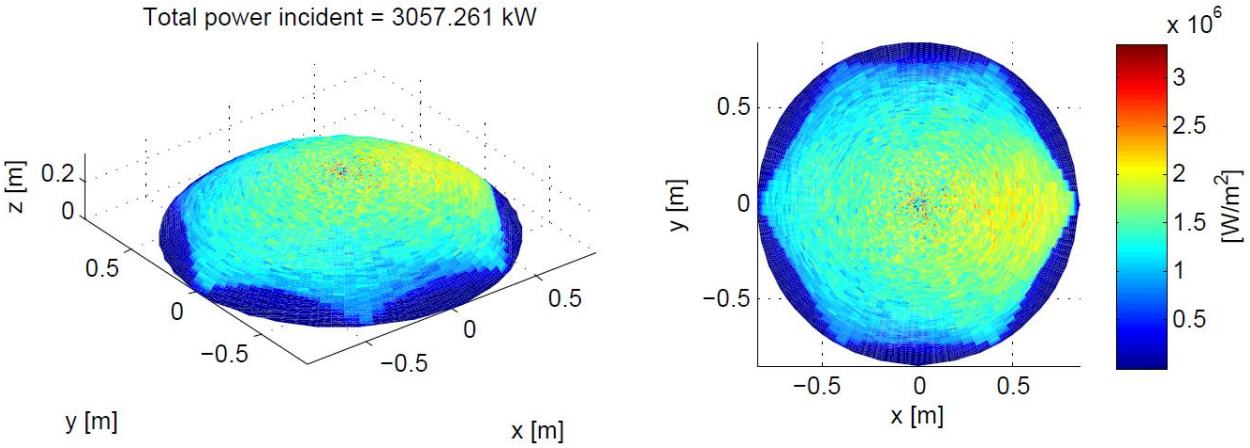

Figure 3-61 Test for hexagonal inlet-outlet for 03/21 at 15:00/16:00 hours

3.2.2.4 Test for 6/21 at 07:00/08:00 hours

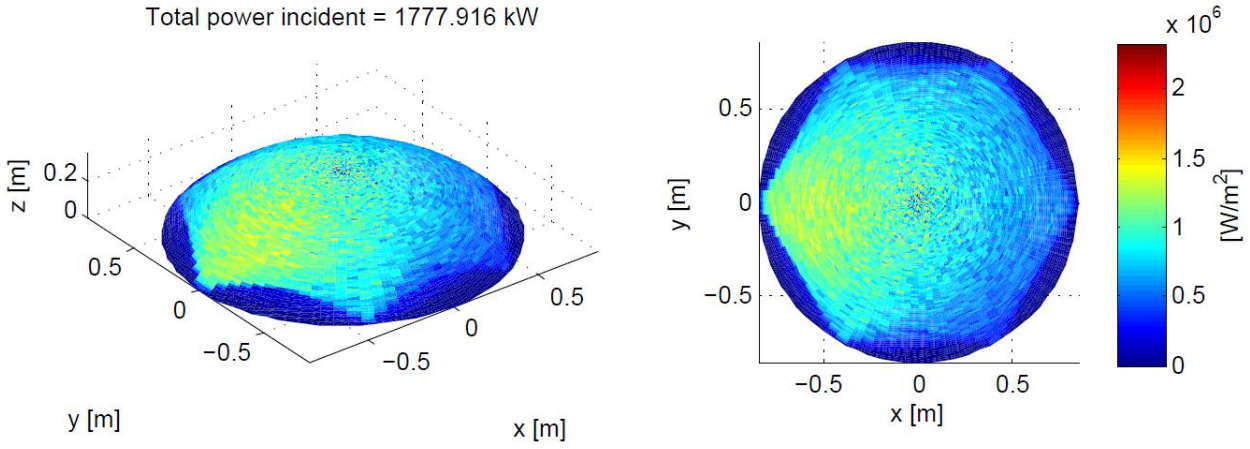

Figure 3-62 Test for hexagonal inlet-outlet for 06/21 at 07:00/08:00 hours

3.2.2.5 Test for 6/21 at 11:00/12:00 hours

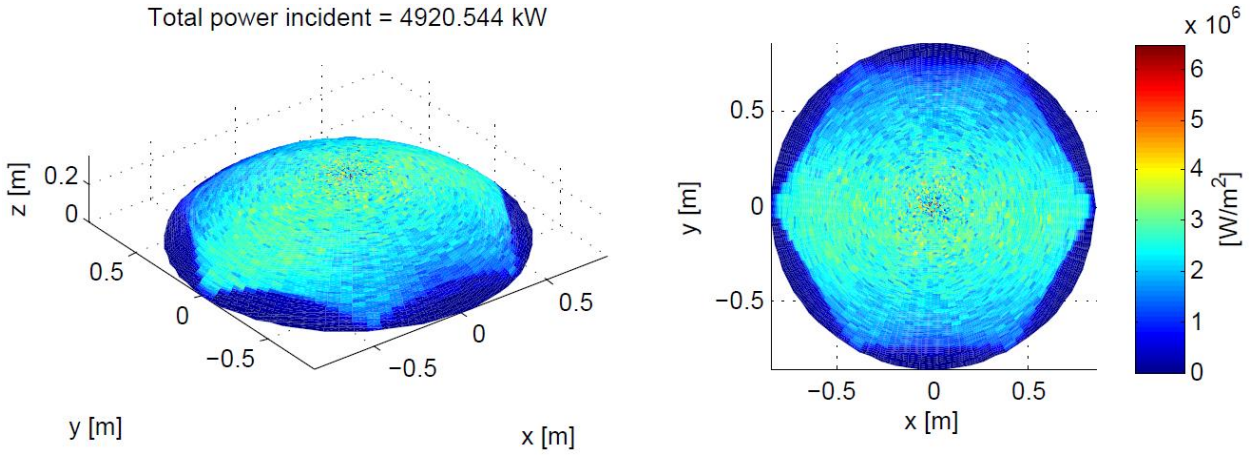

Figure 3-63 Test for hexagonal inlet-outlet for 06/21 at 11:00/12:00 hours

3.2.2.6 Test for 6/21 at 15:00/16:00 hours

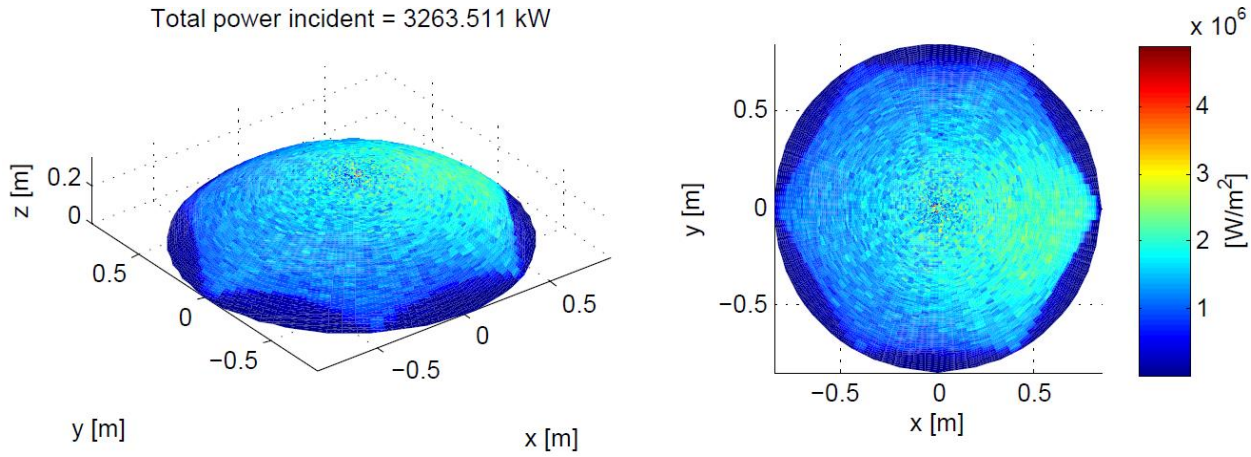

Figure 3-64 Test for hexagonal inlet-outlet for 06/21 at 15:00/16:00 hours

3.2.2.7 Test for 9/21 at 07:00/08:00 hours

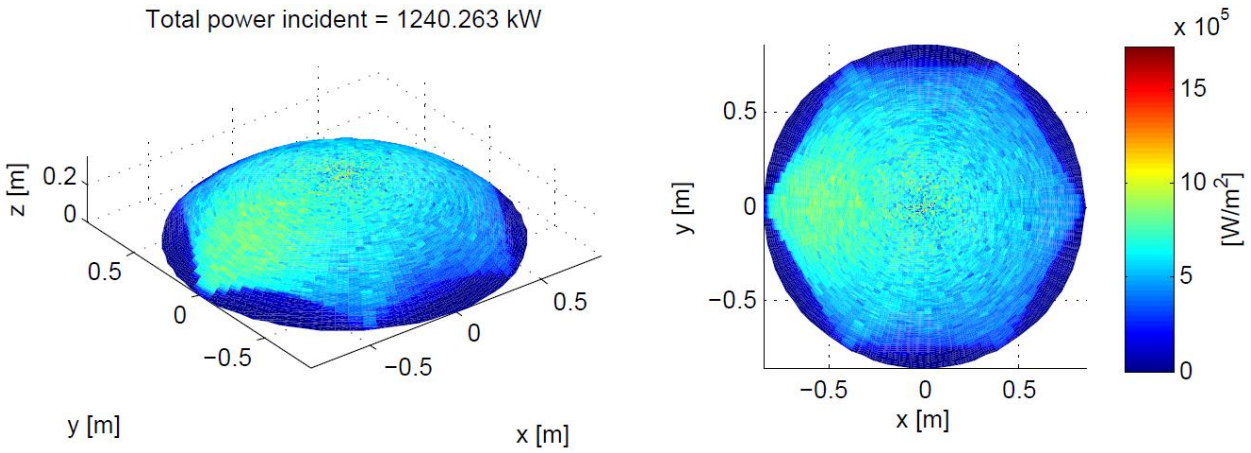

Figure 3-65 Test for hexagonal inlet-outlet for 09/21 at 07:00/08:00 hours

3.2.2.8 Test for 9/21 at 11:00/12:00 hours

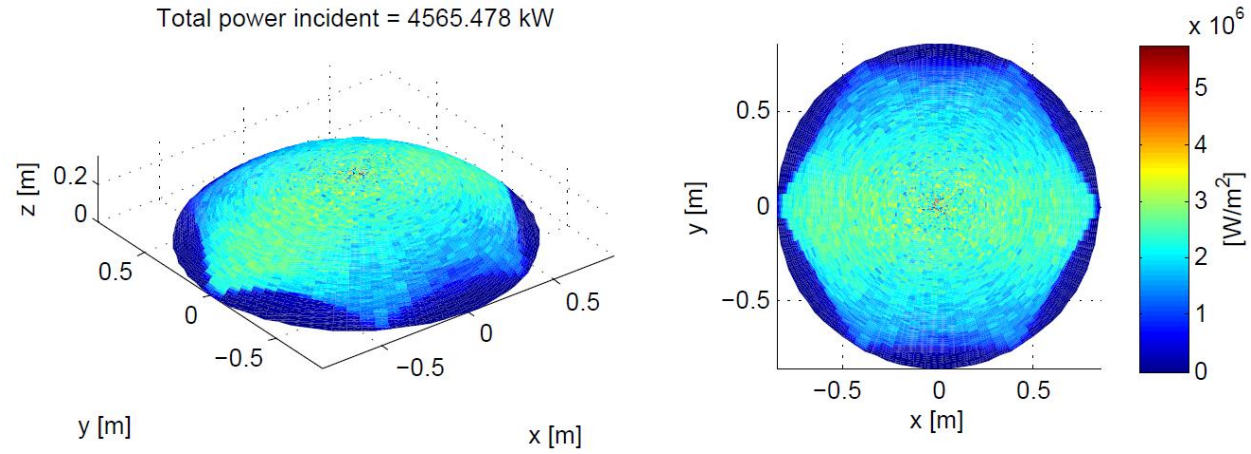

Figure 3-66 Test for hexagonal inlet-outlet for 09/21 at 11:00/12:00 hours

3.2.2.9 Test for 9/21 at 15:00/16:00 hours

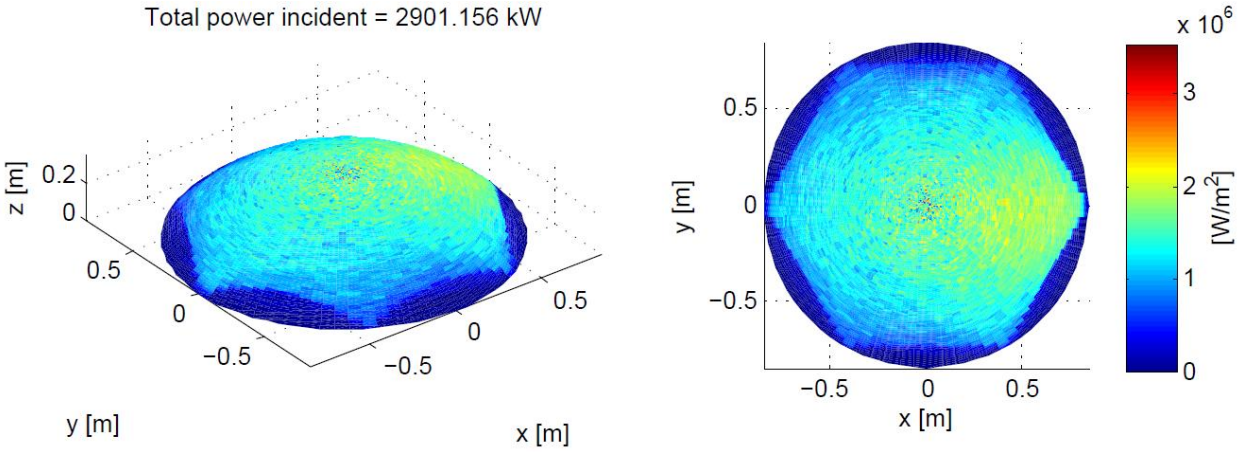

Figure 3-67 Test for hexagonal inlet-outlet for 09/21 at 15:00/16:00 hours

3.2.2.10 Test for 12/21 at 11:00/12:00 hours

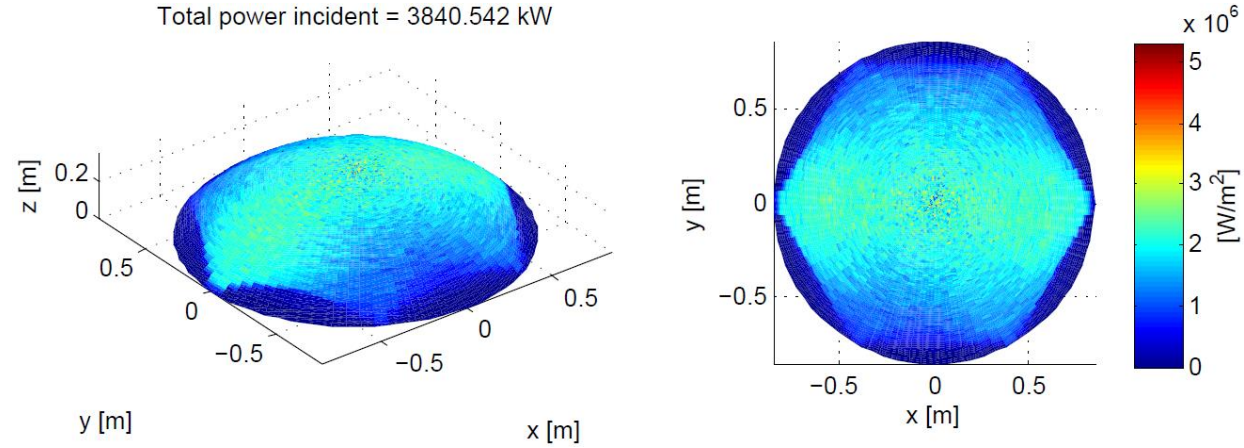

Figure 3-68 Test for hexagonal inlet-outlet for 12/21 at 11:00/12:00 hours

3.2.2.11 Test for 12/21 at 15:00/16:00 hours

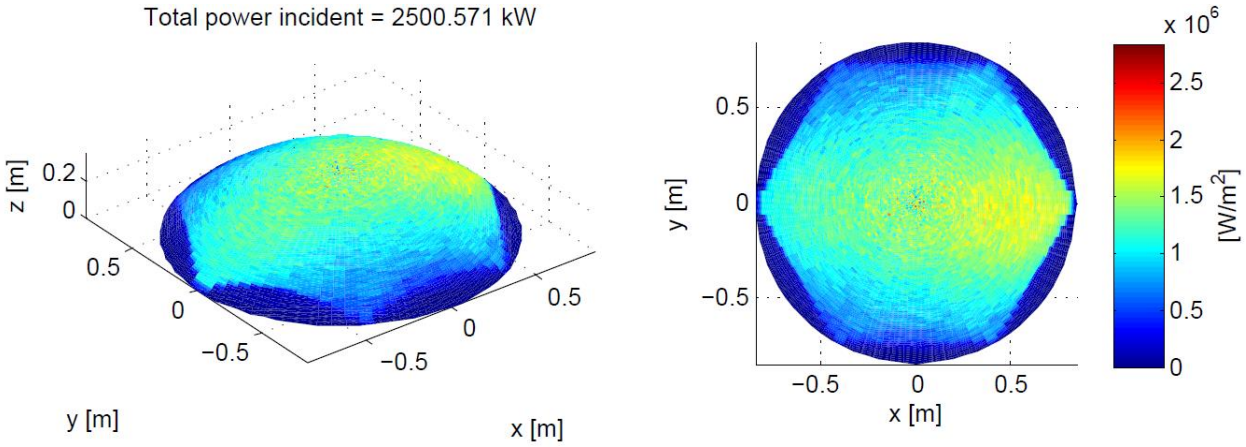

Figure 3-69 Test for hexagonal inlet-outlet for 12/21 at 15:00/16:00 hours

3.2.2.12 Comparison of the hitting power

Day	Hour	Total Power Absorbed
3-21	07:00/08:00	1151.19
	11:00/12:00	4862.63
	15:00/16:00	3057.26
6-21	07:00/08:00	1777.92
	11:00/12:00	4920.54
	15:00/16:00	3263.51
9-21	07:00/08:00	1240.26
	11:00/12:00	4565.48
	15:00/16:00	2901.16
12-21	07:00/08:00	-----
	11:00/12:00	3840.54
	15:00/16:00	2500.57

Table 3-7 Comparison of the hitting power

3.2.3 Berchtold shape with hexagonal entrance.

3.2.3.1 Test for 3/21 at 07:00/08:00 hours

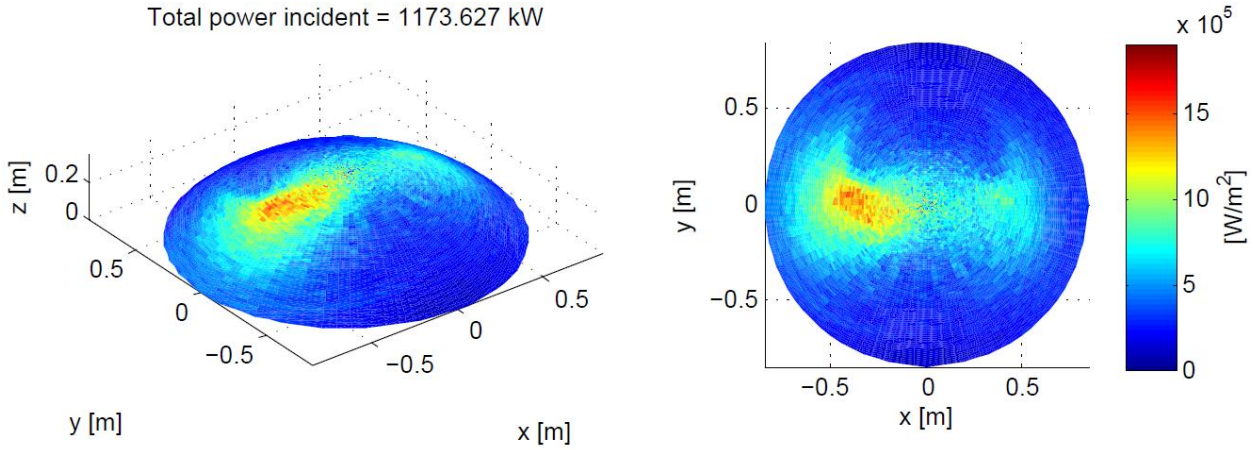

Figure 3-70 Test for Berchtold shape with hexagonal entrance for 3/21 at 07:00/08:00 hours

3.2.3.2 Test for 3/21 at 11:00/12:00 hours

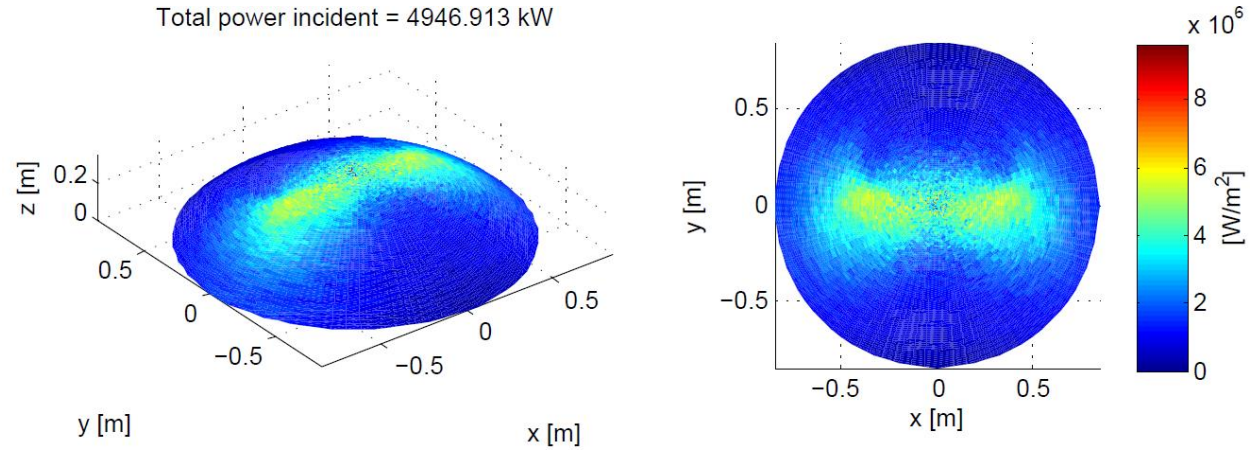

Figure 3-71 Test for Berchtold shape with hexagonal entrance for 3/21 at 11:00/12:00 hours

3.2.3.3 Test for 3/21 at 15:00/16:00 hours

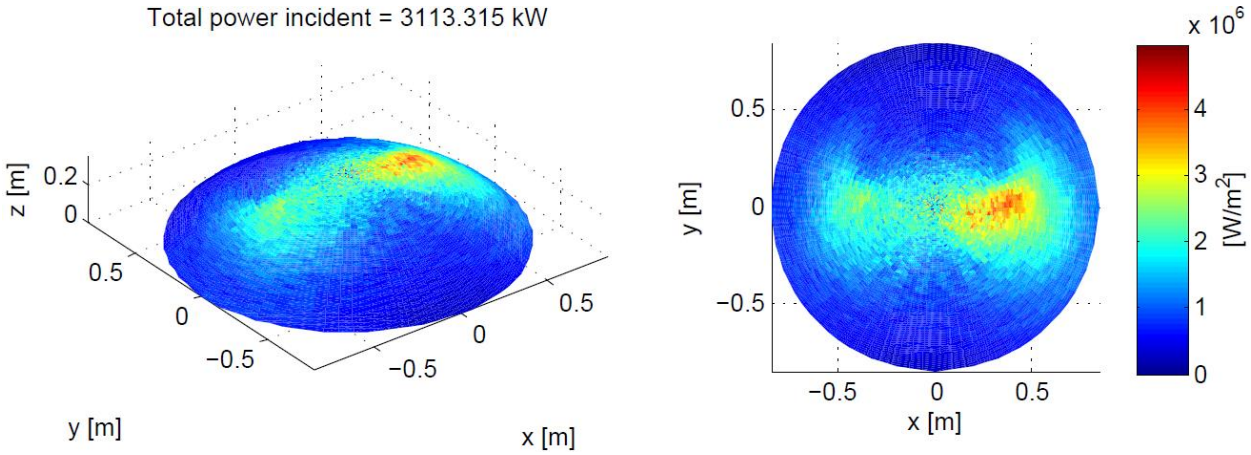

Figure 3-72 Test for Berchtold shape with hexagonal entrance for 3/21 at 15:00/16:00 hours

3.2.3.4 Test for 6/21 at 07:00/08:00 hours

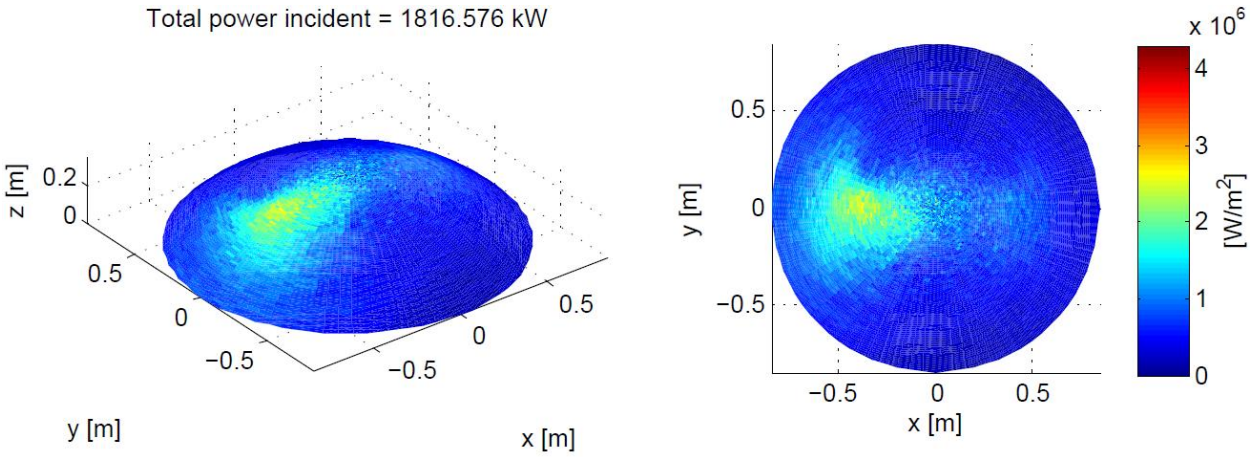

Figure 3-73 Test for Berchtold shape with hexagonal entrance for 6/21 at 07:00/08:00 hours

3.2.3.5 Test for 6/21 at 11:00/12:00 hours

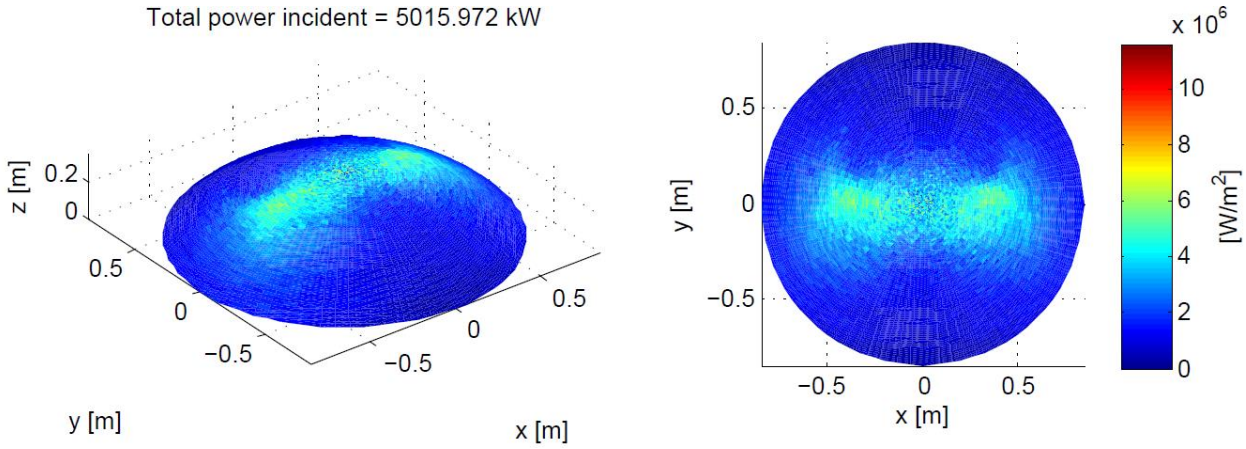

Figure 3-74 Test for Berchtold shape with hexagonal entrance for 6/21 at 11:00/12:00 hours

3.2.3.6 Test for 6/21 at 15:00/16:00 hours

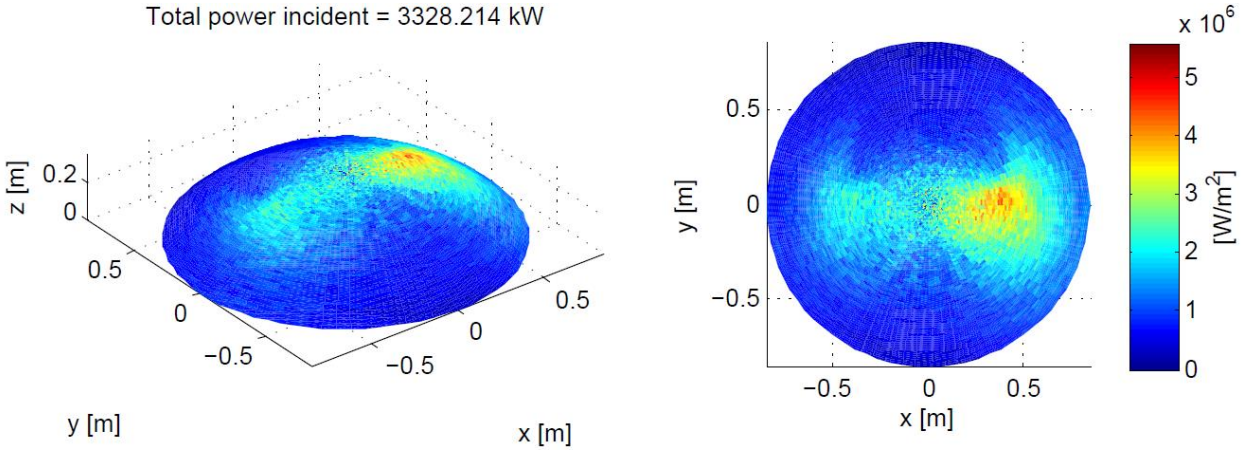

Figure 3-75 Test for Berchtold shape with hexagonal entrance for 6/21 at 15:00/16:00 hours

3.2.3.7 Test for 9/21 at 07:00/08:00 hours

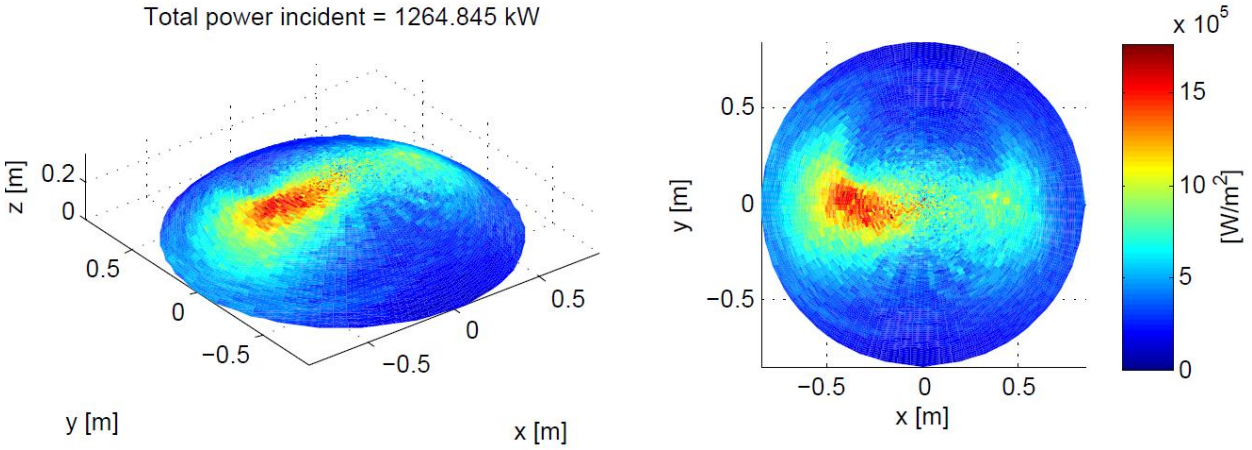

Figure 3-76 Test for Berchtold shape with hexagonal entrance for 9/21 at 07:00/08:00 hours

3.2.3.8 Test for 9/21 at 11:00/12:00 hours

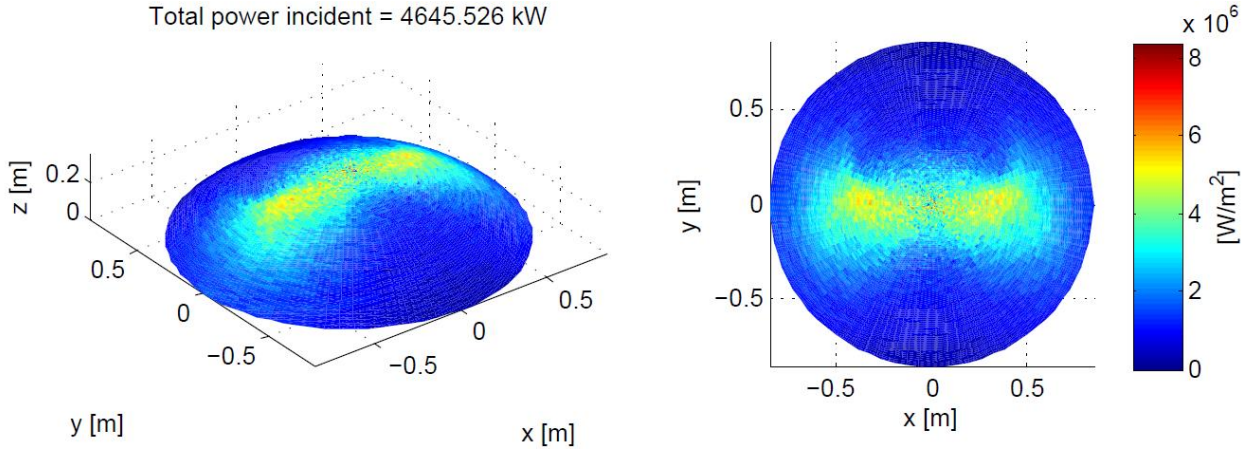

Figure 3-77 Test for Berchtold shape with hexagonal entrance for 9/21 at 11:00/12:00 hours

3.2.3.9 Test for 9/21 at 15:00/16:00 hours

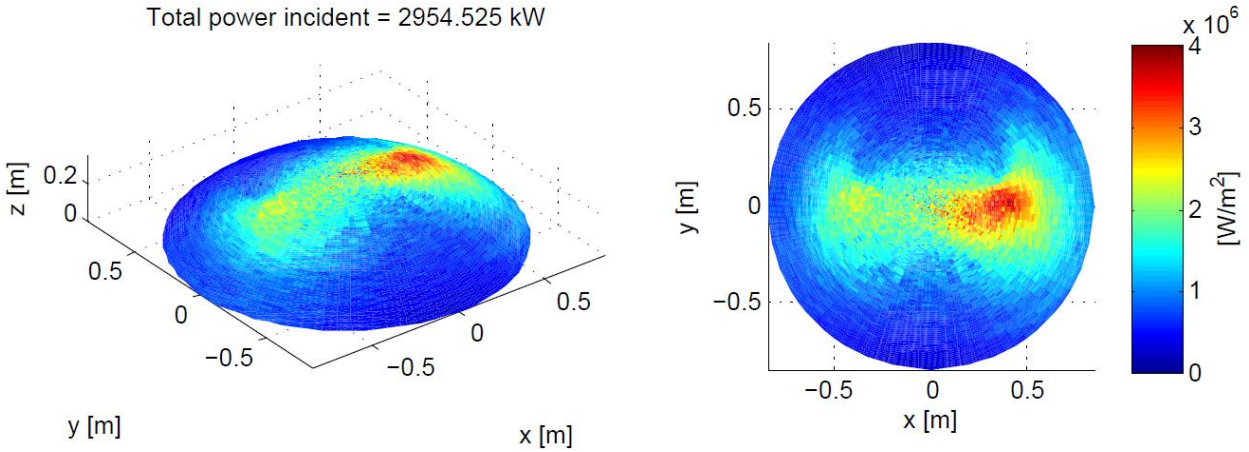

Figure 3-78 Test for Berchtold shape with hexagonal entrance for 9/21 at 15:00/16:00 hours

3.2.3.10 Test for 12/21 at 11:00/12:00 hours

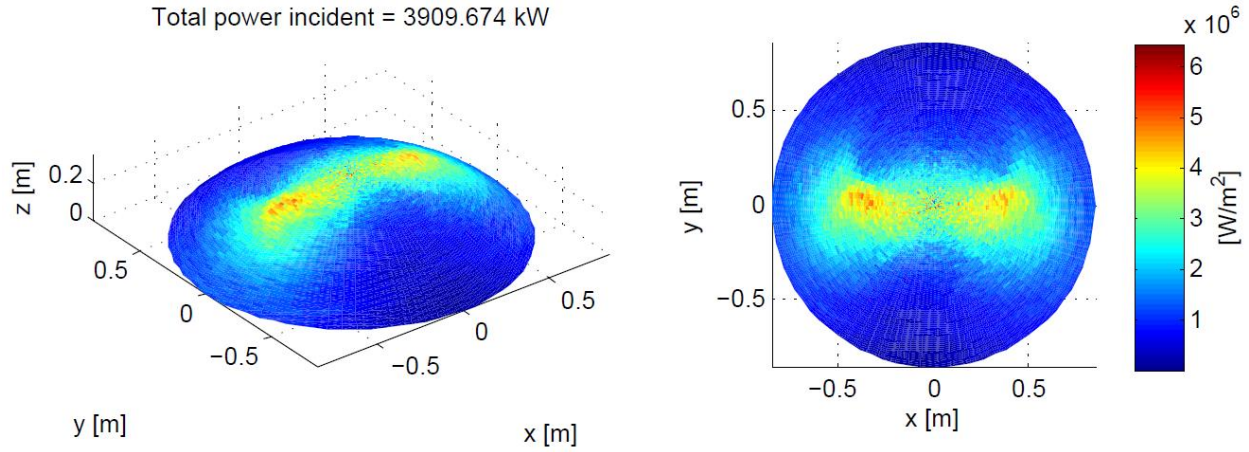

Figure 3-79 Test for Berchtold shape with hexagonal entrance for 12/21 at 11:00/12:00 hours

3.2.3.11 Test for 12/21 at 15:00/16:00 hours

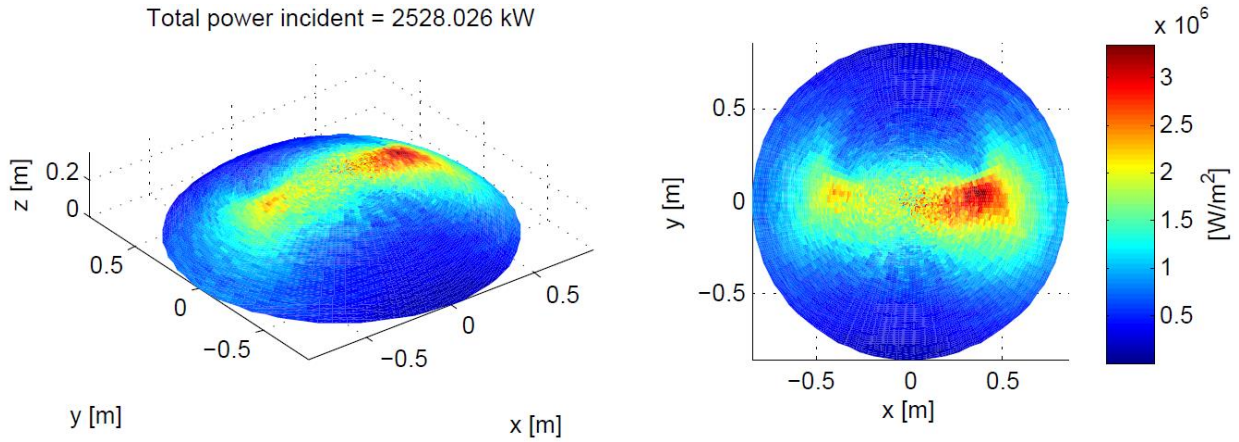

Figure 3-80 Test for Berchtold shape with hexagonal entrance for 12/21 at 15:00/16:00 hours

3.2.3.12 Comparison of the hitting power

Day	Hour	Total Power Absorbed
3-21	07:00/08:00	1173.63
	11:00/12:00	4946.91
	15:00/16:00	3113.32
6-21	07:00/08:00	1816.58
	11:00/12:00	5015.97
	15:00/16:00	3328.21
9-21	07:00/08:00	1264.85
	11:00/12:00	4645.53
	15:00/16:00	2954.53
12-21	07:00/08:00	-----
	11:00/12:00	3909.67
	15:00/16:00	2528.03

Table 3-8 Comparison of the hitting power for Berchtold shape with hexagonal entrance

3.2.4 Comparison of the hitting power in all the shapes

As can be seen the difference in the generated power in the window is not significant in the different shapes, is mandatory to say that the reason of the higher power in the window with the hexagonal inlet circular outlet versus Berchtold's shape is the percentage of rays rejected after reflection, analyzing this percentage is seen that in Berchtold's shape this percentage is bigger which supposed in a decreased of the total power hitting the window, in addition there are no missing ray in the entrance, which makes a part of Berchtold useless.

		Total Power Absorbed	**Total Power Absorbed**	**Total Power Absorbed**
Day	Hour	Berchtold's shape	Hexagonal inlet and outlet	Hexagonal inlet circular outlet
3-21	06:00	1173.40	1151.19	1173.63
	12:00	4945.08	4862.63	4946.91
	21:00	3111.39	3057.26	3113.32
6-21	06:00	1815.00	1777.92	1816.58
	12:00	5010.70	4920.54	5015.97
	21:00	3325.16	3263.51	3328.21
9-21	06:00	1264.16	1240.26	1264.85
	12:00	4642.73	4565.48	4645.53
	21:00	2952.59	2901.16	2954.53
12-21	06:00	-----	-----	-----
	12:00	3907.56	3840.54	3909.67
	21:00	2528.25	2500.57	2528.03

Table 3-9 Comparison of the hitting power for the different shapes

In the simulations can be seen the movement of the hitting rays depending on the hour of the day, it is seen that the hitting rays moves from the left part of the window to the right, being symmetric in the peak hour, but also it is seen that the pattern in the window does not change from month to month, it only depends in the hour of the day, the month is related to the power of the window. It is shown that the power increase during the day until the peak hour around noon and it starts decreasing, this is related to the position of the sun and the quantity of rays in the different hours.

Also, analyzing the pattern in the window is seen that the shapes based in Berchtold´s equation have a similar pattern, concentrating all the rays in the middle of the window, while the hexagonal inlet outlet generate a more dispersed pattern, which can be helpful in order to transfer the heat to the heat transfer fluid.

Although the shapes base in Berchtold´s equation have better power hitting the window, the difficulties of manufacture compare to the hexagonal inlet-outlet make it the best choice for the secondary concentrator.

The good performance of the hexagonal inlet outlet and the ease of manufacture makes it the best shape in the rate price-performance, and in consequence the shape to have in mind in order to increase the heliostat field.

4 Conclusions

A FORTRAN code was developed in order to find the more efficient and cheaper secondary concentrator for a CSP plant. For that a ray tracing code for any shape was developed and validated.

Due to the necessity to be able to test any arbitrary shape, SOLIDWORKS and ANSYS are used to be able to generate the shape in FORTRAN.

In order to generate the rays for the secondary concentrator, MIRVAL is used, a Monte Carlo code that generates the rays that may enter in the concentrator, then it is made the ray tracing of them inside the concentrator.

In order to have no dead space between the concentrators, certain portions of facets near the entrance of the concentrators can be removed to form a closed-packed hexagonal matrix.

Several designs for concentrators were analyzed using the MCRT. The main purpose of the new designs is to be able to allocate more than one concentrator with no dead space between them. The best results, from the point of view of power hitting the window, were obtained for compound parabolic concentrators, although the hexagonal modifications gives in some simulations more power this is due to the dimensions of the MIRVAL file. From the point of view of power distribution, the best result were obtained for the hexagonal inlet- outlet since it gives a more unfocused pattern, and from the economic point the hexagonal inlet-outlet also is better since is built with six planes.

5 Future work

Further power can likely be achieved by coupling the secondary concentrator and the heliostat field, since the shape of the heliostat field affect in the secondary concentrator shape an in consequence in the gain power.

Further power also can be achieved modifying the hexagonal inlet outlet in order to have more rays hitting the window directly since this shapes decreased the percentage of them.

Thirdly, it is necessary to investigate the absorbed power by the secondary concentrator in order to design a cooling system for it.

Fourthly a research about the increase of power allocating more secondary concentrators need to be done.

Finally is necessary to couple the code in MIRVAL in order to make the ray tracing in only one step.

6 Bibliography

[1] G.-K. P. R. K. a. P. F. Susan Solomon, "Irreversible climate change due to carbon dioxide emissions," 2008.

[2] Enerdata, "Global energy Statistical Yearbook 2016," 2016. [Online]. Available: https://yearbook.enerdata.net/CO2-emissions-data-from-fuel-combustion.html. [Accessed 2016].

[3] Engineering Inc., "Engineering library," [Online]. Available: http://www.engineering.com/SustainableEngineering/RenewableEnergyEngineering/SolarEnergyEngineering/WhySolarEnergy/tabid/3893/Default.aspx.

[4] M. C. F. D. F. N. M. J.-G. W. Deliang Chen, "Introduction.," in *Climate Change 2013: The physical Science Basis.*, Cambridge University Press, 2016.

[5] International Energy Agency, "IEA," [Online]. Available: www.iea.org/roadmaps/.

[6] Union of Concerned Scientists, Cambridge, "Union of concerned Scientists," 2013. [Online]. Available: http://www.ucsusa.org/clean_energy/our-energy-choices/renewable-energy/public-benefits-of-renewable.html#.V79wzfkrK71.

[7] G. Petrecca, "Energy Conversion and Management: Principles and Applications," Springer International Publishing Switzerland, 2014.

[8] S. Overgaard, "Standard International Energy Classidication(SIEC) in the International Recommendation on Energy Statistics(IRES)," Statistics Norway, 2008.

[9] A. K. K. M. Omar Behar, "A review of studies on central receiver solar thermal power plants," ELSEVIER, Bouzareah, Algeria, 2012.

[10] Office of Energy Efficiency & Renewable Energy, "U.S. Department of Energy," 20 08 2013. [Online]. Available: http://energy.gov/eere/energybasics/articles/power-tower-system-concentrating-solar-power-basics.

[11] J. Lemmens, "DNV GL," 06 10 2016. [Online]. Available: http://blogs.dnvgl.com/energy/the-future-of-solar-energy-concentrated-solar-power-vs-photovoltaic-power-plants.

[12] R. Gaspar, "How Solar PV is winning over CSP," 2013.

[13] U.S. Department of energy, "ENERGY.GOV," [Online]. Available: http://energy.gov/eere/sunshot/concentrating-solar-power.

[14] J. Lillan, "Extensive US project pipeline awaiting dollars and transmission," Solar Industry, 2010.

[15] A.Hunt, A New Solar Thermal Receiver Utilizing a Small Particle Heat Exchanger, 1979.

[16] M. C.-S. M. R. C. W. c. H. L. M.-A. Aránzazu Fernáandez-García, "Durability Of solar reflector materials for secondary concentrators used in CSP systems," *ELSEVIER*, no. 17 June, p. 13, 2014.

[17] E. S. D. F. L. M. P. S. A. G. a. F. F. David Jafrancesco, "Simple methods to approximate CPC shape to preserve collection efficiency," *International Journal of Photoenergy*, p. 7, 2012.

[18] SOLGATE, "Solar hybrid gas turbine lectric power system," European commision.

[19] O. Berchtold, "The Analysis of a Secondary Concentrator for the Small Particle Heat Exchange Receiver using the Monte Carlo Ray Trace Method," San Diego, 2014.

[20] EPIX ANALYTICS, "Introduction to Monte Carlo Simulation".

[21] J. H. P.L. Leary, "A User's guide for Mirval a computer code for comparing designs of heliostat-receiver optics for central receiver solar power plants," 1979.

[22] E. P. Trullen, "Heliostat field design and optimization for a small particle solar receiver," 2015.

[23] T. B. T. D. M. P. P. S. F. T. Reiner Buck, "Solar-Hybrid Gas Turbine-based Power Tower Systems(REFOS)".

[24] R. A.-D. a. S. M. B. Abdullahi, "Effect of acceptance angle on the design and performance of a heat pipe based compound parabolic collector at Kano, Nigeria," EA4EPQ.

[25] J. m. A.A. Radu, "Ray tracing simulations for a modified compound parabolic concentrator to be considerd for the VERITAS project," ELSEVIER, Boston, 1999.

[26] A. L. Ávila-Marín, "Volumetric receivers in Solar Thermal Power Plants with Central Receiver System technology," ELSEVIER, Madrid, 2011.

[27] J. R. S. A. Aurelian A.Radu, "Design studies for nonimaging light concentrators to be used in very high-energy gamma-ray astronomy," ELSEVIER, Boston, 1999.

[28] X.-L. X. C. S. H.-C. Z. Gui-Long Dai, "Numerical investigation of the solar concentrating characteristics of 3D CPC and CPC-DC," ELSEVIER, 2011.

[29] A. B. V. B. F. C. A. C. D. d. V. T. M. L. P. M. R. f. t. S.-1. s.-C. J.A. Aguilar, "Design, optimization and characterization of the light concentrators of the single-mirror small size telescopes of the cherenkov Telescope Array," ELSEVIER, Geneva, 2014.

[30] J. R. M. S. A. Aurelian A. Radu, "Design studies for nonimaging light concentrators to be used in very high-energy gamma-ray astronomy," ELSEVIER, Boston, 1999.

[31] W. S. A. K. a. H. R. A. Timinger, "Optimized Secondary Concentrators for a partitioned central receiver system," Pergamon, München, 1999.

[32] F. D. ,. G. A. A. P. A. S. Thomas Cooper, "Performance of compound parabolic concentrators with polygonal apertures," ELSEVIER, Zurich, 20113.

[33] T. K. Nazmi Sellami, "Optical efficiency study of PV crossed compound parabolic concentrator," ELSEVIER, Edinburgh, 2012.

[34] A. D. A. L. Tim Wendelin, "Soltrace: A Ray-Tracing Code for Complex Solar Optical Systems," NREL, 2013.

[35] M. C.-S. a. T. A. Fernandez-García, "Examination of naturally weathered REFOS secondary concentrators," 2011.

[36] A. Hunt, "Small Particle Heat Exchangers," Berkeley Lab, 2011.

[37] P. D. R. R. J. K. R. R. S. D. a. E. T. A. Kribus, "A multistage solar receiver: the route to high temperature," Pergamon, Beer-Sheva, 2000.

[38] R. Bertocchi, "Carbon Particle Cloud Generation for a Solar Particle Receiver," Israel, 2002.